Reaction kinetics of the iron-catalysed decomposition of SO3

AF van der Merwe

Dissertation submitted in fulfilment of the requirements for the degree *Magister in Chemical Engineering* at the Potchefstroom Campus of the North-West University

Supervisor: Prof HWJP Neomagus

April 2014

Reaction kinetics of the iron-catalysed decomposition of SO_3

Abraham Frederik van der Merwe

(B.Eng – Chemical Engineering)

Dissertation submitted in fulfilment of the requirements for the degree Masters in Engineering in the School for Chemical and Minerals Engineering at the North-West University, Potchefstroom Campus

Supervisor: Professor H.W.J.P. Neomagus

Declaration

I, Abraham Frederik van der Merwe, hereby declare that the dissertation entitled: Reaction kinetics of the iron-catalysed decomposition of sulphur trioxide, which was done for the completion of a Masters Degree in Chemical Engineering, is my own work.

_____ _____

A.F. van der Merwe Date

Abstract

In this study the performance of pure, very fine iron (III) oxide powder was investigated as catalyst for the decomposition of sulphur trioxide into sulphur dioxide and oxygen. This highly endothermic reaction requires a catalyst to lower the reaction temperature. This reaction forms part of the HyS (Hybrid Sulphur) cycle, a proposed thermochemical process for the industrial scale production of hydrogen and oxygen from water.

The study aimed at obtaining reaction kinetics for this reaction employing pure, unsupported iron (III) oxide as catalyst as a cheaper alternative compared to supported iron catalysts.

It was found that the SO_3 conversion was carried out in the absence of diffusion limitations and that the reverse reaction did not play a significant role. By assuming plug flow conditions in the reactor and 1st order kinetics, the kinetic parameters of the reaction were obtained.

These parameters that form part of the Arrhenius law in describing the reaction rate constant, were determined to be $118\ (\pm 23)\ kJ/mol$ for the activation energy (E_a), and a value of $3\ (\pm 0.5) \times 10^8\ hr^{-1}$ was obtained for the Arrhenius frequency factor (A). Both values correspond to literature, although in general larger activation energies were published for iron (III) oxide derived supported catalysts.

A comparison of the performance of the pure, unsupported iron (III) oxide catalyst with other iron (III) oxide derived supported catalysts (or pellets) has shown that the pure iron (III) oxide catalyst exhibit similar activities. Avoiding expensive catalyst preparation will be an initial step in the direction of developing a cost effective catalyst for the decomposition of sulphur trioxide. It is, however, recommended to investigate different particle sizes as well as purity levels of the unsupported iron (III) oxide to find an optimum cost to performance ratio, as the degree of fineness and the degree of purity will largely influence the final catalyst cost.

A qualitative investigation with various reaction product species as well as water in the reactor feed was conducted to assess the influence of these species on the reaction rate. The addition of these species seems to have a larger influence on the reaction rate at low reaction temperatures around 700°C than at higher reaction temperatures (i.e. 750°C and 825°C). This can be attributed to adsorption rates of such species that reduce at higher temperatures. Observations at higher reaction temperatures also suggest that the reaction is of a first-order nature.

Key words: Decomposition of SO_3, iron (III) oxide catalyst, reaction kinetics

Opsomming

Die gedrag van suiwer, baie fyn yster (III) oksied as katalisator is gedurende hierdie studie ondersoek tydens die ontbinding van swael trioksied na swaeldioksied en suurstof. Hierdie hoogs endotermiese reaksie vereis 'n katalisator om die reaksietemperatuur te verlaag. Hierdie reaksie vorm deel van die HyS (Hibried Swael) siklus, 'n voorgestelde termochemiese proses vir die industriële-skaal vervaardiging van waterstof en suurstof vanuit water.

Die studie het ten doel om reaksiekinetika vir die reaksie in die teenwoordigheid van suiwer, nie-ondersteunde yster (III) oksied as katalisator te verkry as 'n goedkoper alternatief in vergelyking met ondersteunde yster oksied katalisatore.

Daar was bevind dat die omsetting van SO_3 in die afwesigheid van diffusiebeperkings uitgevoer was en dat die omgekeerde reaksie nie 'n noemenswaardige rol gespeel het nie. Deur propvloei toestande in die reaktor aan te neem asook 1^e orde kinetika, was die kinetika parameters van die reaksie bepaal.

Hierdie parameters, wat deel vorm van die Arrhenius wet in die beskrywing van die reaksie-tempo konstante, is bereken op $118\ (\pm 23)\ kJ/mol$ vir die aktiveringsenergie (E_a), en 'n waarde van $3\ (\pm 0.5) \times 10^8\ hr^{-1}$ was verkry vir die Arrhenius frekwensie faktor (A) (oftewel die voor-eksponensiële faktor). Beide waardes vergelyk met gepubliseerde data alhoewel groter aktiveringsenergieë gepubliseer is vir yster (III) oksied gebaseerde ondersteunde katalisatore.

'n Vergelyking van die prestasie van die suiwer, nie-ondersteunde yster (III) oksied katalisator met alternatiewe yster (III) oksied gebaseerde ondersteunde katalisatore (asook korrels) het aangetoon dat die suiwer yster (III) oksied soortgelyke aktiwiteite vertoon. Die vermyding van duur voorbereidingsmetodes vir katalisatore kan dus 'n aanvanklike stap wees in die rigting van die ontwikkeling van 'n koste-effektiewe katalisator vir die ontbinding van swaeltrioksied. Dit word egter aanbeveel dat verskillende partikelgroottes asook verskillende mates van suiwerheid van die nie-ondersteunde yster (III) oksied ondersoek moet word om 'n optimale koste tot prestasie verhouding te vind, aangesien die graad van fynheid asook die graad van suiwerheid 'n noemenswaardige invloed op die finale koste van die katalisator sal uitoefen.

'n Kwalitatiewe ondersoek waarin verskeie reaksieproduk spesies asook water in die reaktorvoer toegevoeg is, is onderneem om die invloed van hierdie spesies op die reaksie te ondersoek. Die toevoeging van hierdie spesies blyk 'n groter invloed op die reaksietempo uit te oefen by lae reaksietemperature naby 700°C as by hoër reaksietemperature (750°C en 825°C). Dit kan toegeskryf word aan adsorpsietempo van hierdie spesies wat afneem met toenemende temperature. Waarnemings by die hoër reaksietemperature kan 'n aanduiding wees dat die reaksie 'n eerste-orde natuur het.

Sleutelwoorde: Ontbinding van SO3, yster (III) oksied katalisator, reaksie kinetika

Table of Contents

List of Figures

List of Tables

List of Symbols

Symbol	Description	Units
Roman Symbols		
A	Arrhenius frequency (or pre-exponential) factor	hr^{-1}
Avg	Average value of population	-
C_a	Concentration of species a exiting the reaction zone	mol/m^3
C_a^o	Initial (feed) concentration of species a	mol/m^3
$\bar{C}_a$	Average concentration of species a in the catalyst bed	mol/m^3
CF	Correction factor for sulphur dioxide measurement	-
CA	Cross sectional area of the tubular reaction zone	m^2
D_{AB}	Binary component diffusion coefficient	m^2/s
d_p	Diameter of catalyst particle	m
d_{rz}	Diameter of reaction zone tube	m
E_a	Activation energy	kJ/mol
F_a	Volumetric flow rate of species a	m^3/hr
F_a^o	Initial (feed) volumetric flow rate of species a	m^3/hr
Δh_r^o	Standard heat of reaction	kJ/mol
j_m	Colburn j-factor for mass transfer	-
K_a	Pressure equilibrium constant for species a	kPa
k	Reaction rate constant	$m^3/kg_{cat}.hr$
k_m	Mass transfer coefficient	m/s
M_a	Molecular mass of species a	g/mol
M_{AB}	Mean molecular mass of binary component gas mixture	g/mol
m_a	Mass of species a	g
m_{cat}	Mass of catalyst	kg
N	Number of samples in population	-
$\dot{n}_a$	Molar flow rate of species a	mol/hr
$\bar{n}_a$	Equilibrium flow rate of species a	mol/hr
$\dot{n}_a^o$	Initial (feed) molar flow rate of species a	mol/hr
n_a	Number of moles of species a	$moles$
$\dot{n}_{SO_2}^{(diss)}$	Rate of dissolution of sulphur dioxide	mol/hr
P_a	Partial pressure of species a	bar
P_T	Total reaction pressure	bar

P^{act}	Actual measured pressure	bar
P^{std}	Standard pressure	bar
R	Universal gas constant	$kJ/mol.K$
R_p	Catalyst particle radius	m
Re	Reynolds number	-
r_a	Reaction rate – rate of consumption of species a	$mol/kg_{cat}.hr$
S	Split factor (splitting of stream into two)	-
Sc	Schmidt number	-
Sh	Sherwood number	-
S_v	Space velocity ($= \dot{v}_t^o/m_{cat}$)	$m^3/kg_{cat}.hr$
SP_{MFC}	Set point of the mass flow controller	$m\ell/min$
St_m	Stanton number for mass transfer	-
Std	Standard deviation value of population	-
T	Temperature	K
T^{act}	Actual measured temperature	K
T^{std}	Standard temperature	K
T_r	Temperature in the reaction zone	K
t	Critical t-value	-
v	Superficial reaction gas velocity	m/s
$\dot{v}_a$	Volumetric flow rate of species a	m^3/hr
$\dot{v}_a^{norm}$	Normal volumetric flow rate of species a	Nm^3/hr
$\dot{v}_t^o$	Total volumetric flow rate of the feed stream	m^3/hr
$\dot{v}_t^{o-norm}$	Total normal volumetric flow rate of the feed stream	Nm^3/hr
$\dot{w}_{H_2SO_4}^o$	Mass flow rate of sulphuric acid to the reactor	g/hr
Y_{SO_2}	Sulphur dioxide measured value	$Vol\ \%$
$Y_{SO_2}^*$	Corrected sulphur dioxide measurement	$Vol\ \%$
y_a	Mole fraction of component a in a mixture	-
$WHSV$	Weight-Hourly-Space-Velocity	$g_{SO_3}/g_{cat}.hr$
X	Conversion	%
y_a	Mole fraction of species a	-
$\bar{y}_a$	Equilibrium mole fraction of species a	-
y_a^o	Mole fraction of species a in reactor feed	-
z	Thickness of the catalyst bed	m

Greek Symbols		
ε_v	Void fraction in packed bed	-
ϵ	Experimental error	-
$\epsilon(\%)$	Error percentage	%
μ_g	Reactant gas viscosity at specific conditions	$Pa.s$
$\dot{\xi}$	Extent of reaction	mol/hr
ρ_b	Bulk density of the catalyst	kg/m^3
ρ_g	Reactant gas density at specific conditions	kg/m^3
Σv_a	Diffusion volume of species a	m^3/mol

List of Abbreviations

HyS	Hybrid Sulphur (Process)
PFR	Plug-flow Reactor
PGM	Platinum Group Metals
PVA	Poly-Vinyl-Alcohol
SEM	Scanning Electron Microscope
SI	Sulphur Iodine (Process)
USA	United States of America
WHSV	Weight-Hourly-Space-Velocity

1. Introduction

1.1 Background to this study

The investigation into small, medium and large scale alternatives for the manufacturing of hydrogen as fuel for hydrogen fuel cell driven applications, or for industrial uses like the manufacturing of synthetic fuels, has received much attention in the last four decades (Brown & Revankar, 2012). Several pathways and technologies have been explored for the manufacturing of hydrogen from different energy sources, of which most are depicted in Figure 1.

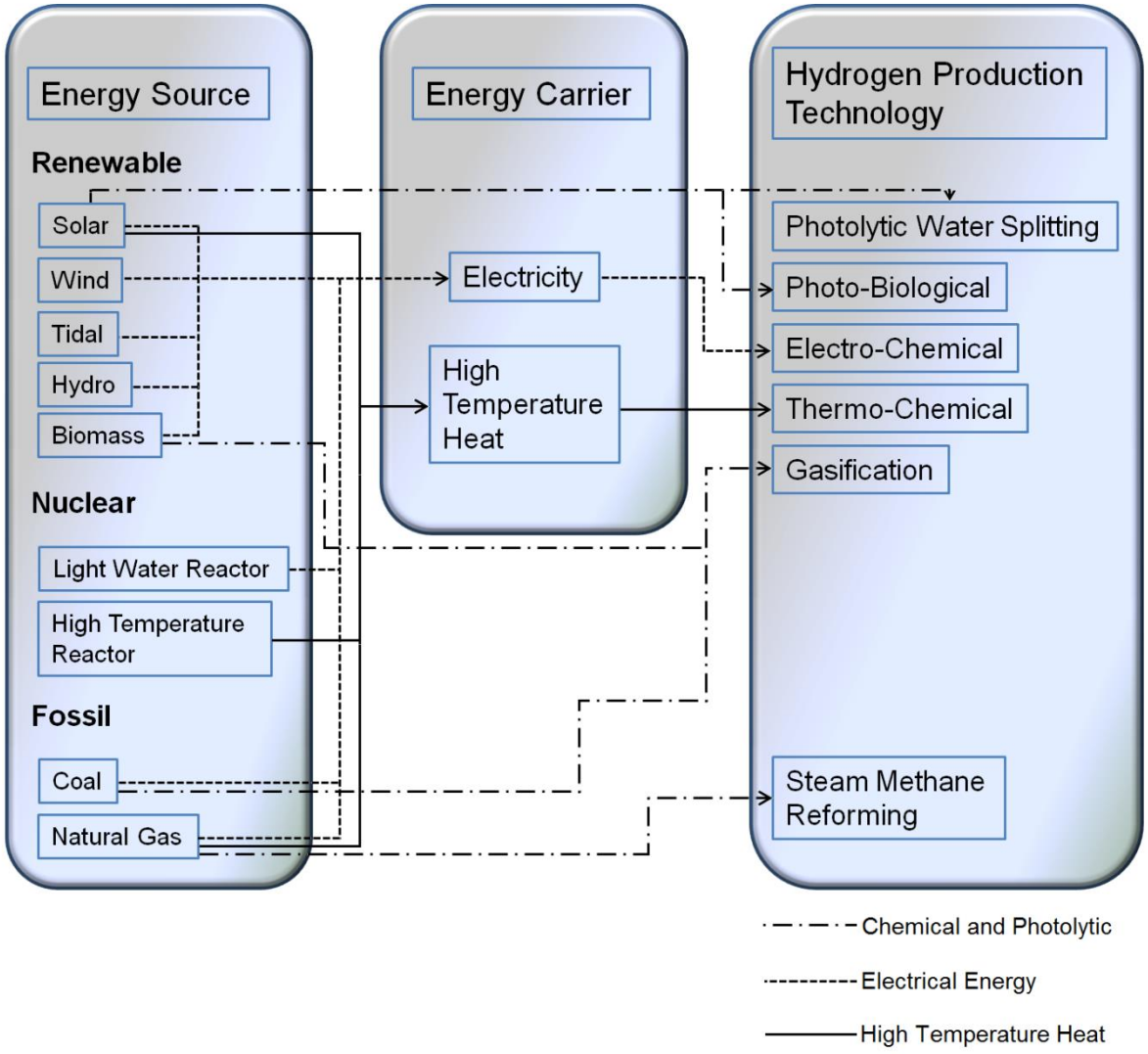

Figure 1 – Pathways and Technologies for Hydrogen Production (Adapted from various sources)

Figure 1 indicates the prominent role that electricity plays in hydrogen production, and research in the field of water electrolysis is receiving international attention (Nagarajan *et al.*, 2009). Various energy sources can be used in the generation of electricity including renewable energy sources, nuclear sources as well as fossil fuel sources, as demonstrated in Figure 1. Electricity production is generally inefficient, expensive and can be polluting (Nagarajan *et al.*, 2009). Other pathways include photo catalytic and photo biological processes which are both limited to solar energy as energy source.

Facing the potential lack of fossil based resources as well as globally enforced limitations on the release of greenhouse gases, water and biomass seem to be the preferred raw materials candidates for the production of hydrogen (Banerjee *et al.*, 2008).

Although the application of thermochemical cycles for hydrogen production, as depicted by the solid lines in Figure 1, has been studied since the energy crisis of the 1970s (Brown & Revankar, 2012), more economical hydrogen production from fossil based fuels prevented large scale investment in research activities and development in this field for the last few decades. Only with recent global interest into high temperature nuclear reactors through the United States of America's Nuclear Hydrogen Initiative (NHI) (Gorensek & Summers, 2009) as well as concentrated solar energy (Thomey *et al.*, 2012) has renewed research efforts gained momentum in these thermochemical cycles.

1.2 The Hybrid Sulphur (HyS) process for hydrogen production

Research initiatives worldwide recognise sulphur-based cycles for the production of hydrogen as high priority candidate technologies, as these have the ability to perform at higher efficiencies than direct water electrolysis (Nagarajan *et al.*, 2009). These cycles are adaptable to large scale hydrogen production and provide an elegant carbon-free means of hydrogen production driven by alternative energy sources (Giaconia *et al.*, 2011). The hybrid sulphur (HyS) as well as the sulphur-iodine (SI) processes have been identified as leading technology candidates for research by the United States of America's Department of Energy's (DOE) Nuclear Hydrogen Initiative (Gorensek & Summers, 2009).

One of the thermochemical processes for the large scale production of hydrogen was proposed by the Westinghouse Electric Corporation, a United States of America based company also specialising in the nuclear industry. This process was extensively researched during the nineteen seventies and -eighties, and became known as the Westinghouse process (Gorensek & Summers, 2009) as it was first proposed by the Westinghouse Electric Corporation. Figure 2 depicts the HyS process schematically.

The HyS process involves a thermochemical cycle wherein sulphur species are continuously cycled in a circuit. From Figure 2 it can be seen that two reaction steps, marked 1 & 2, interact into a net reaction wherein water is split into hydrogen and oxygen (Gorensek & Summers, 2009). The designation "hybrid" in the name "Hybrid Sulphur" indicates that both thermochemical and electrochemical steps are included in the process (Gorensek & Summers, 2009). This implies that electrical energy is required for the production of hydrogen at the sulphur dioxide depolarised electrolyser, indicated as step 2 in Figure 2. In this step, SO_2 is combined with water and fed to the anode of a proton exchange membrane

(PEM) based electrolyser system. The electrical energy requirement for the SO_2 electrolysis process is significantly lower than the energy required for pure water electrolysis, which is visible in the reversible cell potential of the SO_2 electrolyser system of -0.243V at 25°C compared to a value of -1.229V at 25°C for pure water (Gorensek & Summers, 2009).

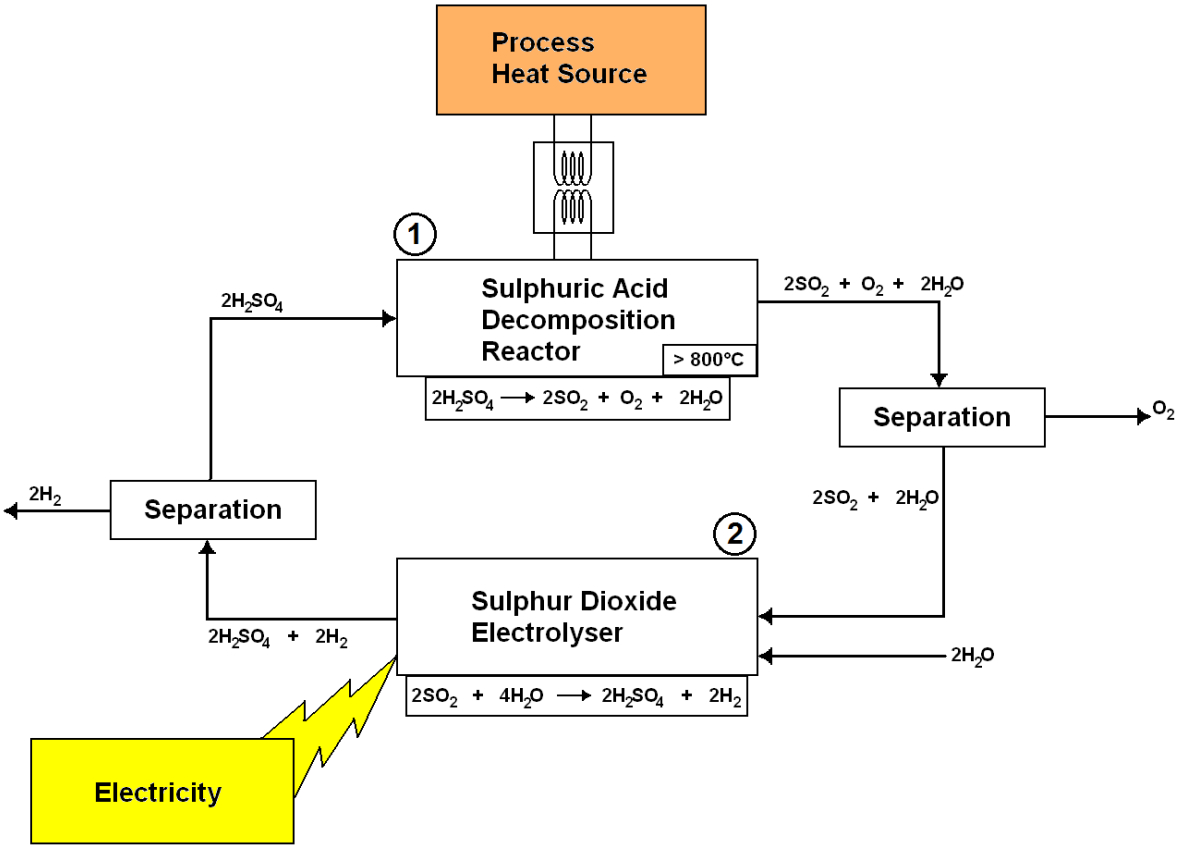

Figure 2 – Schematic Representation of the Hybrid Sulphur (HyS) Process for Hydrogen Production (adapted from Gorensek & Summers, 2009)

A subsequent separation process separates the gaseous hydrogen from the aqueous sulphuric acid that formed in the electrolysis step. The aqueous sulphuric acid is then fed to a reactor wherein it is thermally decomposed into sulphur dioxide, oxygen and water, as seen in step 1 on of Figure 2. At this high-temperature reaction step, oxygen is released through the catalytic decomposition of sulphuric acid. This step receives significant research attention globally (Gorensek & Summers, 2009).

Following the decomposition of the sulphuric acid into sulphur dioxide, oxygen and water, another separation process entails the removal of gaseous oxygen from the other constituents.

The HyS process is one of the simplest thermochemical cycles as it entails only aqueous and gaseous fluids as reactants and products, it comprises of only two reaction steps and it entails only three elements (Gorensek & Summers, 2009).

1.3 Focus of this study

The sulphuric acid decomposition step in the HyS (and SI) thermochemical cycle is receiving substantial research attention in the USA (e.g. Ginosar *et al.*, 2009, Gorensek & Summers, 2009, Brown & Revankar, 2012), Europe (e.g. Barbarossa *et al.*, 2006, Giaconia *et al.*, 2011 etc.), India (e.g. Banerjee *et al.*, 2008 & 2011, Kondamudi & Uphadhyayula, 2012), Japan (e.g. Dokiya *et al.*, 1977 & Karasawa *et al.*, 2006) and South Korea (e.g. Kim *et al.*, 2006). A number of technical challenges surrounding this step still pose threats to commercialisation of this technology. These include materials of construction of the reactors due to the aggressiveness of the reactants, pressures at which the process will be operated at and a proper reactor design for the decomposition reaction of sulphur trioxide due to the absence of reaction kinetics, catalyst choices etc. (Brown & Revankar, 2012).

According to Brown & Revankar (2012), a number of catalysts have been identified and a certain amount of research has already been conducted. Amongst these are supported platinum group metals (PGM) as well as non-PGM based catalysts. Of the latter, iron oxide (Fe_2O_3), some other transition metal oxides as well as more complex combined metal oxides were identified, although very little has been published on intrinsic kinetics of these catalysts.

Iron (III) oxide has been identified as alternative to the more expensive PGM based catalysts. The inexpensiveness and abundance of iron (III) oxide relative to other metals or metal oxides make this an attractive alternative for industrial scale sulphur-based thermochemical cycles (Giaconia *et al.*, 2011). Iron (III) oxide has shown promising catalytic activity, either supported or as pellets (Giaconia *et al.*, 2011, Karasawa *et al.*, 2006, Kondamudi & Upadhyayula, 2012 and Kim *et al.*, 2013).

The performance of unsupported pure Fe_2O_3 powder has not received attention, while this type of catalyst can further reduce catalyst preparation time, effort and the costs involved therein. For these reasons, pure unsupported Fe_2O_3 powder is the focus of this study. A disadvantage of unsupported catalysts in general is the relative small active area, which could possibly be overcome by the use of very small, micronised particles.

1.4 Objectives and Scope of this work

The primary objective of this study is to evaluate the performance of micronized iron (III) oxide powder as candidate catalyst for the decomposition of sulphur trioxide. Results obtained for this pure, unsupported catalyst will subsequently be compared to published results for supported iron (III) oxide catalysts.

A secondary objective is to evaluate the influence of product and reactant gases on the reaction kinetics of the decomposition reaction, which has not received attention in the literature yet.

Figure 3 summarises the scope of the investigation by discussing the layout of this report and subsequently summarising the extent of the investigation.

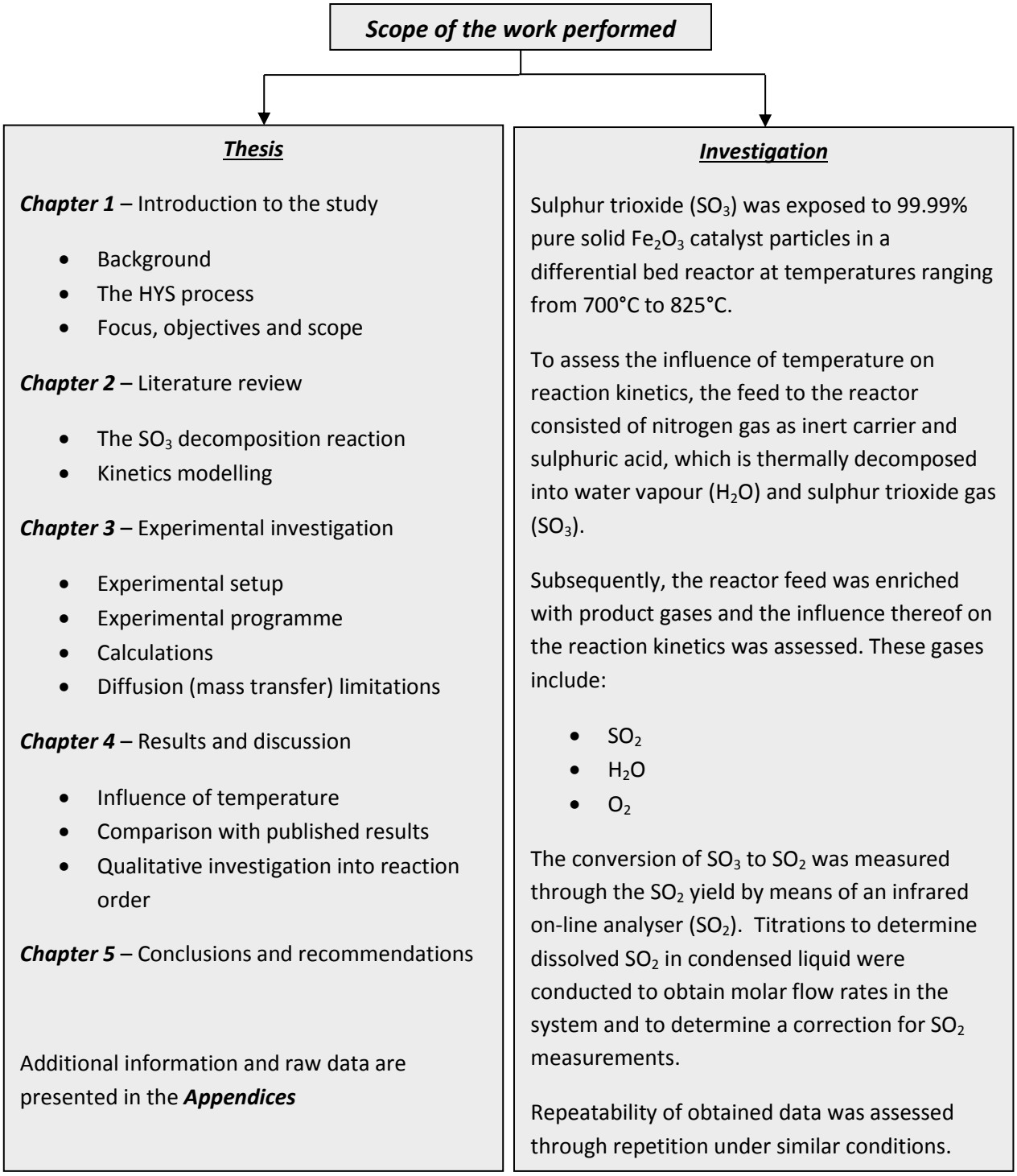

Figure 3 - Scope of this study

2. Literature review

This chapter is divided into two sections. Section 2.1 is a general introductory session that will cover the chemical reaction under investigation followed by a discussion on the catalytic work that has been performed on the reaction. Section 2.2 will focus on the kinetics for the decomposition of sulphur trioxide in the presence of iron (III) oxide as catalyst with emphasis on the modelling and determining of the kinetics parameters.

2.1 The decomposition of sulphuric acid

The decomposition of sulphuric acid, as discussed in available literature sources, takes place according to the following reaction steps.

Step 1:

$$H_2SO_4(g) \rightarrow SO_3(g) + H_2O(g) \qquad \Delta h_r^o = 97.54\ kJ/mol \qquad [1]$$

Step 2:

$$SO_3(g) \rightarrow SO_2(g) + \frac{1}{2}O_2(g) \qquad \Delta h_r^o = 98.92\ kJ/mol \qquad [2]$$

Standard enthalpies of reaction are obtained from Kondamudi *et al.* (2012) wherein the decomposition of sulphuric acid to sulphur trioxide and water assumes that sulphuric acid is in the gaseous phase.

Banerjee *et al.* (2011) describe the decomposition of sulphuric acid as the "most endothermic step" of researched sulphur-based cycles for hydrogen production, which is also observed in the standard heats of the reactions.

Kondamudi *et al.* (2012) also states that the two reactions can take place simultaneously, wherein sulphur trioxide that forms will consecutively decompose into sulphur dioxide and oxygen, but that often a two-stage reactor design, wherein the sulphuric acid is first vaporised and decomposed into sulphur trioxide and water, followed by a second stage wherein the sulphur trioxide is decomposed into sulphur dioxide and oxygen, is used.

2.1.1 The decomposition of sulphuric acid to sulphur trioxide and water

According to Banerjee *et al.* (2008) the decomposition of the sulphuric acid to water and sulphur trioxide (reaction 1) can occur without the presence of a catalyst. Limited information exists on detailed kinetics of this homogeneous reaction shown in Equation 1, and is mainly based on experimental data for the reverse form, wherein sulphuric acid is produced from sulphur trioxide in the well-known contact process (Banerjee *et al.*, 2008).

This reaction is also termed the vaporisation of sulphuric acid by Giaconia *et al.* (2011) and Gorensek & Summers (2009). The latter describes this step as the vaporisation and super heating of sulphuric acid, which spontaneously decomposes into water and sulphur trioxide.

Giaconia *et al.* (2011) mention a temperature of around 400°C for this decomposition step, while Felder and Rousseau (2000:634) indicate that sulphuric acid decomposes (to water and sulphur trioxide) at 340°C. Karasawa *et al.* (2006) briefly discuss a temperature of 500°C for this initial decomposition reaction.

Schwartz *et al.* (2000) describe the predominance of the decomposition of sulphuric acid into sulphur trioxide and water in the temperature range of 400K – 700K (127°C – 427°C), indicating that the reaction equilibrium constant exceeds a value of one for temperatures above 673K (400°C) with rapid increasing of this equilibrium constant with increasing temperature. The reference sources in this section indicate that the decomposition of sulphuric acid according to Equation 1 is relatively fast, resulting in the complete decomposition of the sulphuric acid prior to reaching the catalyst bed (for this study).

2.1.2 The decomposition of sulphur trioxide to sulphur dioxide and oxygen

Due to the focus of this study, more emphasis will be attributed to the second step (or sub reaction) in the decomposition of sulphuric acid, as described by Equation 2. Although a number of articles were published on this sub reaction, the amount of information available on the kinetics of this reaction is limited (Banerjee *et al.*, 2008).

Brown & Revankar (2012) describe this step as the most challenging step of the decomposition reaction due to the severe corrosive effect of the products as well as the high energy requirements due to the endothermic nature.

Although Kim *et al.* (2006) suggest that sulphuric acid can be decomposed either with- or without the aid of a catalyst, the second sub reaction is well known to be a catalytic reaction step. Most literature published on this sub reaction discuss the catalytic nature thereof, but Kondamudi *et al.* (2012) note that published reports focus in principle on the activity of different catalysts, thus failing to address intrinsic reaction kinetics for this reaction.

Karagiannakis *et al.* (2010) describe the decomposition reaction of sulphur trioxide as the step requiring the most energy. Another substantial difference between steps 1 and 2 (as expressed in Equations 1 & 2) is the temperatures whereby these reactions take place. As given in Section 2.1.1, sub reaction 1 takes place at temperatures 300°C – 400°C in the absence of catalysts, while sub reaction 2 requires substantial higher temperatures. Kondamudi *et al.* (2012) stipulate temperatures in excess of 1023K (750°C), Karasawa *et al.* (2006) mention efficient decomposition of sulphur trioxide at 1173K (900°C) while Gorensek & Summers (2009) indicate temperatures exceeding 1073K (800°C).

In addition to the temperature differences between the two sub reactions, the second reaction wherein sulphur trioxide is decomposed into sulphur dioxide and oxygen requires a catalyst. Kondamudi *et al.* (2012) state that a catalyst lowers the activation energy barrier of this dissociation reaction and at the same time improves the efficiency thereof.

The catalyst will have to be robust at high temperatures and in extreme chemically aggressive atmospheres, according to Rashkeev *et al.* (2009). This narrows the selection of potential useable catalysts as these severe conditions can destroy most catalysts within a very short time frame.

2.1.3 Different catalyst types researched for the decomposition of sulphur trioxide

Since the conception of the Westinghouse process (HyS process) for large scale hydrogen production in the mid-1970s, reports on more than thirty different catalysts for the decomposition of sulphuric acid have been published (Karagiannakis *et al.*, 2010). Of all these studies, the transition metal oxides and some of the precious metals from the Platinum Group of Metals (PGMs) are considered promising for the severe conditions the catalyst needs to perform in (Karagiannakis *et al.*, 2010).

The Westinghouse Electric Corporation first published on catalyst research conducted for the sulphuric acid decomposition reaction in 1976. The kinetics of the reaction wherein sulphur trioxide in a 50:50 mixture with argon gas was fed to a small catalyst bed (kept at a constant temperature) employing two proprietary catalysts were reported on (Brown & Revankar, 2012). The study concluded that one of the proprietary catalysts was unsuitable for the application due to a low activity. The other demonstrated an impressive lifetime with no significant loss of catalytic activity over a thousand hours' time on stream.

Dokiya *et al.* (1977) conducted research on metal oxide catalysts for the decomposition of sulphur trioxide. The metal oxides that were investigated include Al_2O_3, ZnO, CuO, NiO, CoO, Co_3O_4, SiO_2, Fe_3O_4, Fe_2O_3, MnO_2, Cr_2O_3, V_2O_5 and TiO_2. Experiments with these catalysts were performed with temperatures ranging from 800°C to 875°C and at atmospheric pressure. In terms of the catalytic activity obtained per unit weight of catalyst, as is shown in Figure 4, iron (III) oxide demonstrated the highest activity, followed by vanadium (V) oxide and with Al_2O_3 showing the lowest activity. The low performance of Al_2O_3, as explained by Norman *et al.* (1982), is due to sulphate formation or $Al_2(SO_4)_3$ poisoning (Brown & Revankar, 2012).

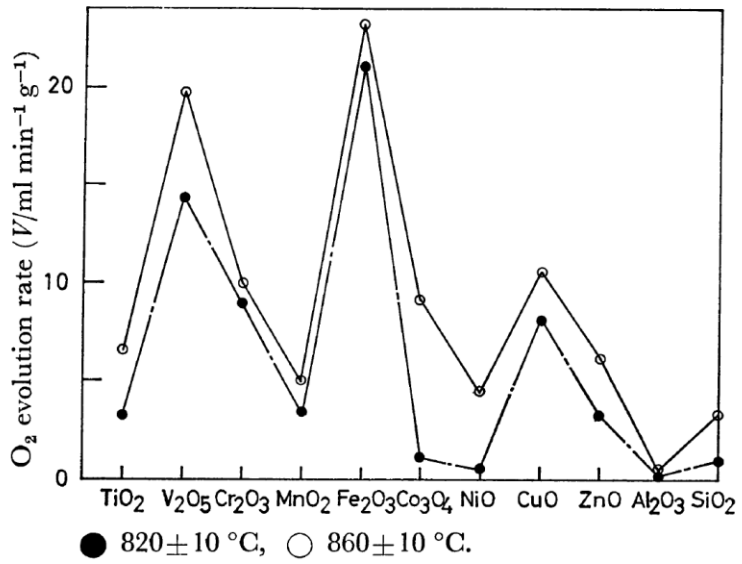

Figure 4 - Catalytic activity per unit catalyst weight (Taken from Dokiya *et al.*, 1977:2658)

Dokiya *et al.* (1977) also compared the catalytic activity obtained per unit specific surface area of the selected oxides. This information is shown in Figure 5. Again the iron (III) oxide demonstrated the highest activity. The interesting disqualifier for vanadium (V) oxide as potential commercial-scale catalyst, although it is predominantly used as catalyst in the reverse reaction for industrial production of sulphuric acid, is that the vanadium (V) oxide liquefies at the relative high operating temperatures. This causes volatilisation of the catalyst.

Brown & Revankar (2012) summarise research conducted by O'Keefe *et al.* (1980) and Norman *et al.* (1982) within General Atomics. They observed declining activities which were attributed to sulphating of the oxides and were normally interpreted as a sign of failure. In this respect, cobalt-, manganese- and nickel oxides indicated excessive sulphate formation resulting in very low activities. Chromium- and vanadium oxides demonstrated high levels of volatility, which allowed these catalysts to migrate and condense in locations downstream in the process where they favour the re-formation of sulphur trioxide. In conclusion, the most active and stable catalysts identified by the research efforts of General Atomics were platinum as noble metal and iron (III) oxide as transition metal oxide.

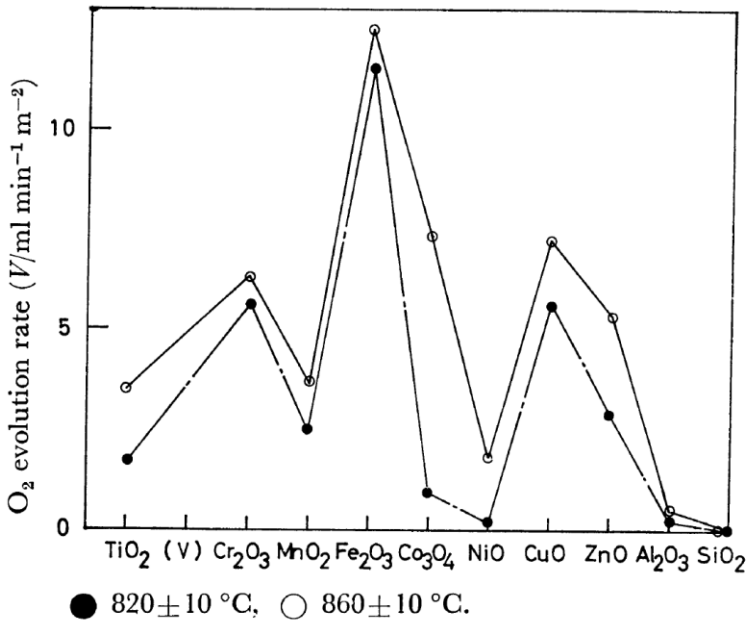

Figure 5 - Comparison of catalytic activity per specific surface area of the catalyst (Taken from Dokiya *et al.*, 1977:2658)

Ishikawa *et al.* (1982) published results of a diverse range of catalysts studied for the decomposition of sulphuric acid. Several metals and metal oxides on a porous support were subjected to experiments wherein the activities of these catalysts were determined. A small packed catalyst bed inside a plug flow reactor was fed with sulphur trioxide gas entrained in argon. The catalyst with the highest activity found in this study was platinum, followed by iron (III) oxide and subsequently vanadium (V) oxide. As with previous studies conducted on Al_2O_3, it exhibits again the lowest activity due to the high stability of the sulphate.

Brown & Revankar (2010) presented a summary of experiments conducted by Brittain & Hildenbrand (1982) wherein, again, platinum was found to have the highest activity in the decomposition of sulphur trioxide, followed by V_2O_4, Cr_2O_3, Fe_2O_3 and lastly, NiO exhibiting the lowest activity. As a confirmation of previous observations, it was found that metal oxide catalysts demonstrates high activities only over temperature ranges wherein the sulphates are less stable.

Tagawa & Endo (1989) conducted experiments wherein catalysts were placed in a quartz tube reactor using nitrogen as carrier gas for the sulphur trioxide. Catalysts pellets of 3mm long and with 3mm diameter were packed to a height of 1cm in the 1.5cm tube (Brown & Revankar, 2010). The main conclusion from this study was that iron-based catalysts have proven high activities with good repeatability at temperatures in excess of 700°C, but that iron sulphate formation was favoured below this temperature, indicated by a loss in activity. Chromium-based catalysts, on the other hand, did not show sulphate formation, thus maintaining high activities at all investigated temperatures. At temperatures exceeding 850°C the platinum-based, iron-based and chromium-based catalysts exhibit similar catalytic activities. Platinum showed the highest overall activity, followed by Cr_2O_3 and Fe_2O_3 with Al_2O_3 showing the lowest activity.

Two catalysts were studied and published on by Barbarossa *et al.* (2006). One is a silver palladium intermetallic alloy while the other is iron (III) oxide supported on a silica (SiO_2) substrate. Sulphuric acid at a concentration of 98% was fed to a decomposition chamber that was considered isothermal. The onset temperature for decomposition of sulphur trioxide in the absence of a catalyst was observed at 1123K (850°C) with complete decomposition observed at 1300K (1027°C). For both catalysts, the observed onset temperature for decomposition was 300°C lower and both catalysts exhibit similar activities. The activity of the iron (III) oxide catalyst remained constant over 16 hours' time on stream (Barbarossa *et al.*, 2006).

A large number of observations and conclusions from published data on iron based catalysts as well as Al_2O_3 as support, were confirmed through studies conducted by Kim *et al.* (2006). The catalyst investigated was iron supported by alumina or titania. For both supports, the molar ratios of iron to support-metal were 0.25, 0.50, 0.75 and 1.00. Experiments were carried out in a quartz decomposition chamber at atmospheric pressure in the temperature range 1023K – 1223K (750°C – 950°C) with the sulphur trioxide entrained in nitrogen gas.

Kim *et al.* (2006) found that the iron-based catalysts maintained their activity over 10 hours' time on stream and that catalytic activity was higher with higher iron load. It was found that iron sulphate decomposes at temperatures higher than 1053K (780°C) and that no iron sulphate was detected on catalyst samples that were operated at 1123K (850°C). Iron sulphate was, however, detected on catalyst samples that were subjected to a temperature of 823K (550°C), indicating that stable iron sulphate remained on the catalyst at this lower temperature range. A minimum temperature for iron catalysts to avoid stable iron sulphate formation was found to be 973K (700°C).

Kim *et al.* (2006) concluded that iron on titania exhibited higher activities than iron on alumina, which is attributed to the sulphating of alumina below 1073K (800°C). Above 1073K (800°C) the alumina sulphate is decomposed, yielding even higher activities than the iron on titania catalysts.

Banerjee *et al.* (2007) investigated the replacement of the iron in Fe_2O_3 in certain step quantities with chromium. The prepared catalysts had the formula $Fe_{2(1-x)}Cr_{2x}O_3$ with x-values ranging from 0 to 1. An x-value of 0 thus indicated pure iron (III) oxide, while a x-value of 1 indicated on pure Chromium (III) oxide. Three catalyst samples were produced: Fe_2O_3, $Fe_{1.8}Cr_{0.2}O_3$ & $Fe_{1.6}Cr_{0.4}O_3$. After 10 hours of catalyst testing, it was found that all these catalysts were stable over the operation time. The highest activity was observed for the $Fe_{1.8}Cr_{0.2}O_3$ catalyst, followed by the Fe_2O_3 and finally the $Fe_{1.6}Cr_{0.4}O_3$. XRD analyses showed that metal sulphates are present in the Fe_2O_3 and $Fe_{1.6}Cr_{0.4}O_3$ samples, but no metal sulphates were detected in the $Fe_{1.8}Cr_{0.2}O_3$ sample.

Banerjee *et al.* (2007) suggested a reaction mechanism that describes the sulphating behaviour of these catalysts wherein minor metastable sulphate formation occurs in the $Fe_{1.8}Cr_{0.2}O_3$ sample in contrast with substantial metastable sulphate formation in the Fe_2O_3 and $Fe_{1.6}Cr_{0.4}O_3$ samples. The catalyst with a lower chromium level has regenerated its oxide after the reaction, thus reducing the formation of metastable sulphates. Temperature-Programmed Reduction (TPR) analyses indicated that the chromium in the catalyst mixture stabilises the catalyst by lowering the formation of stable metal sulphates, lowers the

reduction temperature, minimises sintering of the catalyst and increases the lifetime of the catalyst (Brown & Revankar, 2012).

Brutti *et al.* (2007) studied Fe_2O_3 as catalyst supported on Al_2O_3 in a solar decomposition reactor (Brown & Revankar, 2012). Catalytic activity of this catalyst decreased over the course of the 20 hours experiments by 15-20%. Brutti *et al.* (2007) attributed this decline to sintering of the support, however, the sulphating of the Al_2O_3 substrate cannot be ruled out as contributing factor to the decreasing catalyst activity.

In a few subsequent studies, Ginosar *et al.* (2007), Petkovic *et al.* (2008), Nagaraja *et al.* (2009), Noglik *et al.* (2009) and Rashkeev *et al.* (2009) studied and reported on the decomposition of sulphuric acid using platinum based catalysts.

Noglik *et al.* (2009) included iron (III) oxide in their study, obtaining data that describes the catalytic region as well as the sulphate formation and decomposition region for this specific catalyst, as is depicted in Figure 6 (Brown & Revankar, 2012). According to Figure 6 the sulphate formation and decomposition temperature range for Fe_2O_3 is between 952K and 1052K (679°C and 779°C), a confirmation of the study by Kim *et al.* (2006) wherein no metal sulphates were detected in catalyst samples that were subjected to a reaction temperature of 850°C, with a minimum temperature for decomposition at 700°C (Kim *et al.*, 2006).

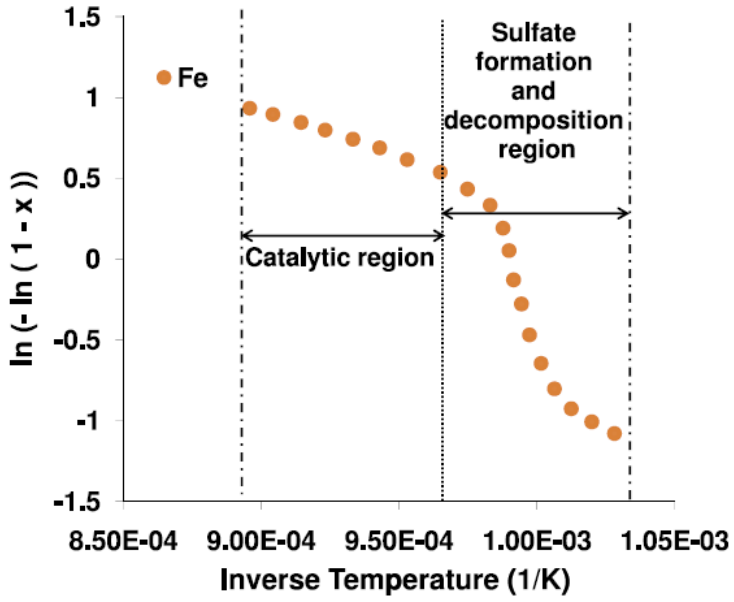

Figure 6 - Sulphate formation region for Fe_2O_3 (Taken from Brown & Revankar, 2012:2694)

Giaconia *et al.* (2011) performed another investigation on Fe_2O_3 as catalyst for the decomposition of sulphur trioxide. The study focused on the effects of reaction temperature, sulphur trioxide partial pressure and Weight-Hourly-Space-Velocity (WHSV) on the conversions and decomposition rate. The Fe_2O_3 showed good performance in the temperature range of 775°C – 900°C, which is a confirmation of data from previous studies. A similar study with quite similar results was performed for Fe_2O_3 by Kondamudi *et al.* (2012) over a temperature range of 750°C to 900°C.

Some more studies that confirmed the temperature dependence of the sulphur trioxide decomposition reaction were reported by Karasawa *et al.* (2006) with the use of ferric oxide (or haematite) and Thomey *et al.* (2012), who investigated Fe_2O_3 and $CuFe_2O_4$ as catalysts.

A summary of past catalyst research activities for the decomposition reaction of sulphur trioxide is presented in Table 1.

Table 1 - Summary of SO_3 decomposition catalyst research activities

Researchers	Catalyst(s) researched	Main conclusions
Abimanyu *et al.* (2008)	Cu-, Fe- & CuFe-Al_2O_3 composites	Cu showed higher activities than Fe due to lower sulphate decomposition temperature (650°C for Cu and 780°C for Fe).
Banerjee *et al.* (2008)	Fe_2O_3, $Fe_{1.8}Cr_{0.2}O_3$, $Fe_{1.6}Cr_{0.4}O_3$	$Fe_{1.8}Cr_{0.2}O_3$ showed less deactivation and improved reproducibility in repeated reduction-oxidation cycles. Improved surface regeneration.
Banerjee *et al.* (2011)	$CoFe_2O_4$, $NiFe_2O_4$, $CuFe_2O_4$	Lowest decomposition temperatures observed for $CuFe_2O_4$. Explained by proposed reaction mechanism. Concluded most promising.
Barbarossa *et al.* (2006)	Ag-Pd alloy & Fe_2O_3 on SiO_2 support	Both catalysts showed high activity; onset temperature reduced by both with 300°C; Fe_2O_3 proved stable over 16 hours of operation.
Brittain & Hildebrandt (1982)	Pt, V_2O_4, Cr_2O_3, Fe_2O_3, NiO	Order of catalytic activity observed: Pt > V_2O_4 > Cr_2O_3 > Fe_2O_3 > NiO. Ru, V_2O_4 & Cr_2O_3 showed poor reproducibility and decreased activity.
Brutti *et al.* (2007)	Fe_2O_3 supported by Al_2O_3	Catalyst activity decreased by 15 – 20% over 20 hours of time-on-stream. Sulphating of the Al_2O_3 substrate played substantial role.
Dokiya *et al.* (1977)	SiO_2, Al_2O_3, ZnO, CuO, NiO, CoO, Fe_2O_3, MnO, Cr_2O_3, V_2O_5, TiO_2	Order of activities per unit weight of catalyst: Fe_2O_3 > V_2O_5 > CuO > Cr_2O_3 > Co_3O_4 > TiO_2 > ZnO > MnO_2 > NiO > SiO_2 > Al_2O_3.
Giaconia *et al.* (2011)	Fe_2O_3 (pellets) or on SiSiC support	Fe_2O_3 showed good catalytic activity (approximately 80% of equilibrium conversion) with negligible deactivation after 100 hrs.
Ginosar *et al.* (2007)	Pt on Al_2O_3, TiO_2 & ZrO_2 supports	Pt on TiO_2 proved stable with deactivation mainly due to Pt loss. Al_2O_3 & ZrO_2 supports showed good activity at 850°C, but activity loss at 800°C
Ginosar *et al.* (2009)	$FeTiO_3$, $MnTiO_3$, $NiFe_2O_4$, $CuFe_2O_4$, $NiCr_2O_4$, $2CuOCr_2O_3$	Order of activities observed for complex metal oxides: $2CuOCr_2O_3$ > $CuFe_2O_4$ > $NiCr_2O_4$ = $NiFe_2O_4$ > $MnTiO_3$ = $FeTiO_3$. Both $2CuOCr_2O_3$ and $NiCr_2O_4$ leached Cr into the sulphur dioxide. FeTiO3 displayed instability at high temperatures (>850°C).
Ishikawa *et al.* (1982)	Pt, Fe_2O_3, V_2O_5, CuO, MnO_2, Cr_2O_3, CeO_2, CoO, ZnO, Al_2O_3	Order of activities observed: Pt > Fe_2O_3 > V_2O_5 > CuO > MnO_2 > Cr_2O_3 > CeO_2 > CoO > ZnO > Al_2O_3.

Karagiannakis *et al.* (2010)	Iron oxides, Al_2O_3, CuO, Cr_2O_3, Pt/Al_2O_3	Fe oxides require substantial temperature for rapid decomposition of iron sulphates. Not the same for Cu. Addition of Al, Cu & Cr to Fe structure enhances conversion.
Karasawa *et al.* (2006)	Ferric oxide (Haematite)	Decomposition rate increased in the presence of the catalyst (compared to thermal decomposition)
Kim *et al.* (2006)	Fe supported by Al and Ti. Fe:support = 25%, 50%, 75% & 100%	Activities increased with increased Fe loading. Fe sulphate not detected on the 850°C sample, but was detected on the 550°C sample. Minimum temperature of 700°C for Fe-based catalysts. Fe-Ti activity higher below 800°C and Fe-Al activity higher above 800°C.
Kondamudi *et al.* (2012)	Fe_2O_3 on Al_2O_3 support	Fe_2O_3 demonstrated good activity at high temperatures (900°C) and 2hrs time on stream.
Nagaraja *et al.* (2009)	Pt supported by $BaSO_4$	Study focussed on catalyst preparation methods with higher activity at higher Pt dispersions.
Noglik *et al.* (2009)	Pt on SiSiC, Fe_2O_3 on SiSiC, blank SiSiC	Pt showed high catalytic activity even at low residence times (0.2 s). Fe2O3 required longer residence times (0.33 s – 1 s) for higher conversion (20% – 85%).
Norman *et al.* (1982)	Supports: Al_2O_3, SiO_2, CeO_2, TiO_2, ZrO_2, Ba_SO_4	Al2O3 supports generally failed due to sulphate formation ($Al_2(SO_4)_3$ poisoning). CuO/SiO_2 failed, but Pt/SiO_2 was active and stable. TiO_2 support generally active and stable. ZrO_2 and $BaSO_4$ supports suffered from sulphate formation.
O'Keefe *et al.* (1980)	Fe_2O_3, V_2O_5 and Cr_2O_3 on supports (see Norman *et al.*)	Fe2O3 most active and stable of the three. Vanadium and Chromium seem volatile at high temperatures, migrating downstream and favouring the re-oxidation of sulphur dioxide.
Petkovic *et al.* (2008)	Pt on TiO_2 support	Activity loss mainly attributed to Pt loss. Pt loss initially high, followed by sulphating of support.
Rashkeev *et al.* (2009)	Pt, Pd, Rh, Ir, Ru supported on TiO_2	Catalytic behaviour is defined by some of the nano scale features, which explains deactivation of the catalyst with time on stream.
Spewock *et al.* (1976)	Proprietary catalysts	One catalyst showed good activity, with an impressive lifetime (no activity loss over 1000 hrs at 850°C). Indication it could be Pt; unconfirmed.
Tagawa & Endo (1989)	Fe_2O_3, Cr_2O_3, Al_2O_3, CeO_2, NiO, CuO	CuO lost activity after a few runs. Cerium activity not impressive. Fe_2O_3 showed good activity > 700°C, but loses activity < 700°C. Pt, Fe & Cr activities were similar > 850°C.
Thomey *et al.* (2012)	Fe_2O_3, $CuFe_2O_4$	Study focused more on solar reactor design – catalyst data scantily presented.
Yannopoulos & Pierre (1984)	$ZnFe_2O_4$, $NiFe_2O_4$	Focussed mainly on preparation. Activities maintained over short test periods. Little data.

2.1.4 Reaction mechanisms with iron (III) oxide as catalyst

A mechanism was proposed by Banerjee *et al.* (2008) who investigated the activities of pure iron (III) oxide, iron (III) oxide of which 10% of the iron was replaced with chromium and iron (III) oxide of which 20% of the iron was replaced with chromium. From thermal analyses of the metal sulphates as well as the metal oxides activities, the conclusion was drawn that both the metal sulphate formation rate and the decomposition rate of the sulphate are the

rate determining steps for the decomposition reaction of sulphur trioxide. A probable route that could describe the decomposition reaction was given as:

$$MO + SO_3 \rightarrow MSO_4 \quad [3]$$

$$MSO_4 \rightarrow MO + SO_2 + \frac{1}{2}O_2 \quad [4]$$

Through analyses the presence of sulphate species was detected on the spent catalysts (Fe_2O_3 & $Fe_{1.6}Cr_{0.4}O_3$), which is a confirmation of the mechanistic approach, depicted by Equations 3 & 4. The final conclusion is that the decomposition of the metal sulphate is the required condition for the decomposition of sulphur trioxide.

Brittain and Hildenbrand (1982) as well as Dokiya *et al.* (1977) found that the onset temperature for the catalytic activity of iron (III) oxide was 793 K (520°C). Barbarossa *et al.* (2006) found this onset temperature at 773K (500°C), which agrees well with the previously observed temperature. Barbarossa *et al.* (2006), who investigated iron (III) oxide on silica, mention further that this observed onset temperature corresponds well with the decomposition temperature of iron (III) sulphate $Fe_2(SO_4)_3$, which is in the order of 780K (507°C) in air. Similar observations were made for other metal sulphates, including $CoSO_4$, $CuSO_4$, $MnSO_4$, $NiSO_4$ and $ZnSO_4$. This could be indicative of the same catalytic mechanism for each, and could entail the formation of a metastable sulphate on the oxide surface.

Tagawa and Endo (1989) found that iron (III) oxide exhibits good catalytic activity when kept beyond 700°C. Reducing the reaction temperature to below 700°C resulted in activity loss for iron (III) oxide. This phenomenon was attributed to the formation of iron sulphate. As the same trends were not observed for chromium- and platinum based catalysts at temperatures lower than 700°C, the activities of these three catalysts were similar beyond 850°C. The mechanism proposed by Tagawa and Endo (1989) is basically a confirmation of that proposed by Banerjee *et al.* (2008) and is depicted in the following two equations:

$$MO + SO_3 \rightarrow MSO_4 \rightarrow MO_2 + SO_2 \quad [5]$$

$$MO_2 \rightarrow MO + \frac{1}{2}O_2 \quad [6]$$

A similar reaction mechanism for the decomposition of sulphur trioxide was proposed by Kim *et al.* (2006).

Karagiannakis *et al.* (2010) contradicted the mechanism proposed by Banerjee *et al.* (2008), Brittain and Hildenbrand (1982), Dokiya *et al.* (1977) and Tagawa and Endo (1989). A strong indication was found that the sulphur trioxide decomposition reaction proceeds rather through the intermediate formation of metal sulphates, and not through repetitive cyclic, reduction-oxidation schemes described by Equations 5 & 6. Should this scheme have been valid, the various oxidation states of e.g. iron would have played a role in the catalytic activity thereof in the order $FeO > Fe_3O_4 > Fe_2O_3$ as the lowest oxidation state of any metal (M) would be the most active in being oxidised to MO_2 through the decomposition of MSO_4. In terms of iron oxide, exactly the opposite in terms of catalytic activity was observed ($FeO < Fe_3O_4 < Fe_2O_3$). Therefore Karagiannakis *et al.* (2010) proposed the following mechanism:

$$MO + SO_3 \rightarrow MSO_4 \rightarrow MO + SO_2 + \frac{1}{2}O_2 \quad [7]$$

In this case the metal (of any oxidation state) is regenerated to its original state. For lower oxidation states of the metal exist a possibility that the metal oxide is further oxidised by the oxygen produced from the reaction shown in Equation 7, yielding:

$$MO + SO_3 \rightarrow MSO_4 \rightarrow MO_2 + SO_2 \quad [8]$$

This latter mechanism can be substantiated by the observation that all FeO and Fe_3O_4 were completely converted to Fe_2O_3 during the reaction, leaving no residual species of FeO and Fe_3O_4 in the spent catalyst. Karagiannakis *et al.* (2010) therefore concluded that the reaction mechanism proposed in Equation 6 does not take place, but that the metal oxide transforms to the active (fully oxidised) form through which the decomposition of the sulphur trioxide is facilitated.

Kondamudi *et al.* (2012) also found that the catalytic activity for metal oxides is closely related to some of their thermodynamic properties, especially the stability of the formed sulphates. With increasing sulphate stability, the tendency to return to the pure oxide form is lower, leading to reduced catalytic activity of the metal oxide.

2.2 Kinetics of sulphur trioxide decomposition with iron (III) oxide as catalyst

2.2.1 Assumptions to kinetics modelling

Spewock *et al.* (1976), Brittain and Hildenbrand (1982), Ishikawa *et al.* (1982), Tagawa and Endo (1989), Ginosar *et al.* (2009), Karasawa *et al.* (2006), Kondamudi & Upadhyayula (2012), Kim *et al.* (2013) & Giaconia *et al.* (2011) proposed ways to obtain kinetic parameters for the decomposition of sulphur trioxide, although only Karasawa *et al.* (2006), Giaconia *et al.* (2011), Kondamudi & Upadhyayula (2012) and Kim *et al.* (2013) published kinetics obtained for supported iron (III) oxide.

Apart from the work by Karasawa *et al.* (2006), who conducted a series of non-isothermal experiments, other authors conducted their experiments isothermally. The way Spewock *et al.* (1976), Kondamudi & Upadhyayula (2012) and Giaconia *et al.* (2011) suggests for the determination of reaction kinetics is adopted for this study, as discussed in Section 2.2.2.

This proposed means to obtain kinetic parameters is done under four assumptions:

- A PFR model is applicable for the kinetics
- The reaction is first-order with respect to sulphur trioxide
- The reaction can be considered irreversible
- Mass transfer limitations can be neglected in the reaction zone

The majority of investigations on the decomposition of sulphur trioxide found in literature are conducted using an integral (fixed-bed-, or plug-flow-) reactor (Brown & Revankar, 2012).

This entails a model of a differential length of reactant fluid that passes through a cylindrical reactor, as described in Appendix A where the kinetics model is derived.

The assumption that the reaction is first-order (in SO_3) will be investigated through the addition of the various reaction products to the reactor feed. In this way, a qualitative investigation will yield information regarding the influence of various SO_3 concentrations in the reaction zone on the reaction.

In order to assume that the reaction is irreversible, observed conversions should be sufficiently below equilibrium conversions at similar conditions. Fogler (1986:59) states that an irreversible reaction behaves as if no equilibrium exists; however, this is only a theoretical concept as no reaction is completely irreversible. Being sufficiently below the equilibrium point (i.e. the equilibrium lies very far to the right of the reaction equation), the reaction can be termed irreversible for practical purposes. To assess whether the assumption of irreversibility can be adopted for this study, the observed conversions should be compared to the equilibrium conversions at the same conditions. Equilibrium conversions are shown in Figure 7.

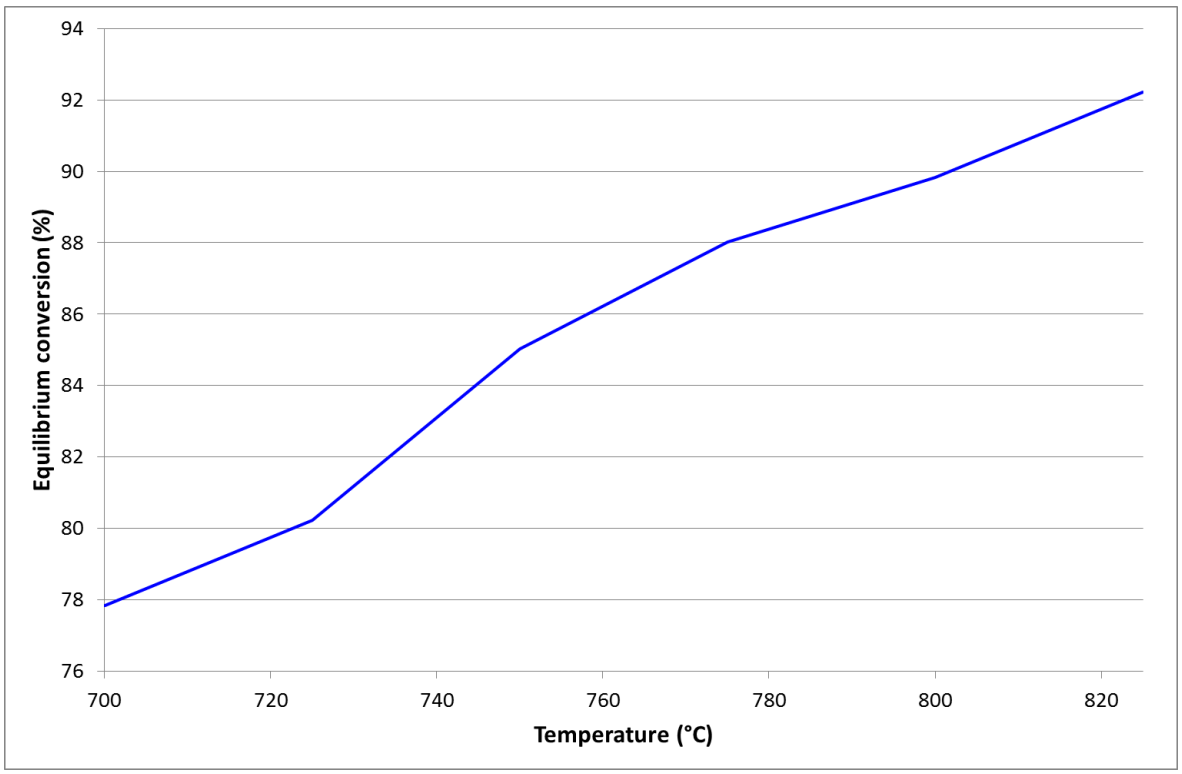

Figure 7 - Equilibrium conversions for SO_3 for the temperature range investigated

The equilibrium conversions were calculated using version 1.1 of the ThermoSolver software program by Connelly Barnes & Milo Koretsky, Oregon State University (2006). Details of the calculations are shown in Appendix B.

The last assumption will be evaluated using the Mears criterion, which is detailed in Section 4.2 and Appendix C.

2.2.2 Kinetics modelling of the trioxide decomposition reaction

Spewock *et al.* (1976), Karasawa *et al.* (2006), Giaconia *et al.* (2011), Kondamudi & Upadhyayula (2012) and Kim *et al.* (2013) arrived at a similar model that relates observed conversions with the reaction rate constant (*k*). This model is derived for a PFR in Appendix A, and can be summarised by Equation 9:

$$k = -\ln\left(\frac{C_{SO_3}}{C^o_{SO_3}}\right).\frac{v^o}{m_{cat}} = -\ln\left(\frac{C^o_{SO_3}(1-X)}{C^o_{SO_3}}\right).\left(\frac{v^o}{m_{cat}}\right) = -\ln(1-X).\left(\frac{v^o}{m_{cat}}\right) \quad [9]$$

Giaconia *et al.* (2011) defines the reaction rate constant *k* as the Arrhenius kinetic constant which is dependent on the reaction temperature according to the Arrhenius law expression:

$$k(T) = A.e^{-E_a/RT_r} \quad [10]$$

By linearizing Equation 10 through taking natural logarithms on both sides, Equation 11 is obtained:

$$\ln(k) = \left(-\frac{E_a}{R}\right)\frac{1}{T_r} + \ln(A) \quad [11]$$

Combining Equations 9, 10 and with linearizing as in Equation 11, the following expression is found:

$$\ln(-\ln(1-X)) = -\ln(v^o/m_{cat}.A) - E_a/RT_r = -\ln(S_v/A) - E_a/RT_r \quad [12]$$

In this model, the activation energy E_a and the Arrhenius frequency factor A are empirically determined from experimental data using Equation 12. These parameters are dependent on a variety of aspects including catalyst loading, catalyst particle sizes and geometry as well as catalyst activity (Brown & Revankar, 2012).

Data from a number of researchers' work on a variety of catalysts, including noble metals, simple metal oxides as well as complex metal oxides, have been plotted according to the model shown in Equation 12. This data is shown in Figure 8 to Figure 11, while data obtained for iron (III) oxide is shown in Figure 6.

Brown & Revankar (2012) observed that, in the temperature range wherein a straight line is achieved, metal sulphates are highly unstable and do not play an important role (i.e. is not the rate-limiting step) in the reaction kinetics. This does not apply to the noble metals, but only to the metal oxides. For the straight-line sections, the activation energy (E_a) is then determined by the slope of the obtained line while the pre-exponential factor (*A*) is determined by the interception.

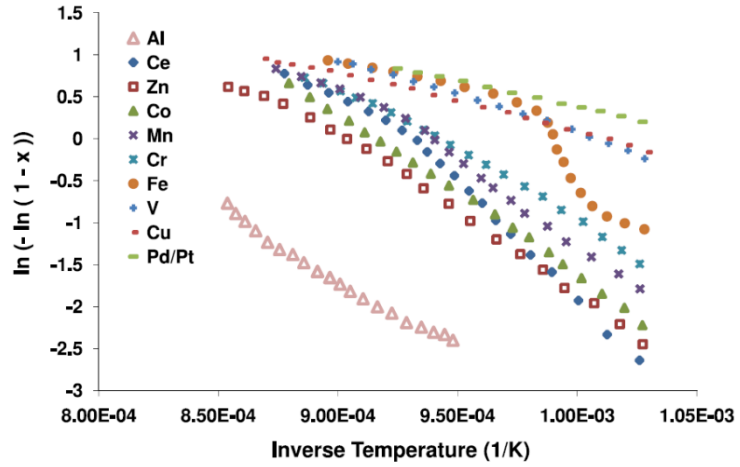

Figure 8 - Experimental data taken from of Ishikawa *et al.* (1982)

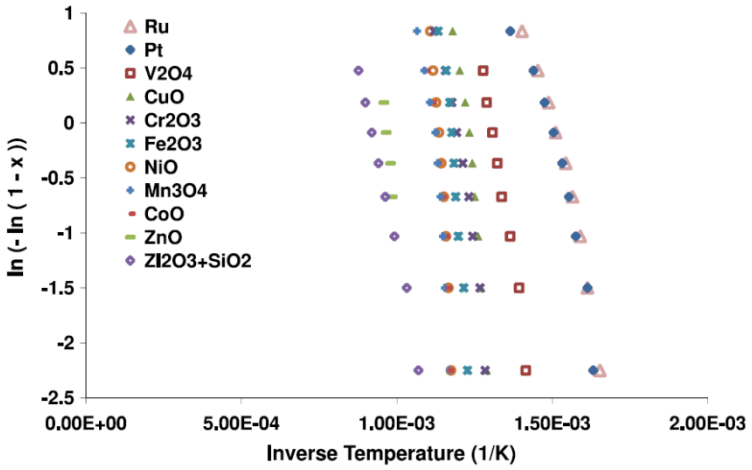

Figure 9 - Experimental data taken from of Brittain and Hildenbrand (1982)

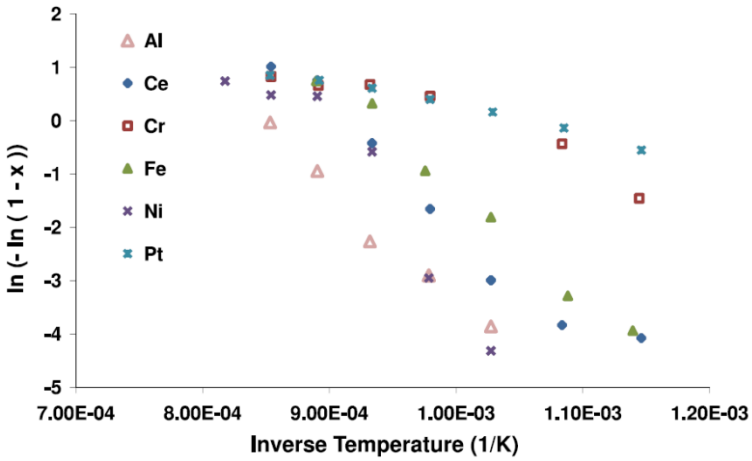

Figure 10 - Experimental data taken from of Tagawa and Endo (1989)

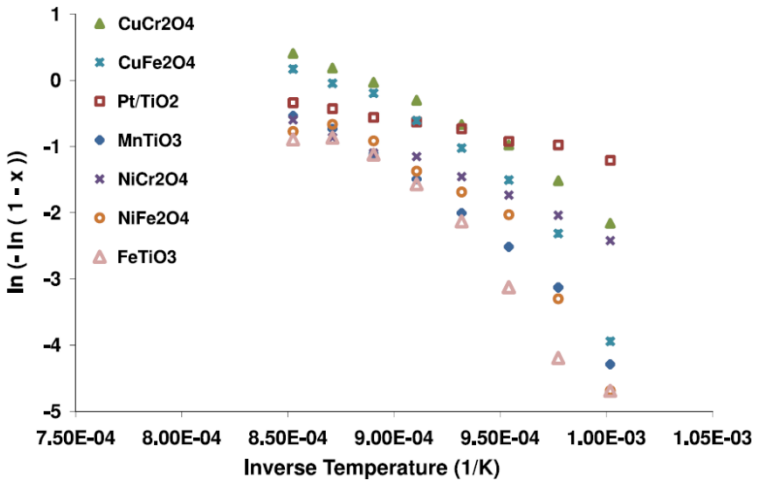

Figure 11 - Experimental data taken from of Ginosar *et al.* (2009)

In the lower temperature range wherein metal sulphate formation and the subsequent decomposition thereof plays an important role in the kinetics of the decomposition of the sulphur trioxide, the plot forms a differently shaped curvature which is distinguishable from the straight line wherein the metal sulphates are unstable. This is visible in Figure 6 and Figure 8 for iron (III) oxide.

Reaction kinetics parameters were obtained by a number of authors for either supported iron (III) oxide, or iron (III) oxide pellets, as shown in Table 2.

Table 2 – Published Arrhenius law kinetic parameters for iron (III) oxide

Author	Catalyst	A	E_a
Giaconia *et al.* (2011)	Fe_2O_3 pellet fragments	2.3×10^8 – $3.0 \times 10^8\ hr^{-1}$	$163 - 166\ kJ/mol$
	Fe_2O_3-coated honey-comb fragments	1.3×10^{11} – $3.1 \times 10^{11}\ hr^{-1}$	$223 - 225\ kJ/mol$
Karasawa *et al.* (2006)	Hematite (mineral form of Fe_2O_3)	$4.7 \times 10^{18}\ hr^{-1}$	$302\ kJ/mol$
Kondamudi & Upadhyayula (2012)	Fe_2O_3 on Al_2O_3	Not reported	$139\ kJ/mol$
	Fe_2O_3 pellets	Not reported	$165\ kJ/mol$
	Fe_2O_3-coated honey-comb fragments	Not reported	$223\ kJ/mol$
Kim *et al.* (2013)	Fe_2O_3 pellets	Not reported	$141\ kJ/mol$

Manufacturing of Fe_2O_3 pellets entailed simply the mixing of Fe_2O_3 powder with Poly-vinyl-alcohol (PVA) binder after which the pellets are shaped in a uniaxial hydraulic press, fired at 900°C, crushed and screened to obtain the desired particle size ranges.

Kondamudi & Upadhyayula (2012) indicates that high activation energies, as reported in Table 2, are an indication that the experiments are conducted in a kinetic controlled regime.

The approach taken in this study to obtain the intrinsic reaction kinetic is similar to that proposed by Spewock *et al.* (1976), Karasawa *et al.* (2006), Giaconia *et al.* (2011),

Kondamudi & Upadhyayula (2012) and Kim *et al.* (2013). The equation that links the reaction rate constant k with the calculated conversion X is given by Equation 9. The linearized Arrhenius equation (Equation 11) relates the calculated k-values with the reaction zone temperature T_r, and a plot of $\ln(k)$ versus $1/T_r$ will yield a straight line from where the activation energy E_a and the Arrhenius frequency factor A are calculated using the slope and offset.

2.2.3 The power rate law applied to the kinetics modelling

The kinetic expression that algebraically relates the rate of a reaction to the concentration of the different species involved in the reaction is termed the rate law (Fogler, 1986:60). For a reaction, the rate law can be expressed by the following equation:

$$-r_a = k(T).f(C_i)\,, \quad f(C_i) = C_a^{\alpha}.C_b^{\beta}.C_c^{\gamma} \ldots \qquad [13]$$

In this equation, the function of the concentrations $f(C_i)$ can be a rate law, based on the order of the reaction $(\alpha, \beta, \gamma, \ldots)$. Under the assumption that the reversible reaction can be neglected as discussed in Section 2.2.1, the rate law for the decomposition of sulphur trioxide can be simplified to the following:

$$-r_{SO_3} = k(T).C_{SO_3}^{\alpha} \qquad [14]$$

Under another assumption of the reaction being first order with respect to sulphur trioxide, as assumed by all the various authors, and since the reaction is a decomposition reaction, the rate law can, again, be simplified to Equation 15.

$$-r_{SO_3} = k(T).C_{SO_3} \qquad [15]$$

Another approach to the reaction rate was investigated by Petropavlovskii *et al.* (1989) who developed a kinetic model for a Pd-Al type catalyst. This model is similar to the Langmuir-Hinshelwood type kinetics, takes the reverse reaction into account and is presented in Equation 16.

$$-r_{SO_3} = \frac{\left[kK_{SO_3}P_{SO_3}\left(1-P_{SO_3}P_{O_2}^{0.5}\right)/K_{SO_3}P_{SO_3}\right]}{\left(1+K_{SO_3}P_{SO_3}+K_{SO_2}P_{SO_2}+K_{O_2}^{0.5}P_{O_2}^{0.5}+K_{H_2O}P_{H_2O}\right)^2} \qquad [16]$$

Petropavlovskii *et al.* (1989) evaluated this pressure dependent kinetic model over a temperature range by obtaining the required pressure equilibrium constants (K-values).

2.2.4 Diffusion-limited and reaction-limited criterion

When investigating the variation of reaction rate with catalyst particle size and velocity of reactant passing the catalyst particle, Fogler (1986:532) describes a general relationship as depicted in Figure 12.

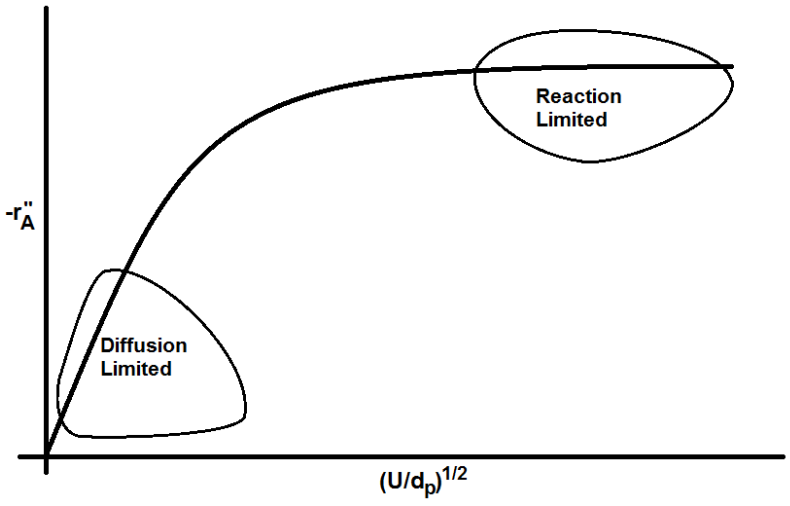

Figure 12 - Mass-transfer-limited and reaction-limited regions (Adapted from Fogler, 1986:532)

At low linear velocities of reactant passing the catalyst particles, it is observed that a relative thick boundary layer dictates that the reaction is diffusion (or mass transfer) limited. This scenario can change and the reaction can become reaction limited with a high-enough linear velocity. Similarly can relatively small particles dictate a reaction-limited reaction for given velocities compared to larger particles, but this can have a larger pressure drop over the catalyst bed as consequence. Fogler (1986:531) states that sufficiently high velocities or small particle sizes are used for obtaining laboratory-scale reaction rate data.

It is important, according to Kondamudi & Upadhyayula (2012), to determine whether mass-transfer limitations can be neglected in studying the decomposition of sulphur trioxide. In this regard, Mears proposed a measure to determine whether mass transfer (or diffusion) effects can be neglected (Fogler, 1986:579). The Mears criterion makes use of a relationship between the measured rate of reaction, the catalyst bulk density and particle radius, the reaction order and a mass transfer coefficient as shown in Equation 17. Mears suggested that by satisfying Equation 17, mass-transfer effects can be neglected.

$$\frac{-r_a \rho_b R_p \alpha}{k_m} < 0.15 \qquad [17]$$

The evaluation of this equation requires the determination of the mass transfer coefficient from modified Reynolds and Chilton-Colburn analogies (Incropera & DeWitt, 2002:981, Perry & Green, 1997:5-48 – 5-49), and is presented in detail in Appendix C. The result from the evaluation is discussed in Chapter 3 in Section 3.4.

3. Experimental Procedures

Chapter 3 is subdivided into three sections. Section 3.1 elaborates on the experimental setup with detailed descriptions of materials used, experimental equipment and treatment of material streams. It concludes with a description of the molar flow calculations over the system for different experimental scenarios. Section 3.2 discusses the experimental programme that was followed and emphasises experimental procedures followed during execution of experimental runs. Section 3.3 contains a discussion of the calculations used to obtain kinetics as well as a section on obtaining the average catalyst particle size. Section 3.4 concludes this chapter with a discussion of the effects of mass-transfer- and diffusion effects and the potential influence it has on studying this catalyst.

3.1 Experimental setup

3.1.1 Materials used in experimental runs

Table 3 summarises the materials that were used during experimental runs together with the respective supplier of each.

Table 3 - Materials used in experimental runs

Material	Remarks	Supplier
H_2SO_4	98% Purity	ACE Chemicals
N_2	99.999% Purity, Process gas	Afrox Industrial Gases Division
Air	99.9% Purity, Process gas	Afrox Industrial Gases Division
$1\%\ SO_2$	$1.0\%\ SO_2, 0.5\%\ O_2$ Balance N_2 Calibration gas	Afrox Speciality Gases Division
$10\%\ SO_2$	$10.0\%\ SO_2, 5.0\%\ O_2$ Balance N_2 Calibration and process gas	Afrox Speciality Gases Division
Fe_2O_3	99.99% Purity	Sigma-Aldrich
Soluble Starch $(C_6H_{10}O_5)_n$	Titration indicator 99.94% Purity	ACE – Associated Chemical Enterprises
$NaOH$	Titrant and scrubber solution 99.96% Purity	Saarchem
$Na_2S_2O_3$	99.90% Purity	ACE – Associated Chemical Enterprises
I_2 – resublimed	99.5% Purity	Rochelle Chemicals

The iron (III) oxide that was used as catalyst was obtained from Sigma-Aldrich as an off-the-shelf material with 99.99% purity. This catalyst material was chosen as no additional preparation measures were required. The solid catalyst particles are in powder form with an

average particle size, as determined with a SEM, of 40(±14) µm, as detailed in Section 3.3.4.

3.1.2 Process flow diagram

A reactor set-up, designed, constructed and commissioned at the laboratories of the School of Chemical and Minerals Engineering at the North-West University for the investigation of the decomposition of sulphur trioxide, was used. The complete setup is shown in Figure 13 and includes the feed system (denoted by the letter A), a quartz bayonet reactor submerged inside the furnace (denoted by the letter B), a Liebig cooler (C), some traps, driers and scrubbers (D) and finally the on-line gas analysers (E).

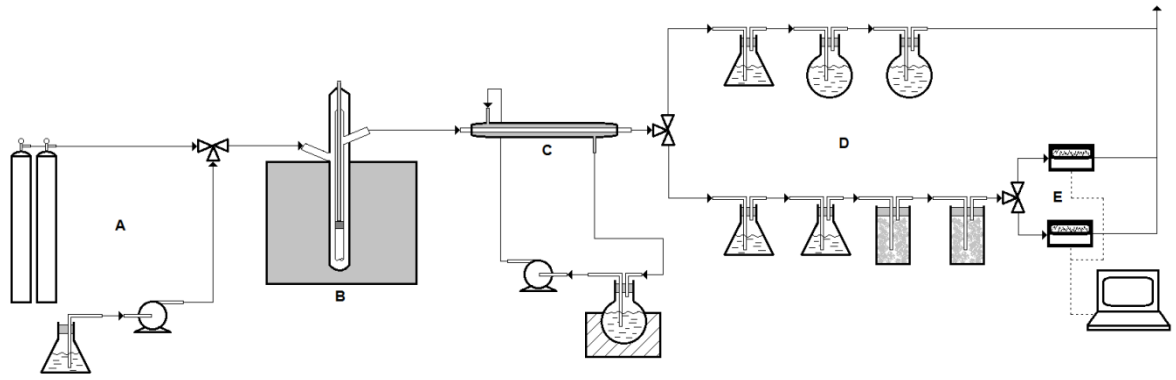

Figure 13 - Complete experimental setup

3.1.3 Feed system

The system feeding the reactor consists of the gas cylinders containing the carrier nitrogen gas as well as additional gases used during the investigation, a sulphuric acid reservoir and a peristaltic pump. This system is depicted in Figure 14 and indicates the position of the pre-calibrated Brooks Instruments, model 0254 4-port mass flow controller.

The sulphuric acid was pumped into the reactor inlet, where it was joined with the gas stream from the mass flow controller, by a Watson Marlow model 120u peristaltic pump. This pump was calibrated and the calibration curve is supplied in Appendix D.

3.1.4 Bayonet reactor

Figure 15 shows a schematic representation of the bayonet reactor used for the decomposition experiments. The reaction zone of the reactor (lower section) is completely submerged in the furnace (A), which was supplied by Hi-Tech elements. The sulphuric acid together with the additional carrier gas stream is fed into the reactor at point D.

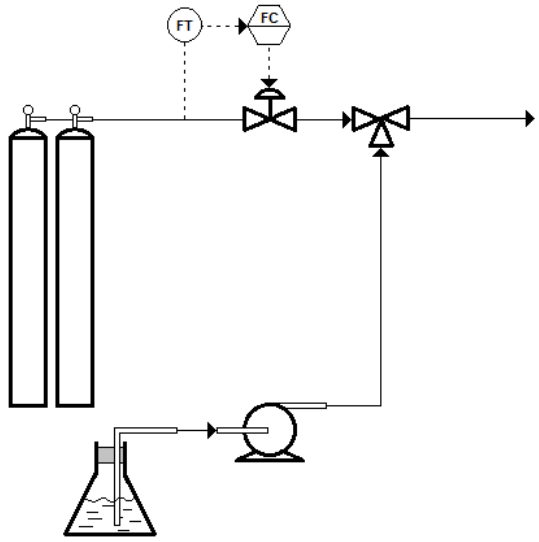

Figure 14 - Feed system schematic representation

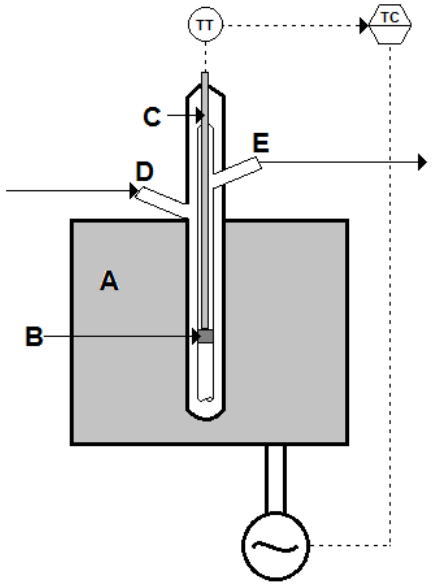

Figure 15 - Schematic representation of the bayonet reactor

The downwards path allows the sulphuric acid to decompose into sulphur trioxide and water according to Equation 1. It is assumed that all sulphuric acid is completely decomposed in this section as the temperature is maintained at a value in excess of 700°C (Giaconia *et al.*, 2011).

Point B indicates the catalytic reaction zone wherein the iron (III) oxide catalyst is maintained in place between two loosely packed plugs of quartz wool which serve as fixation of the catalyst bed. Some of the sulphur trioxide is catalytically decomposed to sulphur dioxide and oxygen in this zone according to Equation 2.

A quartz sleeve (C) is inserted inside the reactor tube and touches the quartz wool at the catalytic zone (B) at the bottom end of the sleeve. The purpose of this sleeve is to host a thermocouple that continuously measures the temperature in the reaction zone. A controller is set up using the temperature signal from this thermocouple to accurately maintain the reaction zone temperature at the desired value. A PID controller is used to avoid oscillatory temperature behaviour in the reaction zone, and the temperature was controlled within 1°C of the set point.

The decomposed gases then flow upward through the reaction tube around the sleeve (C) and exit the reactor at point E.

3.1.5 Cooling system, acid and moisture traps

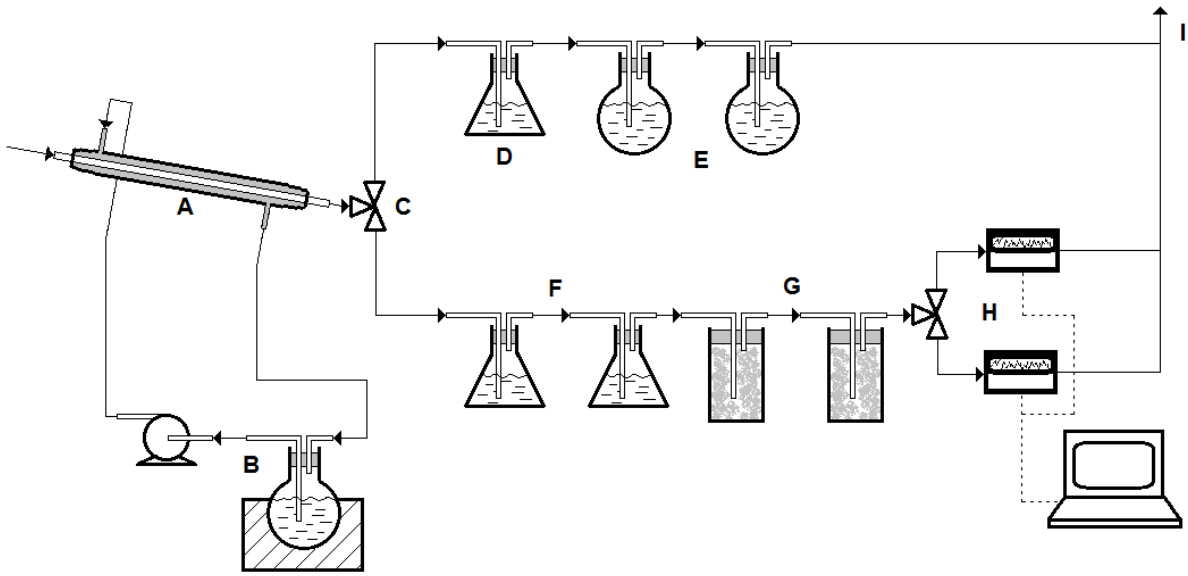

Figure 16 - Balance of plant equipment

The rest of the equipment used in the laboratory scale setup is depicted in Figure 16. The hot gas exiting the reactor enters a Liebig cooler (A) wherein the gas is cooled using water from an ice bath (B). The Liebig cooler is positioned at an angle to facilitate gravitation of formed liquid into the liquid traps. The cooling serves to recombine any unreacted sulphur trioxide with the water in the product gas stream and to condense this again as sulphuric acid in subsequent liquid traps.

The cooled gas stream is split at the junction (C) and a quantity of the gas passes through a water trap (D) wherein any liquid (condensed sulphuric acid and excess water) is collected. Two scrubbers at E containing caustic soda solutions are used to remove sulphur dioxide from the gas stream and the remaining gas is thereafter vented to the atmosphere (I).

From the splitter (C), another stream of the product gas passes through two liquid traps (F) wherein liquid (condensed sulphuric acid and excess water) is collected. Two subsequent

moisture traps (G) are used to remove residual moisture from the gas stream to avoid damage to the analysers (H).

The analysers (H) are discussed in detail in Section 3.1.6.

All junctions in the laboratory scale setup were sealed with polytetrafluoroethylene (PTFE) tape to ensure no leaks. This PTFE tape is inert to the severe corrosiveness of the reactants and products. All junctions were frequently inspected for leaks using soap water. The junctions around the reactor were sealed with graphite powder and high-temperature resistant copper compound paste.

3.1.6 Handling and analyses of product gas

The liquid traps at points D and F in Figure 16 consist of conical flasks placed inside a container that is filled with ice. This cools the passing gas and vapours, enhancing further condensation, and maintaining condensed liquid in the liquid state. Liquid that formed in the Liebig cooler (point A in Figure 16) gravitates into the liquid traps as the Liebig cooler is slightly elevated relative to these traps.

Prior to the analysers are two driers, which consist of conical flasks packed with porcelain marbles. The additional cooled surfaces assist in removing any moisture from the gas through condensation, thus protecting the analyses equipment from exposure to moisture and acid.

The scrubbers at point E in Figure 16 consist of large 5 litre flasks that were partially filled with sodium hydroxide solution. With the sulphuric acid removed from the product gas, the remaining sulphur dioxide is removed from the passing gas for safety and environmental reasons. In the scrubbers, the sulphur dioxide reacts with the sodium hydroxide to form sodium sulphite, according to the following reaction:

$$2NaOH + SO_2 \rightarrow Na_2SO_3 + H_2O \quad [18]$$

The analysers at point H in Figure 16 comprise of a Teledyne Analytical Instruments model 7500 E infrared sulphur dioxide analyser and a Teledyne Analytical Instruments model 3300 MA paramagnetic oxygen analyser. Both analysers are connected to a computer where software is used for the logging of gas analyses data. The sulphur dioxide analyser has a sensitivity range on one channel of 0 – 1% and on another channel of 0 – 10%. Pre-prepared calibration gases, as specified in Table 3, were obtained in order to calibrate this analyser prior to each experimental run. The oxygen analyser had a range of 0 – 25%, rendering the sensitivity of this analyser improper for the analyses of the product gas. General trends could, however, be observed in the oxygen data, but exact values were of little use.

To compensate for the dissolution of sulphur dioxide in the traps, both a titration of the liquid in the traps as well as a solubility test wherein the traps were changed from ambient temperature to an ice environment were conducted. The titration test entailed the reaction of sulphur dioxide with sodium hydroxide to form sodium sulphite according to Equation 18.

This was followed by a titration with an excess amount of iodine. The iodine reacts with the sodium sulphite according to the following equation:

$$Na_2SO_3 + I_2 + H_2O \rightarrow Na_2SO_4 + 2HI \quad [19]$$

Using a solution with known concentration of sodium thiosulphate, a back-titration will reveal the amount of sulphur dioxide dissolved in the traps. The back-titration reaction is shown in Equation 20.

$$2Na_2S_2O_3 + I_2 \rightarrow 2NaI + Na_2S_4O_6 \quad [20]$$

Based on the procedure discussed, a 10ml sample of the liquid in the liquid traps was taken and treated with a standard solution of 1.000 mole/litre sodium hydroxide solution. This sample was then titrated with iodine in the presence of starch as indicator, which turns from dark blue to colourless once all the sodium sulphite is converted. Correction calculations and titration results are shown in Appendix E.

3.2 Experimental phase

3.2.1 Experimental programme

The experimental programme followed is summarised in Table 4.

Table 4 - Experimental programme

Tempe-rature	H_2SO_4 & air in feed	H_2SO_4 & additional H_2O in feed			H_2SO_4 & additional SO_2 in feed
		Molar ratio 1:1 (base case)	Molar ratio 1:2	Molar ratio 1:3	$4.9\%\ SO_2$ $2.4\%\ O_2$ $balance\ N_2$
700°C	1 run	3 runs	2 runs	1 run	1 run
725°C		3 runs			
750°C	2 runs	3 runs	2 runs	1 run	2 runs
775°C		4 runs			
800°C		2 runs			
825°C	1 run	2 runs	1 run	1 run	1 run

In the third column, the base case refers to the specific conditions used for all temperature variation experiments.

The three base case runs conducted at a temperature mid-point of 750°C were used to determine the experimental error expected in the experiments and the calculation of the experimental error together with the experimental data obtained are shown in Section 3.3.2.

In the second- and also fourth- to the sixth columns of Table 4 the feed compositions to the reactor were varied to qualitatively assess the influence of product gases and the variation of reagent concentration on the reaction kinetics. The feed was varied as follow:

- **Column 2:** air was used instead of pure nitrogen to assess the influence of oxygen on the reaction kinetics.
- **Columns 4 - 5:** the sulphuric acid was further diluted with water to assess the influence of water on the reaction kinetics. Water was added in three quantities so that the molar ratios of sulphur trioxide to water equal 1:1 (base case), 1:2 and 1:3. With the water addition, the sulphur trioxide concentration in the feed was reduced.
- **Column 6:** sulphur dioxide was added to the feed by replacing the pure nitrogen as carrier gas a mixture of 50:50 pure N_2 and a mixture of $10\%_{(volume)}$ SO_2, $5\%_{(volume)}$ O_2 and $85\%_{(volume)}$ N_2.

3.2.2 Experimental procedure

The catalytic zone of the reactor (section B, Figure 15) was loaded each time with exactly 80.00mg of iron (III) oxide catalyst powder. The catalyst was suspended between two loosely packed quartz wool plugs to form a packed bed. The reactor was subsequently positioned with the whole reaction section submerged inside the oven. All junctions were sealed properly as discussed in Section 3.1.4. The carrier gas (normally N_2, but also air and SO_2 gas mixture – refer to Table 4) flow was started at a pre-determined set point and the furnace was switched on to warm up.

During furnace heating the analysers were switched on, calibrated and the computer logging software were started and kept in stand-by mode.

Once the desired temperature inside the reaction zone was reached, the acid pump was started at the desired revolutions per minute to feed the exact desired amount of acid. The experimental setup was then allowed to reach steady state conditions (approximately 2 – 3 hours) after which the data logging was started on the computer. All experimental runs were conducted over a twelve hours period.

The procedure outlined above was repeated for the temperature range of 700°C up to 825°C with 25°C increments for the 98% sulphuric acid and nitrogen feed scenario (base case).

3.2.3 Variation of temperature and feed composition

Additional experimental runs, similar to the procedure outlined in Section 3.2.2, were conducted with diluted sulphuric acid, air instead of nitrogen and a sulphur dioxide gas mixture instead of pure nitrogen (refer to Table 4) in the reactor feed to assess the influence of the reaction products (H_2O, O_2 and SO_2) as part of the reactor feed on the reaction. These additional experiments were repeated at temperatures 700°C, 750°C and 825°C, as summarised in Table 4.

The calculations to obtain a 2:1 molar ratio of H_2O:SO_3 in the feed as well as a 3:1 ratio is shown with the different feed scenario mole balances in Appendix F. The feed rate for the liquid feed to the reactor was determined from the pump calibration data as discussed in Appendix D.

3.3 Molar flow rates and various calculations

3.3.1 Molar flow rates

Based on a simplified flow diagram of the experimental setup, as shown in Figure 17, molar flow rates at each indicated point (points A through E) were calculated to facilitate the rest of the calculations shown in Section 3.3.2.

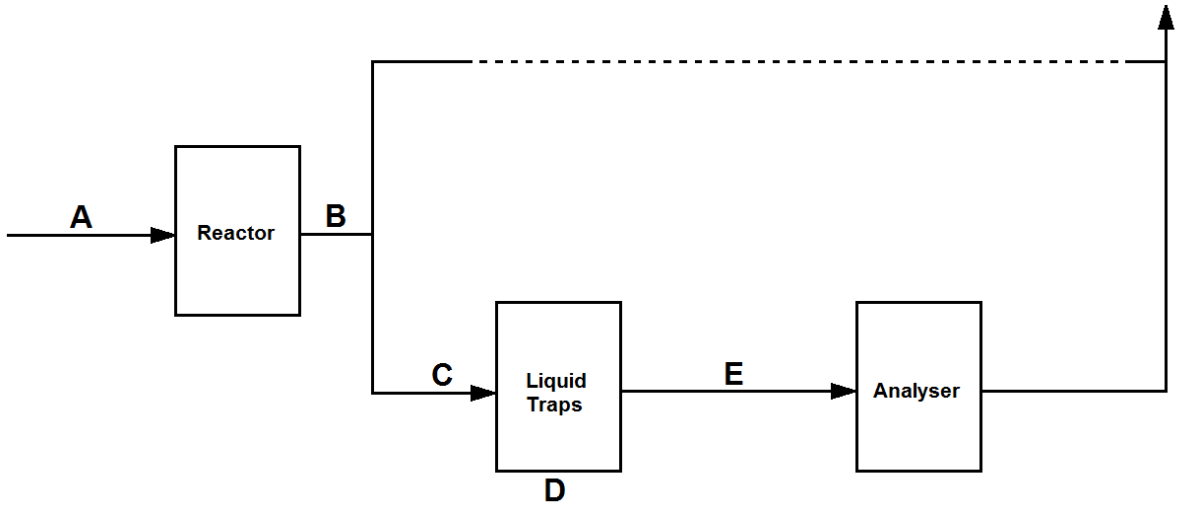

Figure 17 - Simplified flow diagram of the experimental setup

These molar flow calculations were conducted using the following steps:

- Specifying the exact feed rates of the different components in the feed scenario based on the pre-calibrated mass flow controller and acid feed pump set points,
- Subsequent calculation of the sulphur dioxide and oxygen that formed in the reactor based on the measured and corrected SO_2 value (refer to Appendix E),
- Calculation of the split of the reactor product stream (refer to point C in Figure 16) based on the gas flow requirement by the analysers and the assumption that all H_2O and SO_3 in the reactor product condensate as H_2SO_4 (aq) in the liquid traps,
- Calculation of liquid H_2SO_4 as well as dissolved SO_2 in the liquid traps (refer to point F in Figure 16) based on titration results and the assumption that all H_2O and SO_3 are removed from the gaseous reactor product as aqueous H_2SO_4 (aq).

The detailed molar flow rate calculation formulae as well as examples based on the different feed scenarios are presented in Appendix F. The flow rates were recalculated for each scenario, including the base case scenario (only N_2 and H_2SO_4 in the feed), the air-fed instead of N_2 scenario, additional water in the feed scenario as well as additional SO_2 in the reactor feed scenario.

The flow rate of the product gas was measured and correlated with the feed flows to ensure that the flow rate readings on the analysers' flow rate indicators were correct. The amount of dissolved sulphur dioxide in the liquid traps, as determined from the titration of the liquid according to Section 3.1.6, was used to correct the analyser measurements.

3.3.2 Calculating conversions, reaction rates & reaction rate constants

The calculation of the molar flow rates (refer to Section 3.3.1 & Appendix F) required the calculation of the extent of the reaction for each scenario, based on the corrected sulphur dioxide measurement $Y^*_{SO_2}$ (refer to Appendix E). The formula derived for both the base-case- and additional water in the feed scenarios is given by Equation 21.

$$\dot{\xi} = \frac{\dot{n}^o_{N_2} Y^*_{SO_2}}{\left(1 - \frac{3}{2} Y^*_{SO_2}\right)} \quad [21]$$

For the air-fed case, the extent of the reaction is determined by Equation 22 and for the additional SO_2 in the feed scenario Equation 23 shows the derived formula.

$$\dot{\xi} = \frac{\left(\dot{n}^o_{N_2} + \dot{n}^o_{O_2}\right) Y^*_{SO_2}}{\left(1 - \frac{3}{2} Y^*_{SO_2}\right)} \quad [22]$$

$$\dot{\xi} = \frac{\left(\dot{n}^o_{N_2} + \dot{n}^o_{SO_2} + \dot{n}^o_{O_2}\right) Y^*_{SO_2} - \dot{n}^o_{SO_2}}{\left(1 - \frac{3}{2} Y^*_{SO_2}\right)} \quad [23]$$

These formulae are derived in Appendix F.

With the extent of the reaction known for each condition, the conversion could be obtained using Equation 24.

$$X = \frac{\dot{\xi}}{\dot{n}^o_{SO_3}} \quad [24]$$

The rate of the reaction at each condition (for each of the feed scenarios) was calculated using Equation 25.

$$r_{SO_3} = \frac{\dot{\xi}}{m_{cat}} \quad [25]$$

Using the average value of the conversions obtained at each temperature studied, the reaction rate constant k, discussed in Section 2.2.2 and shown by Equation 10, can be obtained for each temperature and feed scenario, as shown in Equation 26.

$$k = -\ln(1 - X) \cdot \left(\frac{v^o}{m_{cat}}\right) \quad [26]$$

Equation 26 is derived in Appendix A, Section A.4.

3.3.3 Experimental error calculation

The experimental error was obtained from the three data sets of the base case at 750°C, as represented by the green data points in Figure 36. The calculation is based on the T-test method with a confidence interval of 95%. The results of the calculation are shown in Table 5 and explained by the subsequent equations.

Table 5 - Determination of experimental error

Calculated conversion at T_r = 750°C		Experimental error analysis	
Experimental run 1	9.187%	Avg	8.477
Experimental run 2	8.394%	Std	0.672
Experimental run 3	7.850%	N	3.0
		Critical t-value	4.303
		ϵ	1.670
		ϵ (%)	19.696

After obtaining the average (Avg), standard deviation (Std) and the number of observations (N) of the experimental values, the critical value of t was obtained from Berenson & Levine (1989:831) that corresponds with the degrees of freedom (N – 1) and the confidence interval selected.

The error is then calculated with the following equation:

$$\epsilon = \frac{t.Std}{\sqrt{N}} \quad [27]$$

And the error percentage is calculated as:

$$\epsilon(\%) = \frac{\epsilon}{Avg} \times 100\% \quad [28]$$

From the table it is seen that an experimental error of 20% is determined.

Raw data for all the experimental runs are shown in Appendix G.

3.3.4 Catalyst particle size determination

A scanning electron microscope (SEM) was used to determine the average particle size of the iron (III) oxide catalyst particles. Figure 18 shows a selection of the catalyst particles as viewed by the microscope, with size measurements indicated on them. An average particle size of 40(±14) µm is found from several similar measurements, which indicates that the catalyst is of a fine nature.

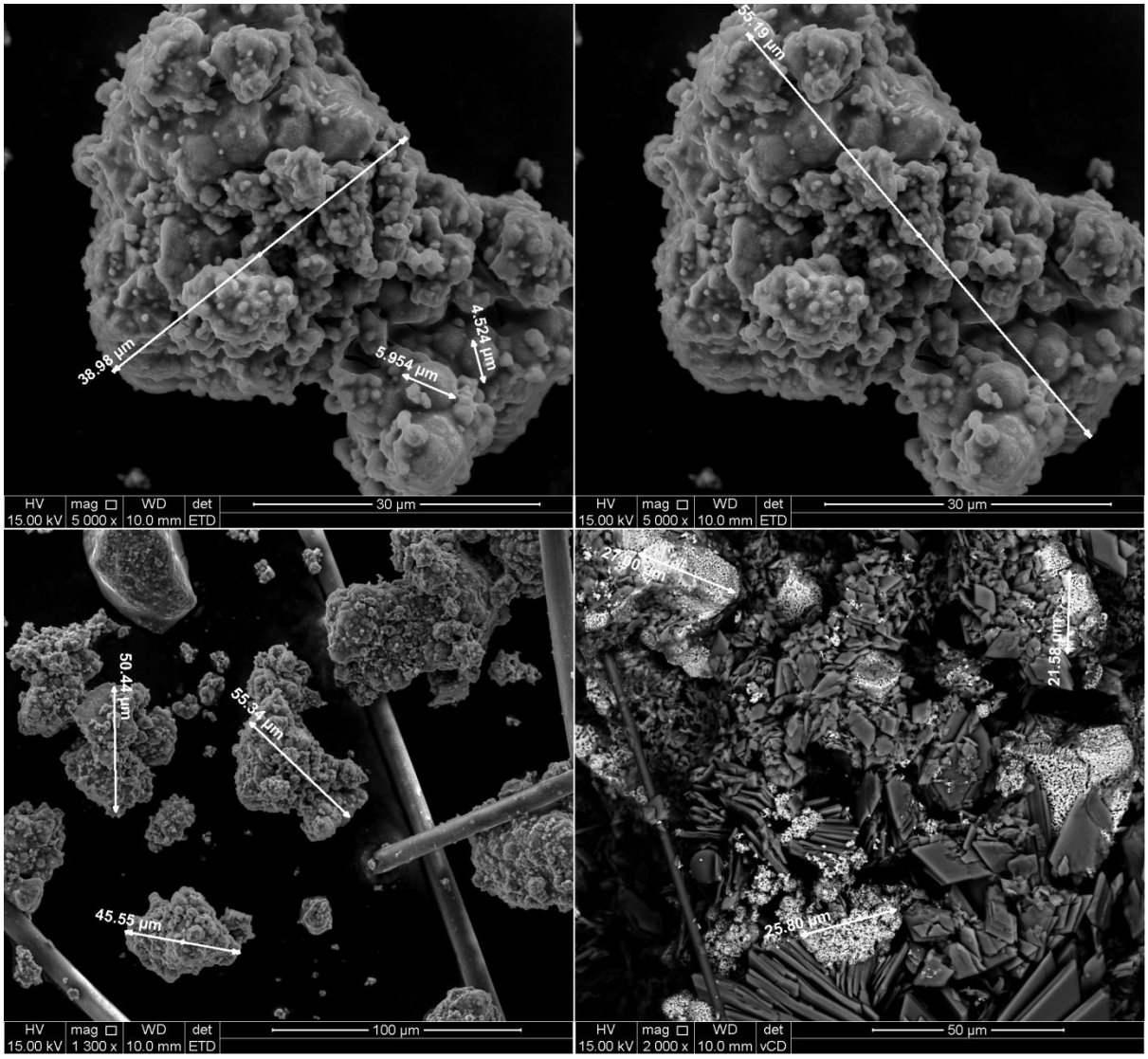

Figure 18 - SEM photographs of the iron (III) oxide catalyst particles

3.4 Reaction-limited region

The Mears criterion was used to assess whether mass transfer effects play an important role in the experiments performed in this study, or whether these effects can be neglected. The Mears criterion is discussed in detail in Section 2.2.4 and the evaluation of the Mears criterion is detailed in Appendix C.

From the result obtained in the evaluation of the Mears criterion, which yielded a value of 3.4×10^{-6} for these experiments – a value substantially lower than 0.15 according to the Mears criteria (Equation 17) – it can be concluded that any mass transfer effects can be neglected for the experiments performed during the course of this study. It is also found that variations in flow rate have not significant effect on the performance of the catalyst as studied, which support the absence of external mass transfer limitations.

4. Results and discussion

In this chapter, Section 4.1 covers the reaction kinetics based on different temperatures for the base case wherein the only feed to the reactor is pure nitrogen and sulphuric acid. Section 4.2 subsequently compares the results obtained for the base case with published results from various authors. Section 4.3 includes different reactor feed scenarios wherein experiments were conducted with additional oxygen, additional water and additional sulphur dioxide respectively added to the reactor feed to qualitatively substantiate the influence of reactants and products on the reaction rate.

4.1 Influence of temperature on conversion

Experiments with nitrogen and sulphuric acid only as reactor feed, referred to as the base-case experiments, were conducted in the temperature range from 700°C to 825°C in 25°C steps. Between 2 and 3 repetitions were conducted at each temperature. The average conversions obtained at these temperatures are shown in Figure 19. From this figure, it can be seen that the conversion of sulphur trioxide, which is defined by Equations 21 & 24, increases with temperature.

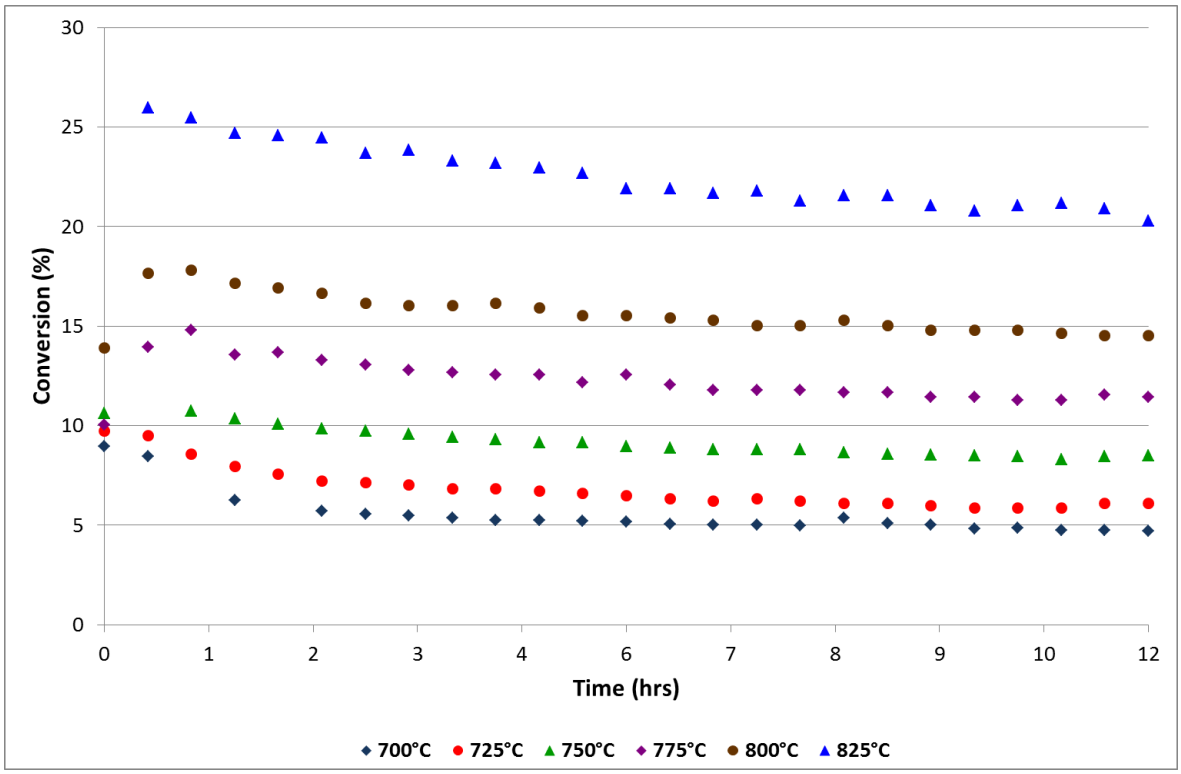

Figure 19 - Sulphur trioxide conversion at different temperatures

The trends in Figure 19 show that initial conversions are high compared to later conversions, but that steady state, wherein conversions tend to stabilise at a specific value, is mostly obtained after 4 to 7 hours' time-on-stream, as can be seen for the 700°C – 800°C reaction temperature data. At 12 hours' time-on-stream, steady state is reached for all conditions within the experimental error.

The steady state conversion data points obtained for each temperature at 12 hours of time-on-stream are plotted against the reaction temperature, and given in Figure 20, confirming the increasing conversion as the reaction temperature increases.

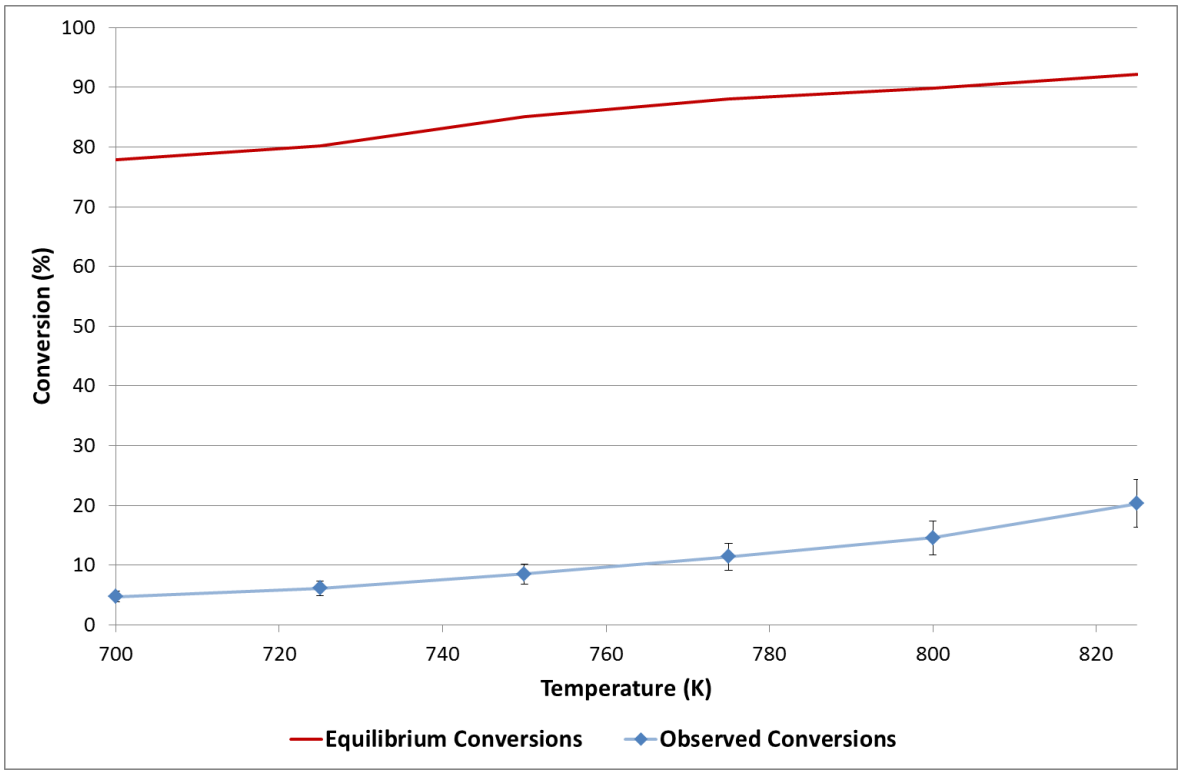

Figure 20 - SO_3 conversion and equilibrium conversion as a function of temperature

To assess whether the experimental data can be modelled as an irreversible reaction, as discussed in Section 2.2.1, the obtained conversions are compared with equilibrium conversions. This comparison is shown in Figure 20 wherein it is found that the conversions obtained in this experimental program is at most 25% of the theoretical equilibrium conversions at these reaction temperatures. Based on this observation it can be concluded that the equilibrium point for this reaction lies far to the right hand side of the chemical reaction (shown by Equation 2) and the effects of the reversible reaction can be neglected (Fogler, 1986:59).

The reaction rates for the decomposition of sulphur trioxide, as determined from Equation 25 in Section 3.3.2, are shown in Figure 21 for each of the reaction temperatures investigated.

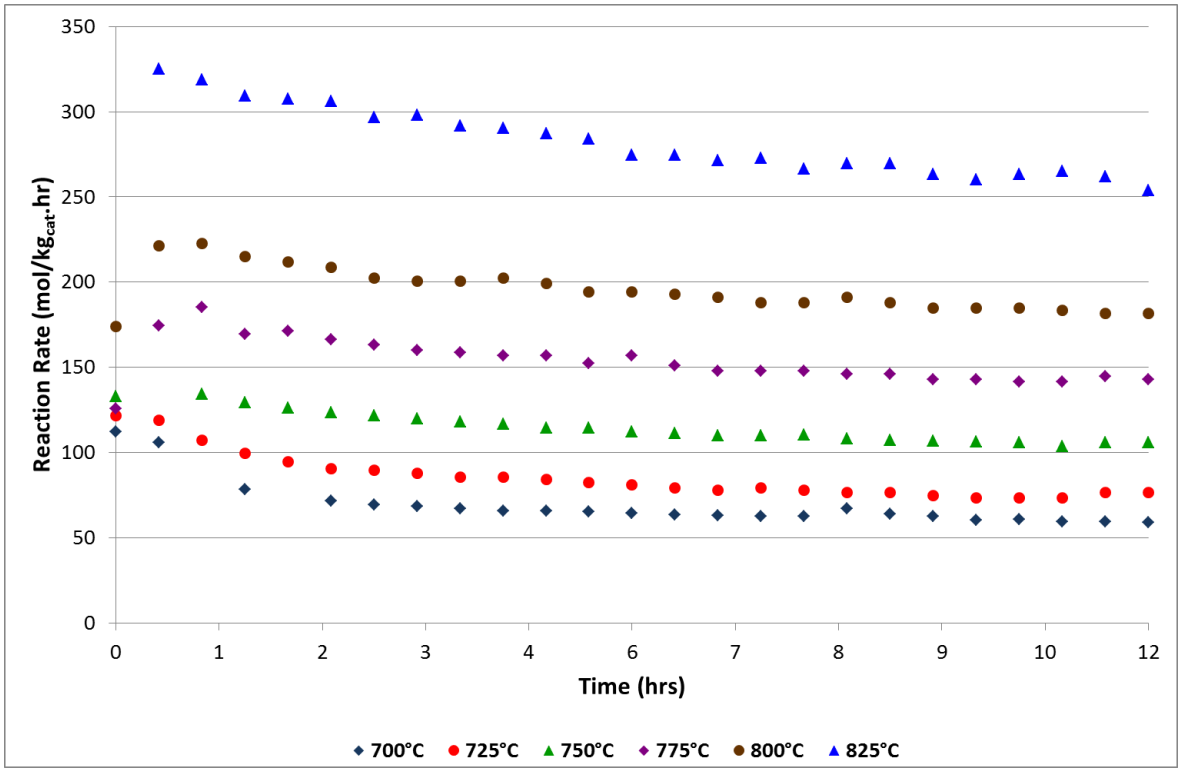

Figure 21 - Reaction rate at various reaction temperatures over duration of experiments

By taking the steady state values of the reaction rates obtained at 12 hours of time-on-stream and by plotting these values against the reaction temperatures, the graph shown in Figure 22 is obtained.

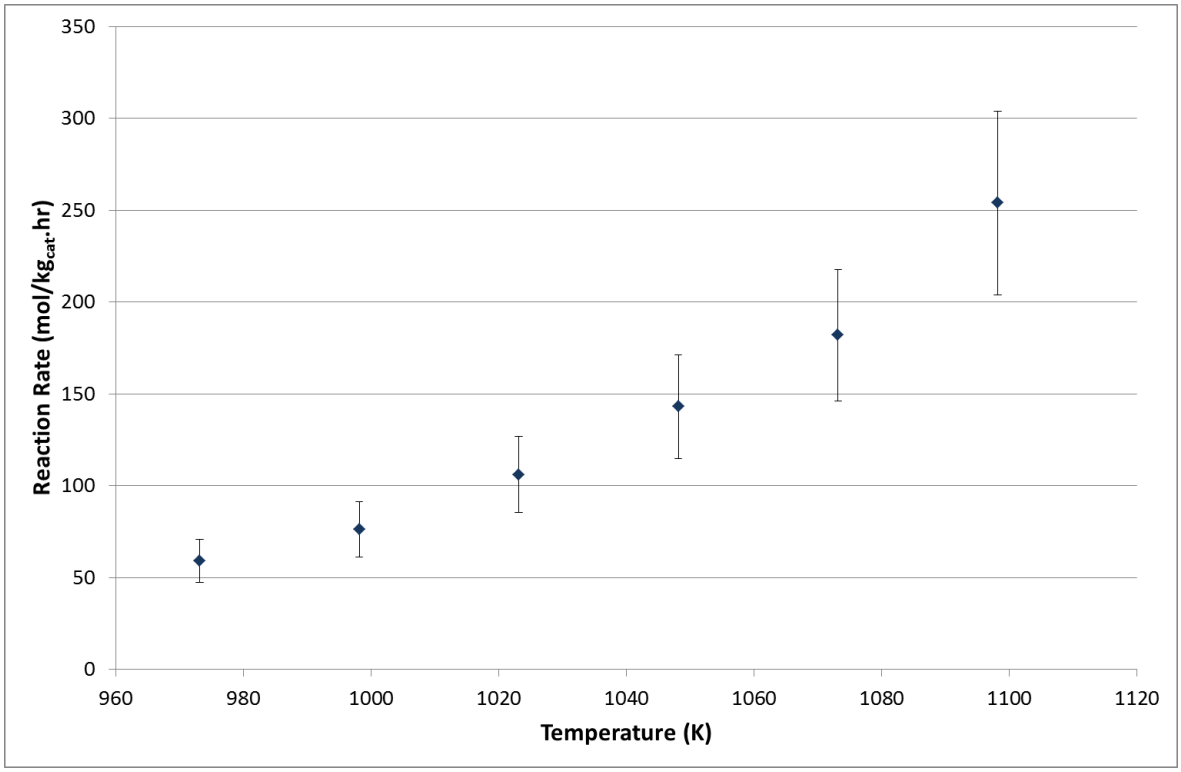

Figure 22 - Reaction rate versus reaction temperature for the base-case scenario

It is seen from both this graph that the reaction rate increases with increasing reaction temperature and follows a similar trend as the conversions, shown in Figure 19 and Figure 20. The increasing reaction rate with increasing reaction temperature was also observed by other authors (Kim *et al.*, 2006, Kondamudi *et al.*, 2012, Giaconia *et al.*, 2011 & Karasawa *et al.*, 2006), mostly for iron (III) oxide supported catalysts, or iron (III) oxide pellets (or fragments of such pellets) as discussed in Section 2.2.2.

With the conversions at the different reaction temperatures known, and under the assumption of a first-order reaction, the reaction rate constants k can be evaluated by using Equation 26 for the different reaction temperatures. Average conversion values at each of the reaction temperatures were used in the calculation. An experimental error of 20% was obtained as described in Section 3.3.3.

Table 6 - Base-case conversions and reaction rate constants

Temperature (K)	Conversion (%)	Reaction rate constant (k) $\left(m^3/kg_{cat}.hr\right)$
973	4.7 (±0.9)	128 (±25)
998	6.1 (±1.2)	172 (±34)
1023	8.5 (±1.7)	248 (±49)
1048	11.4 (±2.2)	347 (±68)
1073	14.5 (±2.9)	460 (±91)
1098	20.3 (±4.0)	680 (±134)

Table 6 summarises the calculated reaction rate constants. These values are used to obtain the Arrhenius frequency factor, A, and the activation energy, E_a, that describe the reaction rate constant k as a function of reaction temperature according to Equation 10. The linearized form of this equation, as given by Equation 11 in Section 2.2.2, is used to fit a straight line through a plot of the natural logarithm of the calculated reaction rate constants versus the reciprocal of the temperature, which allows the determination of the Arrhenius frequency factor A and the activation energy E_a from respectively the offset and slope of the line. This graph of $ln(k)$ versus $1/T$ is shown in Figure 23.

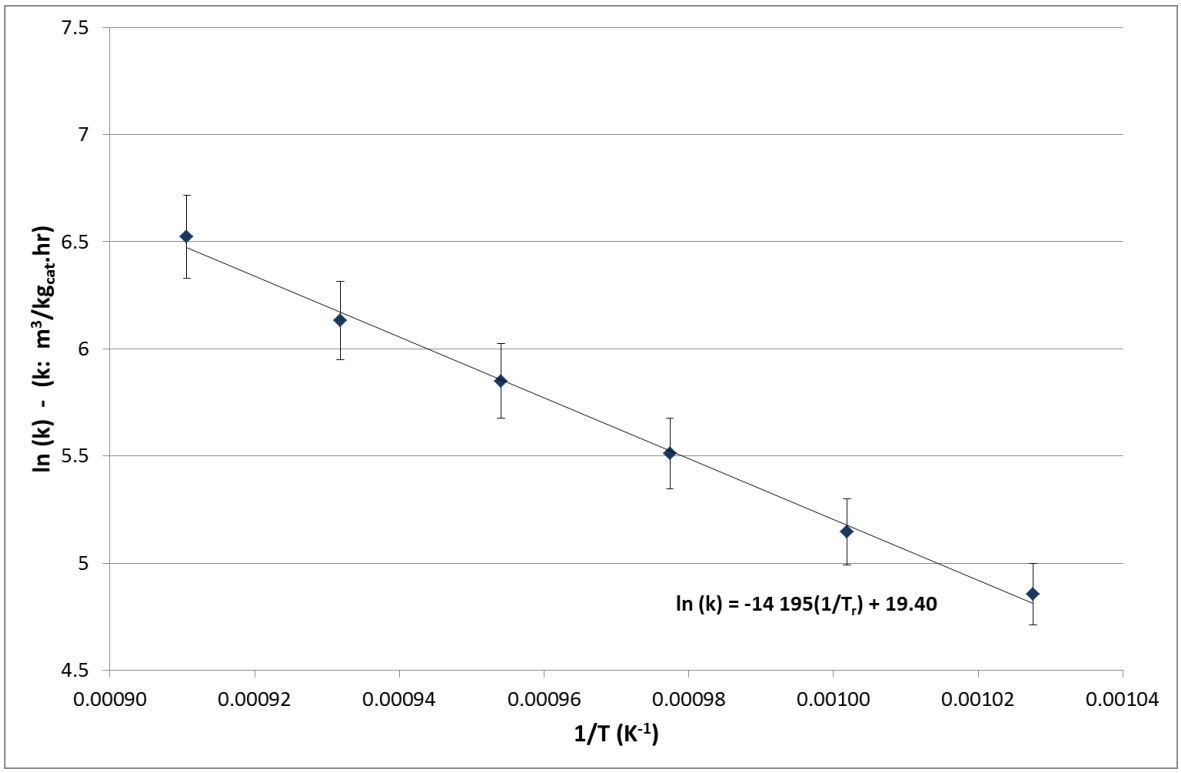

Figure 23 - Natural logarithm of k versus reciprocal of temperature

Figure 23 shows that the data points can be linearized to within the experimental error margins. The equation of the straight line that is obtained is shown in Figure 23. Following Equation 11, the slope of the line equals the term $(-E_a/R)$, while the offset equals the term $ln(A)$. Table 7 summarises the activation energy E_a and the Arrhenius frequency factor A.

Table 7 - Kinetics parameters obtained for the sulphur trioxide decomposition reaction

Activation energy (E_a)	Arrhenius frequency factor (A)
$118\ (\pm 23)\ kJ/mol$	$3 \times 10^8\ hr^{-1}$

Although on the low side compared to values reported on in literature (see Table 2 in Section 2.2.2), the activation energy is comparable to values obtained by Kondamudi & Uphadhyayula (2012) for Fe_2O_3 pellets as well as to values obtained by Kim *et al.* (2013) for Fe_2O_3 pellets. Activation energies of twice this magnitude were published for Fe_2O_3-coated

SiSiC honeycomb fragments by both Giaconia *et al.* (2011) and Kondamudi & Uphadhyayula (2012) while a value three times as high was published for haematite, of which the form is unknown, by Karasawa *et al.* (2006).

Giaconia *et al.* (2011) published similar activation energies (E_a) and Arrhenius frequency factors (A) for Fe_2O_3 pellets compared to the values obtained for pure unsupported iron (III) oxide obtained in this study (Refer to Table 2 & Table 7). It was also found that higher values for both these parameters were reported for Fe_2O_3-coated SiSiC honeycomb fragments by Giaconia *et al.* (2011) and for haematite by Karasawa *et al.* (2006).

4.2 Comparison of base-case results with published results

The results presented in Section 4.1 are subsequently compared with the results obtained by Kim *et al.* (2006), Kondamudi & Uphadhyayula (2012) and Giaconia *et al.* (2011), as sufficient relevant data were published by these authors for comparison purposes.

4.2.1 Comparison with Kim *et al.* (2006)

Kim *et al.* (2006) investigated the decomposition of sulphur trioxide on catalysts with varying iron to substrate ratios ranging from molar ratios (Fe_2O_3:Al_2O_3) of 0.25 to 1.00 and molar ratios (Fe_2O_3:TiO_2) of 0.25 to 1.00. Studies were conducted at reaction temperatures of 775°C, 800°C and 825°C respectively for each of the mentioned catalysts. Published data from Kim *et al.* (2006) were used to obtain reaction rates at different reaction temperatures and the calculations are discussed in Appendix H (Section H1). Figure 24 shows a comparison of the reaction rates obtained in this study with the results obtained by Kim *et al.* (2006). The results obtained by Kim *et al.* (2006) were corrected for the amount of iron (III) oxide in the catalyst.

It is found that reaction rates obtained for pure iron (III) oxide in this study is lower than the values obtained by Kim *et al.* (2006) for different supported iron (III) oxide catalysts, especially at higher reaction temperatures, as is shown by the purple triangles in Figure 24. It has to be mentioned that inlet concentrations of sulphur trioxide was on average between 0.42 and 0.44 mol/m^3 in this study while the data reported by Kim *et al.* (2006) was between 3.7 and 3.9 mol/m^3, indicating that the concentrations used by Kim *et al.* (2006) were in the order of 10 times higher than concentrations used in this study.

By assuming a first order reaction as dictated by Equation 15 in Section 2.2.3, the reaction rate constant k is related to the reaction rate and concentration of sulphur trioxide leaving the reaction zone, and is subsequently evaluated for the case of Kim *et al.* (2006) and the base-case scenario in this study. Figure 25 shows the results obtained.

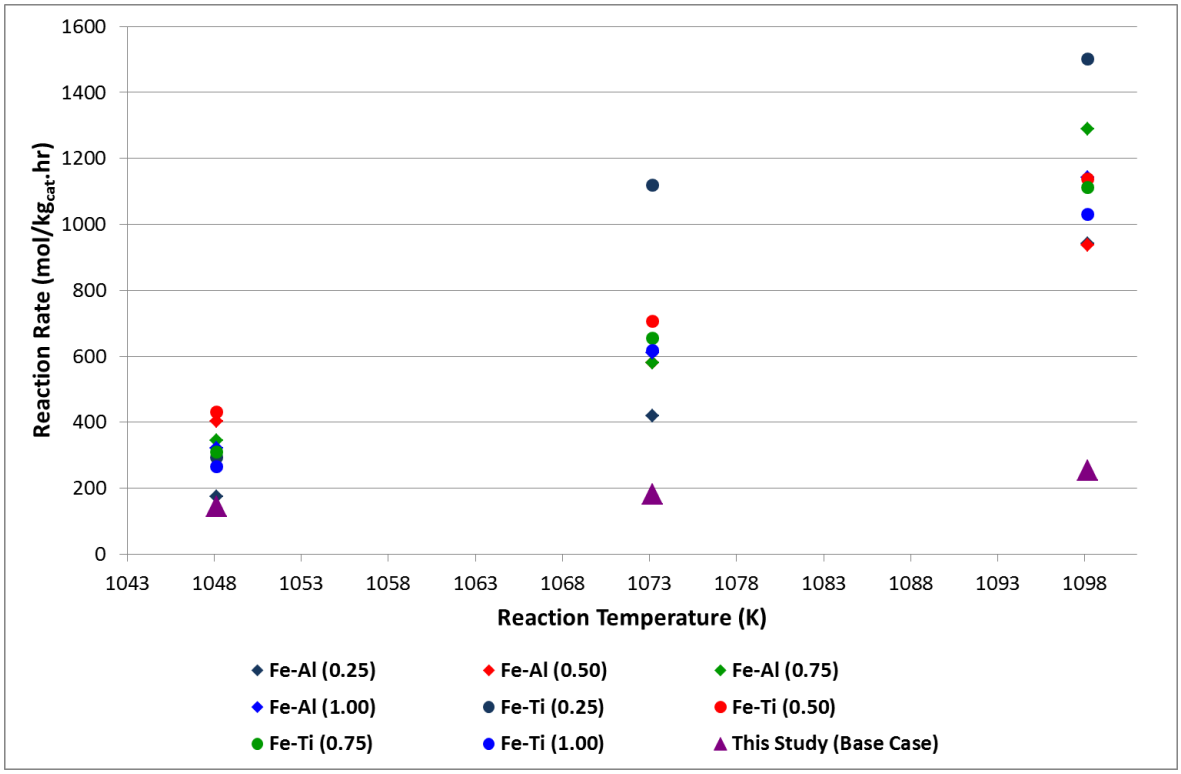

Figure 24 - Comparison of base-case reaction rates with results of Kim *et al.* (2006)

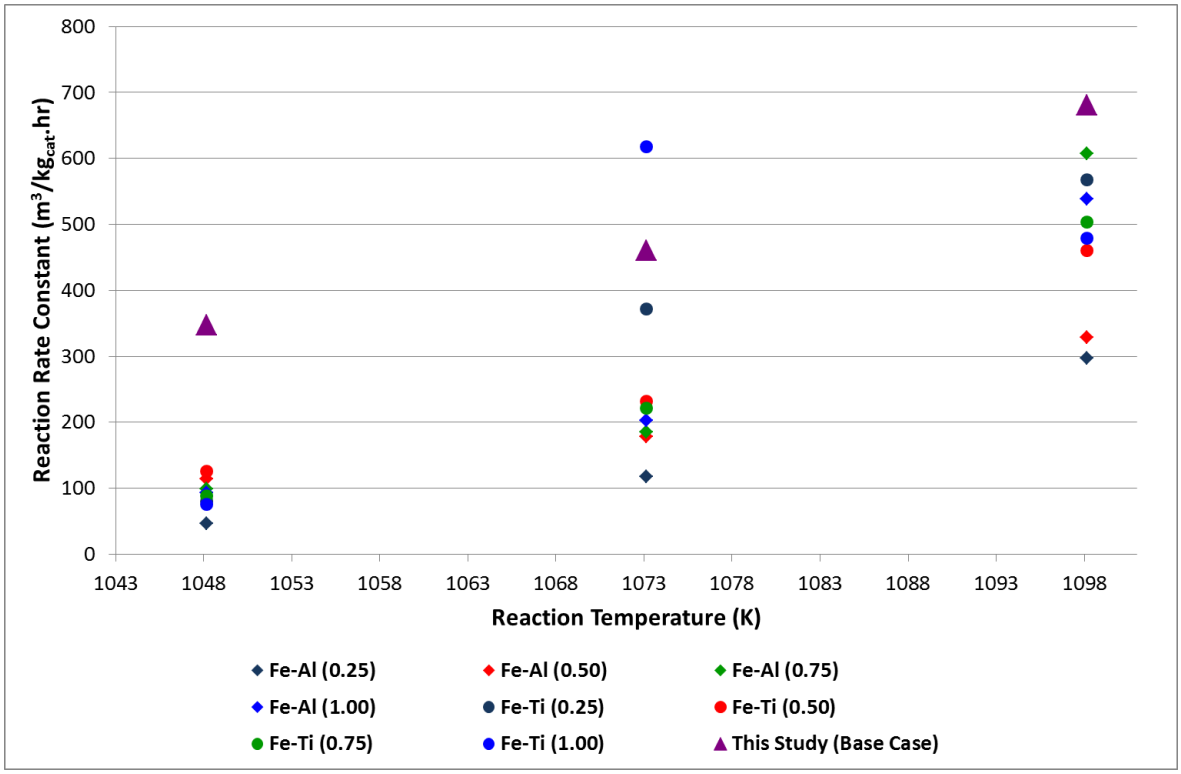

Figure 25 - Comparison of base-case reaction rate constants with results of Kim *et al.* (2006)

In Figure 25, where the published results are again corrected for the iron (III) oxide load in the catalyst, it is observed that higher reaction rate constants are (on average) observed for pure iron (III) oxide catalyst than for supported catalysts, as published by Kim *et al.* (2006). Under the assumption of a first-order reaction, these higher reaction rate constants indicate that similar reaction rates can be expected for pure iron (III) oxide than for supported catalyst should similar sulphur trioxide concentrations be used in this study than concentrations used by Kim *et al.* (2006), which then would result in similar reaction rate constants.

In general it can be seen that activities (reaction rates and reaction rate constants) in a first-order reaction suggest that the unsupported iron (III) oxide catalyst performs similar to the supported catalysts investigated by Kim *et al.* (2006).

4.2.2 Comparison with Kondamudi & Uphadhyayula (2012)

The study conducted by Kondamudi & Uphadhyayula (2012) focused on iron (III) oxide supported on alumina (Al_2O_3). All feed conditions were specified for the experiments conducted and the calculations of reaction rates and reaction rate constants are supplied in Appendix H (Section H2). As Kondamudi & Uphadhyayula (2012) did not specify the iron content of the supported catalyst in their investigation, the data obtained from this publication could not be corrected for the amount of iron (III) oxide in the total catalyst mass. Figure 26 shows a comparison of the reaction rates obtained in this study with the reaction rates obtained by Kondamudi & Uphadhyayula (2012).

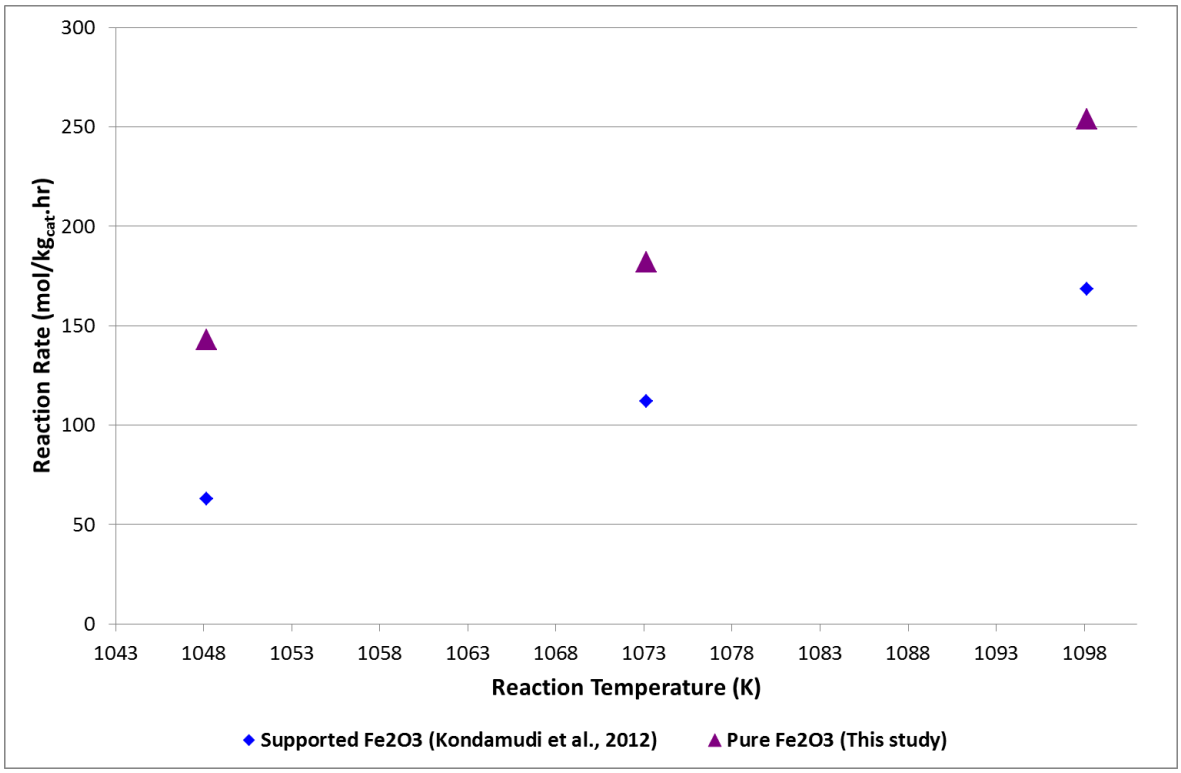

Figure 26 - Comparison of base-case reaction rates with results of Kondamudi & Uphadhyayula (2012)

It is seen this graph that lower reaction rates were observed for the supported catalyst (Kondamudi & Uphadhyayula, 2012) compared to the pure unsupported iron (III) oxide that is being studied here. These results could be attributed to the concentration of sulphur trioxide to the reactor wherein the concentration used for pure iron (III) oxide (± 0.42 mole/m^3 on average) in this study is approximately half the magnitude of the concentration used for supported iron (III) oxide (± 0.80 mole/m^3 on average) by Kondamudi & Uphadhyayula (2012).

However, by assuming a first order reaction as dictated by Equation 15 in Section 2.2.3, it would be expected that reaction rate constants should be similar for the supported catalyst and the pure unsupported iron (III) oxide in this study at the stated conditions. The reaction rate constants are shown in Figure 27 and it is observed that the reaction rate constant obtained by Kondamudi & Uphadhyayula (2012) is approximately half of that obtained in this study.

The observation of lower reaction rates as well as lower reaction rate constants for supported catalysts at lower concentrations compared to the pure unsupported iron (III) oxide case suggests that the supported catalyst studied by Kondamudi & Uphadhyayula (2012) exhibit lower activity at similar reaction temperatures than the unsupported iron (III) oxide catalyst of this study. The absence of information on the iron content in the supported catalyst studied by Kondamudi & Uphadhyayula (2012), however, increases the difficulty to compare the reaction rates and reaction rate constants obtained by these authors with values obtained in this study and the study of Kim *et al.* (2006), and could even prove similar activities for these two catalyst types.

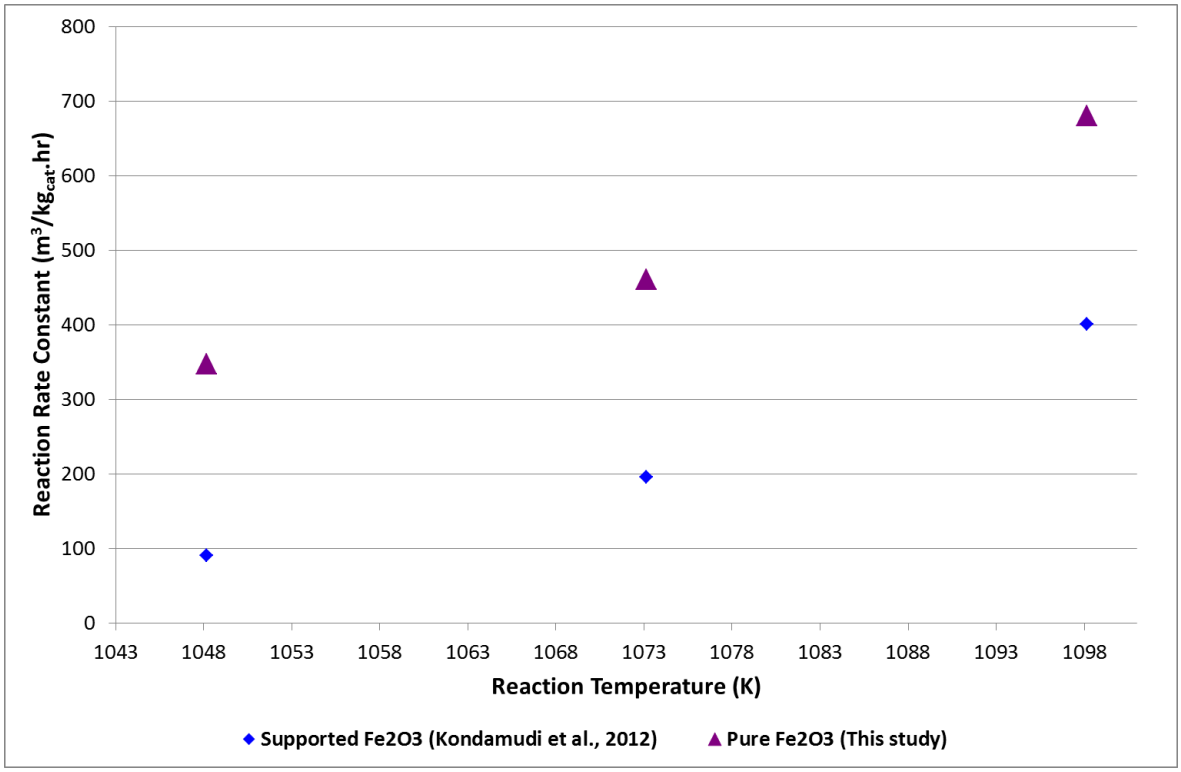

Figure 27 - Comparison of base-case reaction rate constants with results of Kondamudi & Uphadhyayula (2012)

4.2.3 Comparison with Giaconia *et al.* (2011)

Giaconia *et al.* (2011) conducted three experiments on iron (III) oxide pellets as well as three experiments on Fe_2O_3-coated SiSiC honeycomb fragments. Giaconia *et al.* (2011) mentions that their Fe_2O_3-based catalysts have an iron load of 14.9 - 18.5wt%. The pellets were prepared as discussed in Section 2.2.2.

By taking information published by Giaconia *et al.* (2011) on the feed composition, conversions and reported WHSV, the reaction rates and reaction rate constants were calculated as detailed in Appendix H (Section H3). The calculations were conducted by correcting the published data for the iron (III) oxide load in the catalyst. Table 8 summarises the different conditions for the different catalyst types tested by Giaconia *et al.* (2011).

Figure 28 shows that higher reaction rates were obtained in this study with pure iron (III) oxide powder than for both the Fe_2O_3 pellet fragments and the supported Fe_2O_3 fragments at the three reaction conditions studied. The calculated values indicate that the reaction rates obtained for pure iron (III) oxide is on average 2 times higher than for the Fe_2O_3 pellets and on average 3 times higher than for the Fe_2O_3-coated SiSiC fragments studied by Giaconia *et al.* (2011).

Table 8 - Feed conditions of experiments conducted by Giaconia *et al.* (2011)

Experiment	Catalyst	Feed Composition (Vol. %)			WHSV (h^{-1})
		SO_3	H_2O	N_2	
A	Pellets	44	54	2	13.9
B	Pellets	44	53	3	7.1
C	Pellets	42	52	6	3.2
A	Fe_2O_3-coated SiSiC	44	55	1	49
B	Fe_2O_3-coated SiSiC	44	53	3	16.7
C	Fe_2O_3-coated SiSiC	43	52	5	8.4

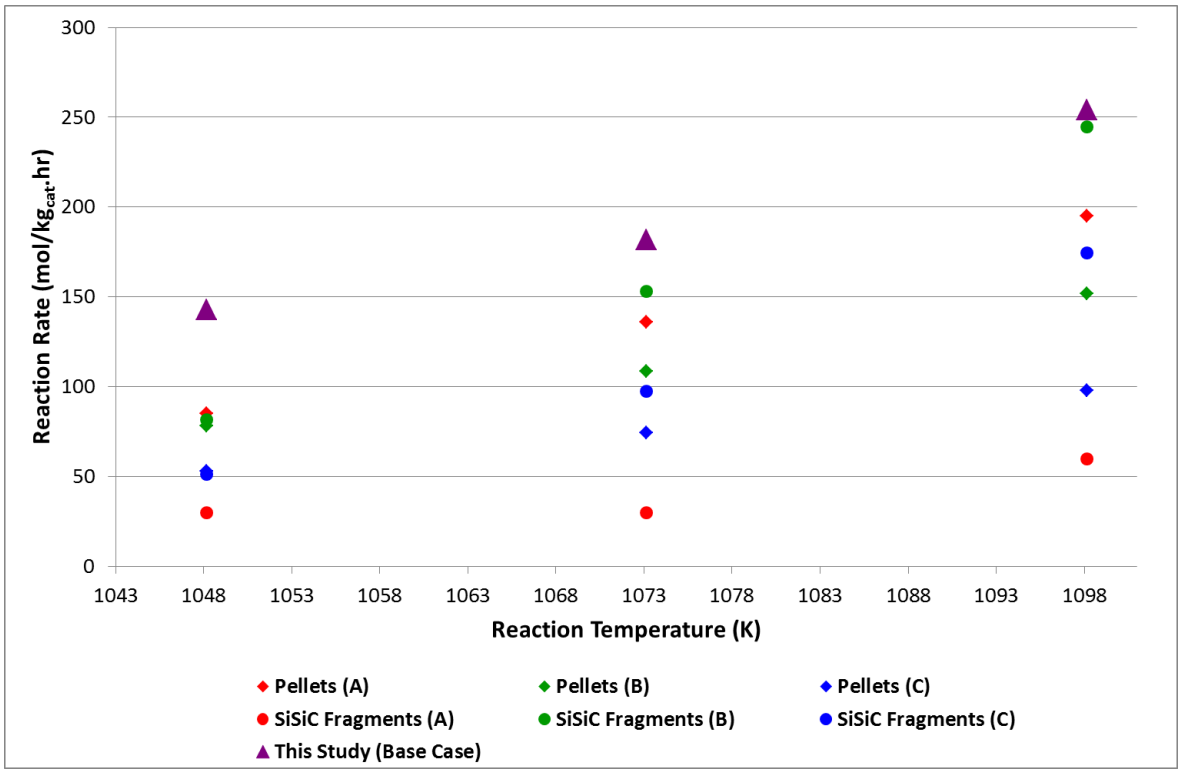

Figure 28 - Comparison of base-case reaction rates with results of Giaconia *et al.* (2011)

With the sulphur trioxide concentration used in the base-case experiments of this study being about 10% on average of the concentrations used by Giaconia *et al.* (2011), and assuming a first order reaction, reaction rate constants that are much higher for the base-case experiments of this study than those determined for Giaconia *et al.* (2011) are to be expected. This, however, is seen in Figure 29 wherein reaction rate constants for pure iron (III) oxide seem to be on average 20 times higher than the reaction rate constants calculated for pellets, and on average 34 times higher than those calculated for Fe_2O_3-coated SiSiC fragments.

This indicates that activities of the pure unsupported iron (III) oxide tend to be similar to that of supported iron (III) oxide or iron (III) oxide pellets investigated by Giaconia *et al.* (2011),

as, based on a first-order reaction, reaction rates and reaction rate constants in conjunction with the concentration of sulphur trioxide in the feed to the reactor are comparable to the results found in this study.

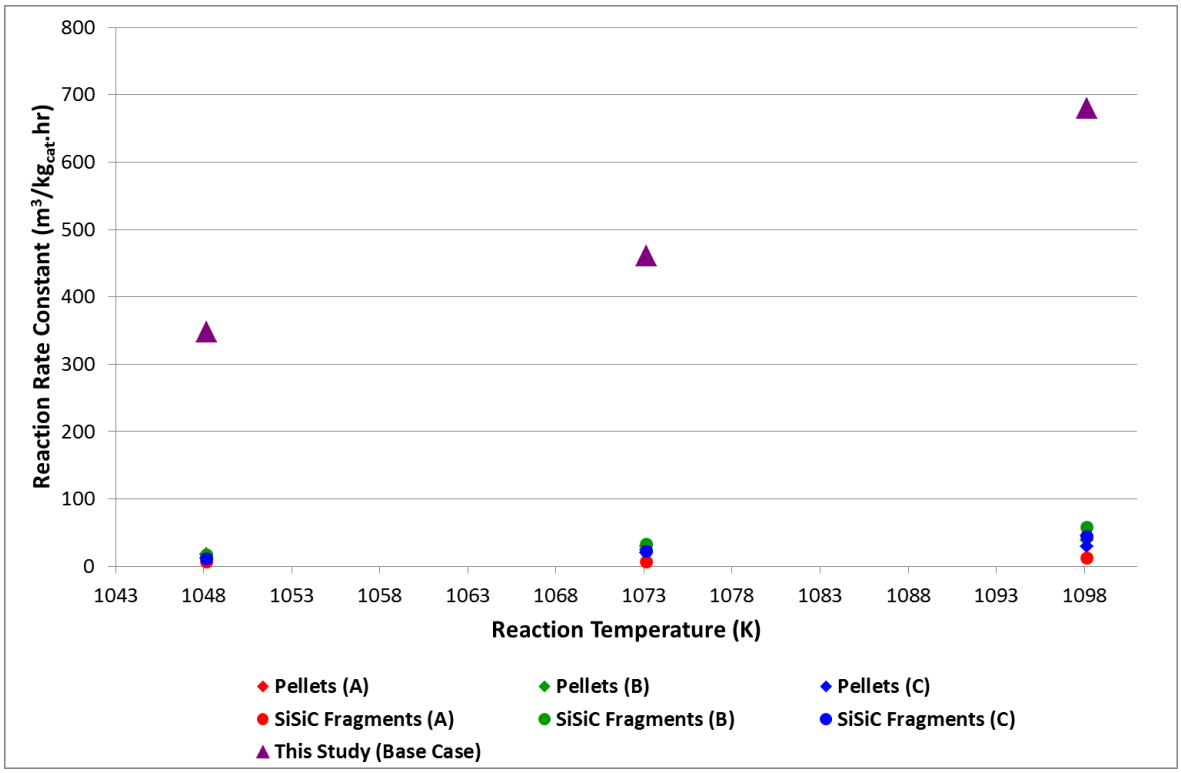

Figure 29 - Comparison of base-case reaction rate constants with results of Giaconia *et al.* (2011)

4.3 Effect of feed concentration variations on conversion

A qualitative investigation was conducted to assess the influence of various reactants and reaction products on the reaction rate. The details of the experimental runs are shown in Table 4 in Section 3.2.1.

For this analysis, the reaction rate of the specific experiment was plotted against an average sulphur trioxide concentration throughout the reaction zone. This average concentration in the reactor was calculated for each of the experimental runs using the following equation:

$$\bar{C}_{SO_3} = \frac{C^o_{SO_3} + C_{SO_3}}{2} \qquad [29]$$

The results of the different feed scenarios are shown in Figure 30, Figure 31 and Figure 32 for the different reaction zone temperatures respectively. Assuming a first-order reaction, the experimental line for the reaction links the reaction rate versus sulphur trioxide concentration data point of the base case experiments with the origin on the graph, while the dotted lines indicate the boundaries of the experimental error.

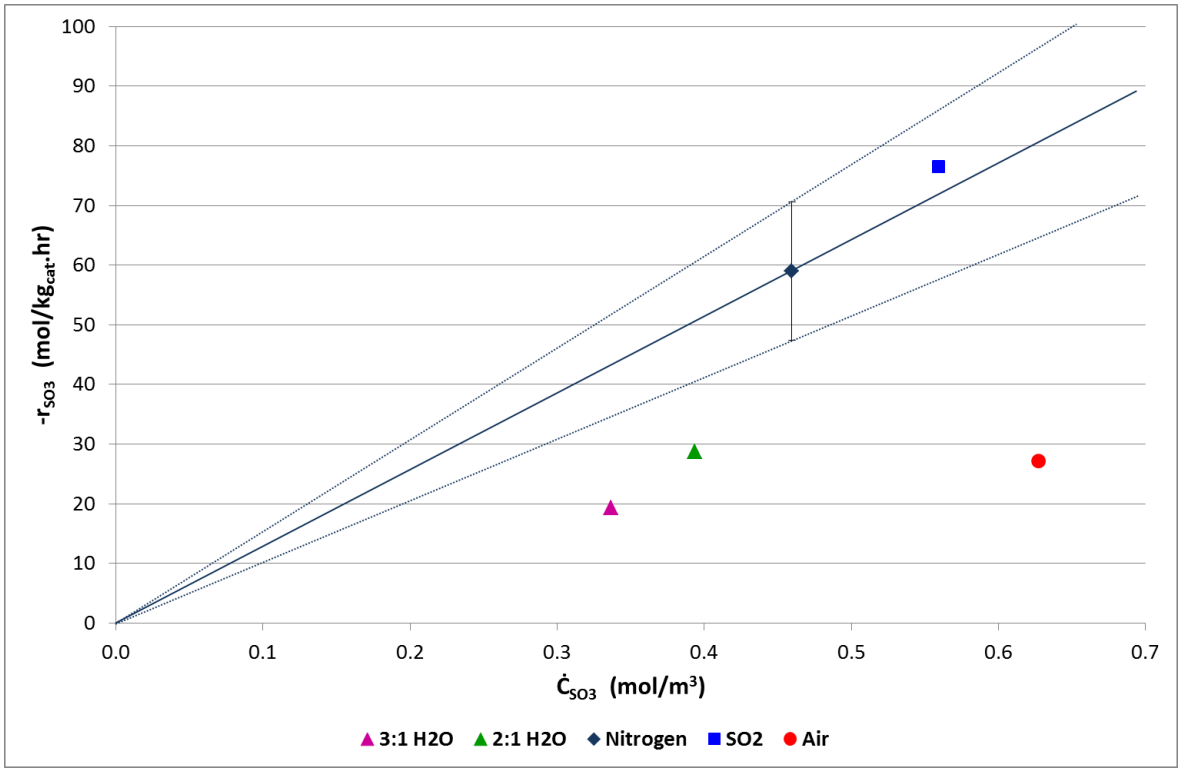

Figure 30 - Influence of product gases and H_2O on the reaction at 700°C

Figure 30 shows the reaction rates versus the average sulphur trioxide concentrations in the reaction zone for the different reactor feed scenarios at a reaction temperature of 700°C. It is noted that only the data point wherein additional sulphur dioxide was added to the reactor feed lies within the experimental error band of the base case. All other data points lie below this error zone. This data suggests that, at the lower reaction temperature of 700°C, water and oxygen do have an influence on the reaction, and could be attributed to adsorption of these species on the active catalyst surface, leaving less active surface for the reaction mechanism as proposed by Karagiannakis *et al.* (2010), which is discussed in Section 2.1.4.

The concentration of oxygen exiting the reactor is of importance when air is used as carrier gas instead of pure nitrogen. This concentration was approximately 40 times higher than the oxygen that develops due to the reaction itself. The significance of this is seen at lower reaction temperatures of 700°C and 750°C (Figure 30 and Figure 31) where reaction rates are more influenced than at the higher reaction temperature (Figure 32).

In each of the investigated reaction temperatures a tendency is observed that reaction rates decline with the addition of water as part of the reactor feed, which could indicate that competitive adsorption may be of importance. This finding is strengthened by the observation of the influence of water on the reaction rate; Both reaction rates in the presence of water in the feed show smaller reaction rates, and the effect is stronger for the 3:1 (water:SO_3) molar ratio than for the 2:1 ratio.

According to Tagawa and Endo (1989) the catalytic activity at and below 700°C was found to be reduced due to metal sulphate formation. This could also explain the observations for the different feed scenarios at 700°C. These water- and air fed data points may indirectly

suggest a reaction order of less than one, and point towards a Langmuir-Hinshelwood type of reaction kinetics.

Figure 31 shows the reaction rates versus average sulphur trioxide concentrations for the different reactor feed scenarios at 750°C. It is seen that all data points except for one (the data point for air instead of nitrogen as feed to the reactor) falls within the experimental Error band of the base case data point.

Figure 32 represents the reaction rate data versus average sulphur trioxide concentration for the different reactor feed scenarios at 825°C reaction temperature. In this figure it can be seen that the addition of reaction product species and water does not significantly influence the reaction rate of this reaction. At the elevated reaction temperatures of 750°C and 825°C, the influence of reactant and product species on the reaction seem less prominent, which is probably attributable to a less stable metal sulphate that forms as intermediate species during the reaction mechanism proposed by various authors (refer to Section 2.1.4). Adsorption of these species on the catalyst surface is in general less pronounced at elevated reaction temperatures, since adsorption is generally an exothermic process (Fogler, 1986:240).

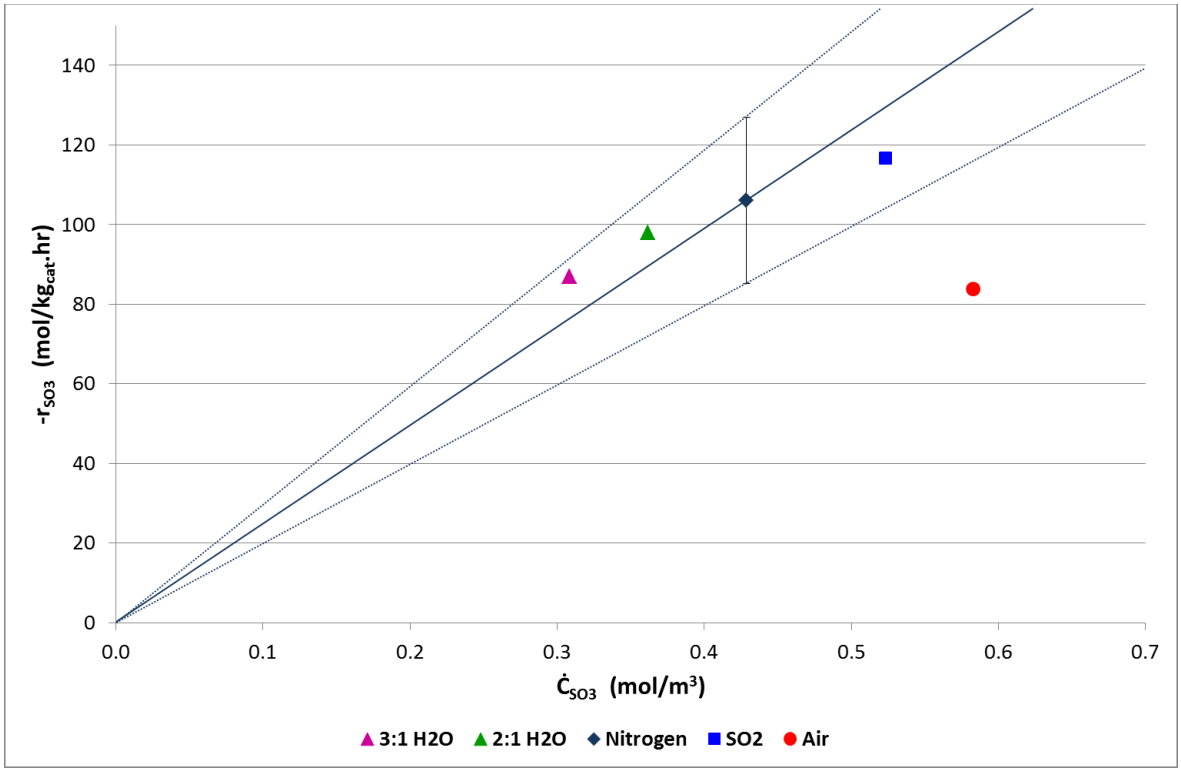

Figure 31 - Influence of product gases and H_2O on the reaction at 750°C

Unlike the data presented in Figure 30, the tendencies in Figure 31 and Figure 32 suggest that, with the exception of one of the data points each time, the reaction is of a first-order nature. Based on this observation, the conclusions drawn from the reaction kinetics determination, presented in Section 4.1, as well as the comparisons with published data from other authors in this field, presented in Section 4.2, can be termed sound based on the assumption of a first-order reaction in sulphur trioxide.

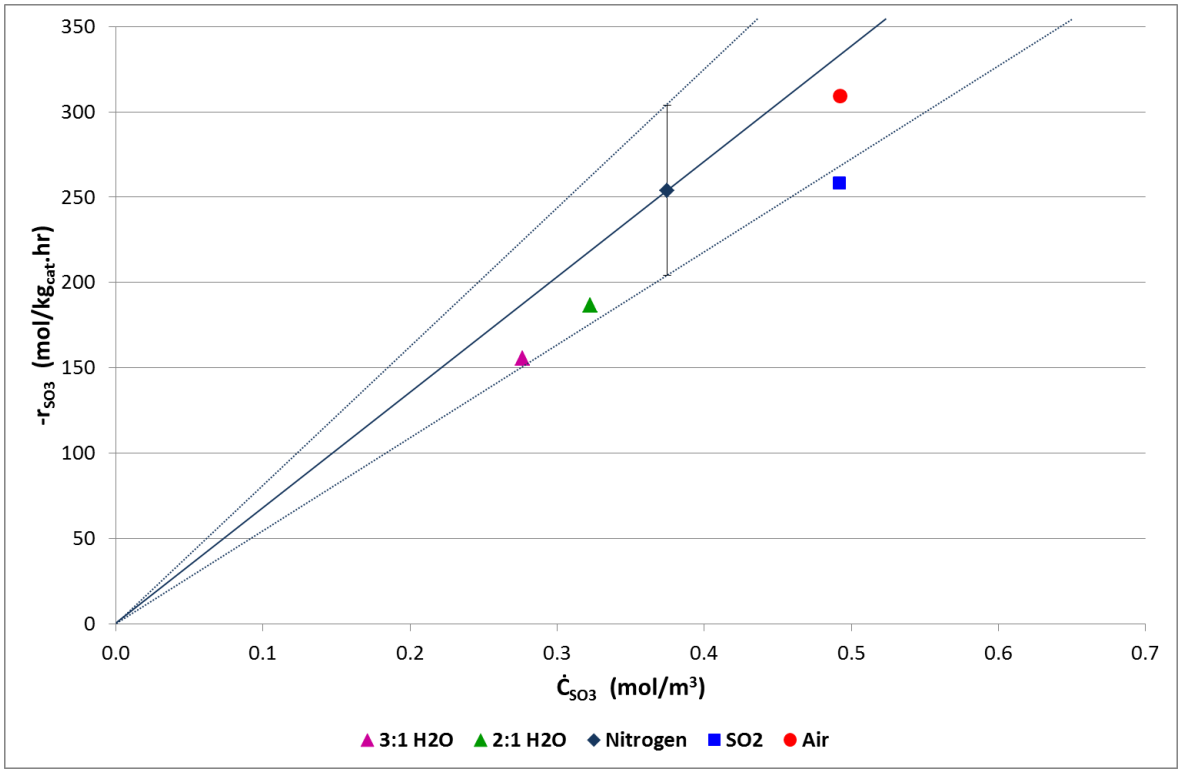

Figure 32 - Influence of product gases and H_2O on the reaction at 825°C

5. Conclusions and recommendations

This chapter covers conclusions drawn from the study and concludes with recommendations for subsequent work on the reaction kinetics of the catalytic decomposition of sulphur trioxide using iron (III) oxide as catalyst.

5.1 Conclusions

Experimental runs at different temperatures with only pure nitrogen as carrier gas and 98%$_{(mass)}$ sulphuric acid provided sufficient information in order to obtain the reaction kinetic parameters for the decomposition of sulphur trioxide into sulphur dioxide and oxygen. Assuming plug-flow conditions and a first-order reaction with respect to sulphur trioxide, values were obtained for the activation energy E_a and the Arrhenius frequency factor A for pure iron (III) oxide powder. These values are comparable to the values found for iron (III) oxide pellets published by Giaconia *et al.* (2011), but substantially higher values were published by other authors (Giaconia *et al.*, 2011, Kondamudi & Upadhyayula, 2012 & Kim *et al.*, 2006) on various other catalyst derivatives employing iron (III) oxide. The main reason for this phenomenon could be that this study focused on very fine (40±14µm) very pure solid iron (III) oxide particles as catalyst, while the mentioned researchers focused mainly on iron (III) oxide supported by either alumina, titania or honeycomb fragments as well as iron (III) oxide pellets.

The performance in terms of reaction rates and reaction rate constants of pure iron (III) oxide powder is comparable to iron (III) oxide pellets or supported iron (III) oxide fragments. This conclusion can be drawn from the comparison of the results obtained for pure iron (III) oxide with data published by Giaconia *et al.* (2011), Kim *et al.* (2006) and Kondamudi & Upadhyayula (2012). In these comparisons, under the assumption of a first-order reaction, the combined reaction rates and the reaction rate constants obtained for pure iron (III) oxide in conjunction with the feed concentrations of sulphur trioxide to the reactor, were similar to the values found for iron (III) oxide supported on titania and on alumina published by Kim *et al.* (2006) as well as for iron (III) oxide pellets and iron (III) oxide supported on SiSiC honeycomb fragments published by Giaconia *et al.* (2011). The comparison with iron (III) oxide supported on alumina, as published by Kondamudi & Uphadhyayula (2012) was inconclusive due to a lack of information on the iron-load in the catalyst. It can therefore be concluded that pure iron (III) oxide powder exhibits similar activities than other iron (III) oxide derived catalysts.

The PFR model as well as a first-order reaction approach has been adopted by the majority of authors who published results on a similar investigation (Brown & Revankar, 2012). Based on the obtained conversions and an evaluation of the Mears criterion, it can be concluded that the reaction was carried out in the absence of diffusion limitations and that the reversible reaction does not play a significant role.

Observations from the qualitative investigation into the influence of reaction product species and water on the reaction show that reaction products have little to no influence on the reaction at higher reaction temperatures, while reaction rates were reduced at lower reaction temperatures, which can be attributed to adsorption of such species on the active catalyst surface as well as the metal sulphate that forms as intermediate species on the active catalyst surface according to the suggested reaction mechanism.

Overall it can be concluded that unsupported Fe_2O_3 is a suitable candidate for the commercial conversion of SO_3 to SO_2 in the HyS cycle. The catalyst show similar activities to supported iron catalysts, but the production of this type of catalyst has economic advantages above the supported counterpart.

5.2 Recommendations

In order to demonstrate potential cost savings related to the use of iron (III) oxide as catalyst for the decomposition reaction of sulphur trioxide to sulphur dioxide and oxygen, a very fine powder (with particle sizes of 40 ± 14μ) at 99.99% Fe_2O_3 purity was used. This catalyst has shown excellent activities during the course of the investigation. The direct use of the micronised material may cause practical challenges, due to the very small particle diameter. For subsequent investigations on pure, unsupported iron (III) oxide, it is therefore recommended also to investigate different particle sizes, and to determine the effect of the particle size on the reaction rate. The level of purity could also contribute to the activity of the catalyst and should also receive attention.

A subsequent study could include a proper microscopic analysis of fresh- and spent catalyst, including mass spectrometric analyses at different temperatures. This would assist in verifying the reaction mechanism proposed by several authors (Banerjee *et al.*, 2008, Brittain and Hildebrand, 1982, Dokiya *et al.*, 1977, Tagawa and Endo, 1989, Kim *et al.*, 2006, Karagiannakis *et al.*, 2010 & Kondamudi *et al.*, 2012), as discussed in Section 2.1.4. It would also shed light on possible physical phenomena around the catalyst particles, e.g. agglomeration or potential fusion of particles at the different operating reaction temperatures.

The qualitative study on the influence of reaction products on the reaction can be expanded into a proper quantitative study in order to confirm the reaction mechanism and also to substantiate the initial assumption of working with a first-order reaction with respect to sulphur trioxide. Also, the reaction should preferably be studied with higher SO_3 concentrations, in order to come closer to industrial conditions.

Finally, a detailed economic analysis should be initiated to assess whether this catalyst would outperform PGM-based catalysts as well as supported iron (III) oxide catalysts.

6. References

Banerjee A.M., Pai M.R., Meena S.S., Tripathi A.K. & Bharadwaj S.R. 2011. Catalytic activities of cobalt, nickel and copper ferrospinels for sulfuric acid decomposition: The high temperature step in the sulphur based thermochemical water splitting cycles. *International Journal of Hydrogen Energy,* 36(2011):1-13.

Banerjee A.M., Pai M.R., Bhattacharya K., Tripathi A.K., Kamble V.S., Bharadwaj S.R. & Kulshreshtha S.K. 2008. Catalytic decomposition of sulphuric acid on mixed Cr/Fe oxide samples and its application in sulphur-iodine cycle for hydrogen production. *International Journal of Hydrogen Energy*, 33(2008):319-326.

Barbarossa V., Brutti S., Diamanti M., Sau S. & De Maria G. 2006. Catalytic thermal decomposition of sulphuric acid in sulphur-iodine cycle for hydrogen production. *International Journal of Hydrogen Energy*, 31(2006):883-890.

Berenson B.L. & Levine D.M. 1989. Basic Business Statistics – Concepts and Applications. 4th Edition. Prentice-Hall International Editions. p.831.

Brittain R., Hildebrand D. 1983. Catalytic decomposition of gaseous SO_3. *Journal of Physical Chemistry*, 87(1983):3713-3717.

Brown N.R. & Revankar S.T. 2012. A review of catalytic sulphur (VI) oxide decomposition experiments. *International Journal of Hydrogen Energy*, 37(2012):2685-2698.

Brutti S., De Maria G., Cerri G., Giovanelli A., Brunetti B., Cafarelli P. 2007. Decomposition of H_2SO_4 by direct solar radiation. *Ind End Chem Res*, 46(2007):6393-6400.

Dokiya M., Kameyama T., Fukuda K., Kotera Y. 1977. The study of thermochemical hydrogen preparation. III. An oxygen-evolving step through the thermal splitting of sulfuric acid. *Bulletin of the Chemical Society of Japan*, 50(10):2657-2660

Fogler H.S. 1986. Elements of chemical reaction engineering. Prentice-Hall International Editions.

Giaconia A., Sau S., Felici C., Tarquini P., Karagiannakis G., Pagkoura C., Agrafiotis C., Konstandopoulos A.G., Thomey D., de Oliveira L., Roeb M. & Sattler C. 2011. Hydrogen production via sulphur-based thermochemical cycles: Part 2: Performance evaluation of Fe_2O_3-based catalysts for the sulfuric acid decomposition step. *International Journal of Hydrogen Energy*, 36(2011):6496-6509.

Ginosar D., Petkovic L., Glenn A., Burch K. 2007. Stability of supported platinum sulfuric acid decomposition catalysts for use in thermochemical water splitting cycles. *International Journal of Hydrogen Energy*, 32(2007):482-488.

Ginosar D.M., Rollins H.W., Petkovic L.M., Burch K.C. & Rush M.J. 2009. High-temperature sulfuric acid decomposition over complex metal oxide catalysts. *International Journal of Hydrogen Energy*, 34(2009):4065-4073.

Gorensek M.B. & Summers W.A. 2009. Hybrid sulfur flowsheets using PEM electrolysis and a bayonet decomposition reactor. *International Journal of Hydrogen Energy*, 34(2009):4097-4114.

Incropera, F.P. & DeWitt, D.P. 2002. Fundamentals of Heat and Mass Transfer. 5th Edition. New Jersey: John Wiley & Sons. p981.

Ishikawa H., Ishii E., Uehara I., Nakane M. 1982. Catalyzed thermal decomposition of H_2SO_4 and production of HBr by the reaction of SO_2 with Br_2 and H_2O. *International Journal of Hydrogen Energy*, 7(1982):237-246.

Karagiannakis G., Agrafiotis C.C., Zygogianni A., Pagkoura C. & Konstandopoulos A.G. 2010. Hydrogen production via sulfur-based thermochemical cycles: Part 1: Synthesis and evaluation of metal oxide-based candidate catalyst powders for the sulfuric acid decomposition step. *International Journal of Hydrogen Energy*, 35(2010):1-14.

Karasawa H., Sasahira A. & Hoshino K. 2006. Thermal Decomposition of SO_3. *International Journal of Nuclear Hydrogen Production and Applications*, 1(2/2006):134-143.

Kim T., Gong G., Lee B.G., Lee K., Jeon H., Shin C., Kim H. & Jung K. 2006. Catalytic decomposition of sulfur trioxide on the binary metal oxide catalysts of Fe/Al and Fe/Ti. *Applied Catalysis A: General*, 305(2006):39-45.

Kondamudi K. & Upadhyayula S. 2012. Kinetic studies of sulfuric acid decomposition over Al-Fe_2O_3 catalyst in the sulfur-iodine cycle for hydrogen production. *International Journal of Hydrogen Energy*, 37(2012):3586-3594.

Nagaraja B., Jung K., Ahn B., Abimanyu H., Yoo K. 2009. Catalytic decomposition of SO_3 over Pt/$BaSO_4$ materials in sulfur-iodine cycle for hydrogen production. *Ind Eng Chem Res*, 48(2009):1451-1457.

Nagarajan V., Ponyavin V., Chen Y., Vernon M.E., Pickard P. & Hechanova A.E. 2009. CFD modeling and experimental validation of sulfur trioxide decomposition in bayonet type heat exchanger and chemical decomposer for different packed bed designs. *International Journal of Hydrogen Energy*, 34(2009):2543-2557.

Noglik A., Roeb M., Sattler C., Pitz-Paal R. 2009. Experimental study on sulfur trioxide decomposition in a volumetric solar receiver-reactor. *International Journal of Energy Resources*, 33(2009):799-812.

O'Keefe D., Norman D., Williamson D. 1980. Catalyst research in thermochemical hydrogen water-splitting processes. *Catal Rev –Sci Eng.*, 22(1980):325-369.

Perry, R.H. & Green, D.W. 1997. Perry's Chemical Engineers' Handbook. 7th Edition. McGraw-Hill. pp. 5-48 – 5-49.

Petkovic L., Ginosar D., Rollins H., Burch K., Pinhero P., Farrell H. 2008. Pt/TiO_2 (rutile) catalysts for sulphuric acid decomposition in sulfur-based thermochemical water-splitting cycles. *Appl Catal A*, 338(2008):27-36.

Petropavlovskii A., Kovalev V., Soroko V., Forsov A. 1989. Kinetics of decomposition of sulfuric acid on an alumina-palladium catalyst. *Zh Prik Khim*, 62(1989)2183-2185.

Rashkeev S.N., Ginosar D.M., Petkovic L.M. & Farrell H.H. 2009. Catalytic activity of supported metal particles for sulfuric acid decomposition reaction. *Catalysis Today*, 139(2009):291-298.

Schwartz D., Gadiou R., Brilhac J., Prado G. & Martinez G. 2000. A kinetic study of the decomposition of spent sulfuric acids at high temperature. *Industrial and Engineering Chemical Research*, 39(2000):2183-2189.

Spewock S., Brecher L.E., Talko F. 1976. The thermal catalytic decomposition of sulfur trioxide to sulfur dioxide and oxygen. *Proceedings of the 1st world hydrogen energy conference. Coral Gables, Fl.* 1976.

Tagawa H., Endo T. 1989. Catalytic decomposition of sulfuric acid using metal oxides as the oxygen generating reaction in thermochemical water splitting process. *International Journal of Hydrogen Energy*, 14(1989):11-17.

Thomey D., de Oliveira L., Sack J., Roeb M. & Sattler C. 2012. Development and test of a solar reactor for decomposition of sulphuric acid in thermochemical hydrogen production. *International Journal of Hydrogen Energy*, 37(2012):16615-16622.

Appendices

Appendix A – Rational followed in calculations and derivations

The order in which calculations were conducted to finally obtain reaction kinetics from the measured SO_2 values is discussed in this appendix.

A.1 Correction for SO_2 measurements

It was important to determine with how much the measured SO_2 values need to be corrected due to SO_2 dissolution in the liquid traps over the duration of each experiment. This was determined based on titration results of liquid samples that formed in the liquid traps for different experimental cases, and the results are discussed in detail in Appendix E.

A.2 Molar flows for each different feed scenario

Molar flow rates were subsequently calculated as outlined in Section 3.3.1 for each of the reactor feed scenarios detailed in Table 4. These flow rates for the different scenarios are detailed in Appendix F.

A.3 Determining conversions, reaction rates and WHSV

Based on the mole balances discussed in Section A.2 above as well as the calculation of the SO_2 formed each time in the reactor ($\dot{\xi}$, detailed by Equations F2, F4 & F5 in Appendix F) based on the corrected SO_2 measurement as discussed in Section A.1 and Appendix E, the conversion and rate of reaction was calculated for each data point.

The conversion X is calculated for each of the experimental scenarios as outlined by the following equation:

$$X = \frac{\dot{\xi}}{\dot{n}^{o}_{SO_3}} \qquad [A1]$$

The rate of reaction r_{SO_3} is calculated according to Equation A2.

$$r_{SO_3} = \frac{\dot{\xi}}{m_{cat}} \qquad [A2]$$

It is also of importance to mention the equation used for the calculation of the weight-hourly-space-velocity (WHSV).

$$WHSV = \frac{\dot{m}_{SO_3}}{m_{cat}} \qquad [A3]$$

A.4 Relating conversion with the reaction kinetic constant k

With the conversion known for each data point in each experimental run, a steady-state conversion value (the last value obtained at 12 hours of operation) was taken to obtain the reaction rate constant k. The model was derived to relate k with X and is subsequently presented.

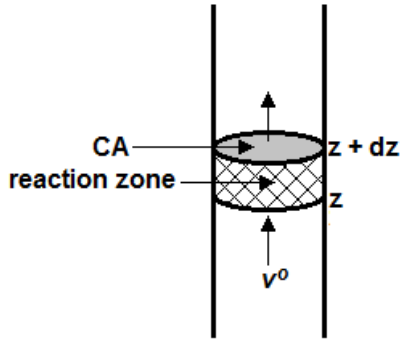

Figure 33 - Fixed bed reactor model

With the catalyst bed (reaction zone) in the reactor being represented by the shaded section in Figure 33 and with CA representing the cross-sectional area of the reaction zone, a simple balance over this section is given by:

$$F_{SO_3}\big|_z - F_{SO_3}\big|_{z+dz} - k.C_{SO_3}.\rho_{cat}.CA.dz = 0 \qquad [A4]$$

By assuming a constant volumetric flow rate ($\dot{v}_t^o$), the following can be obtained:

$$\dot{v}_t^o.C_{SO_3}\big|_z - v_t^o.C_{SO_3}\big|_{z+dz} - k.C_{SO_3}.\rho_{cat}.CA.dz = 0 \qquad [A5]$$

$$\therefore \quad \dot{v}_t^o\left(C_{SO_3}\big|_z - C_{SO_3}\big|_{z+dz}\right) = k.C_{SO_3}.\rho_{cat}.CA.dz \qquad [A6]$$

However,

$$\lim_{dz\to 0}\left(C_{SO_3}\big|_z - C_{SO_3}\big|_{z+dz}\right) = -dC_{SO_3}$$

Equation A6 will thus reduce to:

$$-\frac{dC_{SO_3}}{C_{SO_3}} = \frac{k.\rho_{cat}.CA}{\dot{v}_t^o}.dz \qquad [A7]$$

Integrating both sides of Equation A7 leads to the following:

$$\int_{C_{SO_3}^o}^{C_{SO_3}} \frac{dC_{SO_3}}{C_{SO_3}} = \frac{-k.\rho_{cat}.CA}{\dot{v}_t^o}.\int_0^z dz$$

$$\therefore \ \ln\left(\frac{C_{SO_3}}{C^o_{SO_3}}\right) = \frac{-k.\rho_{cat}.CA.z}{\dot{v}^o_t} \quad [A8]$$

But, since:

$$\rho_{cat}.CA.z = m_{cat}$$

$$k = -\ln\left(\frac{C_{SO_3}}{C^o_{SO_3}}\right).\frac{\dot{v}^o_t}{m_{cat}} = -\ln\left(\frac{C^o_{SO_3}(1-X)}{C^o_{SO_3}}\right).\left(\frac{\dot{v}^o_t}{m_{cat}}\right) = -\ln(1-X).\left(\frac{\dot{v}^o_t}{m_{cat}}\right) \quad [A9]$$

In this equation, the molar flow rate $\dot{v}^o_t$ is obtained by taking the normal volumetric flow rate of the reactor feed and correcting it with the reaction zone temperature:

$$\dot{v}^o_t = \dot{v}^{o-norm}_t.\frac{T_r}{T^{std}} \quad [A10]$$

The initial concentration of SO_3 in the feed was obtained by dividing the molar flow rate of SO_3 in the feed stream by the molar flow obtained in Equation A10.

$$C^o_{SO_3} = \frac{\dot{n}_{SO_3}}{\dot{v}^o_t} \quad [A11]$$

A.5 Obtaining activation energy E_a and Arrhenius frequency factor A

Using the linearized form of the Arrhenius equation as presented below, a plot of $ln(k)$ versus $1/T$ should yield the opportunity to determine the activation energy E_a from the slope of the obtained straight line, and the Arrhenius frequency factor A from the offset.

$$\ln(k) = \left(-\frac{E_a}{R}\right)\frac{1}{T_r} + \ln(A) \quad [A12]$$

The slope of the line represents the value of $(-E_a/R)$ and the offset represents $\ln(A)$.

Appendix B – Equilibrium conversion calculations

The equilibrium conversions were calculated using version 1.1 of the ThermoSolver software program by Connelly Barnes & Milo Koretsky, Oregon State University (2006). The calculations yield the equilibrium conditions as detailed in Table 9.

Table 9 - Equilibrium data obtained from ThermoSolver

Equilibrium at T_r = 700°C				
Species (a)	$\dot{n}_a^o$	y_a^o	$\bar{n}_a$	$\bar{y}_a$
N_2	4.09E-2	0.921	4.09E-2	0.907
SO_3	1.67E-3	3.76E-2	3.64E-4	8.09E-3
H_2O	1.85E-3	4.17E-2	1.85E-3	4.11E-2
SO_2	0	0	1.30E-3	2.90E-2
O_2	0	0	6.52E-4	1.45E-2
Equilibrium at T_r = 725°C				
Species (a)	$\dot{n}_a^o$	y_a^o	$\bar{n}_a$	$\bar{y}_a$
N_2	4.09E-2	0.921	4.09E-2	0.907
SO_3	1.67E-3	3.76E-2	3.29E-4	7.30E-3
H_2O	1.85E-3	4.17E-2	1.85E-3	4.11E-2
SO_2	0	0	1.34E-3	2.97E-2
O_2	0	0	6.70E-4	1.49E-2
Equilibrium at T_r = 750°C				
Species (a)	$\dot{n}_a^o$	y_a^o	$\bar{n}_a$	$\bar{y}_a$
N_2	4.09E-2	0.921	4.09E-2	0.906
SO_3	1.67E-3	3.76E-2	2.53E-4	5.60E-3
H_2O	1.85E-3	4.17E-2	1.85E-3	4.10E-2
SO_2	0	0	1.42E-3	3.14E-2
O_2	0	0	7.08E-4	1.57E-2
Equilibrium at T_r = 775°C				
Species (a)	$\dot{n}_a^o$	y_a^o	$\bar{n}_a$	$\bar{y}_a$
N_2	4.09E-2	0.921	4.09E-2	0.906
SO_3	1.67E-3	3.76E-2	2.02E-4	4.49E-3
H_2O	1.85E-3	4.17E-2	1.85E-3	4.10E-2
SO_2	0	0	1.47E-3	3.25E-2
O_2	0	0	7.33E-4	1.62E-2
Equilibrium at T_r = 800°C				
Species (a)	$\dot{n}_a^o$	y_a^o	$\bar{n}_a$	$\bar{y}_a$
N_2	4.09E-2	0.921	4.09E-2	0.905
SO_3	1.67E-3	3.76E-2	1.71E-4	3.79E-3
H_2O	1.85E-3	4.17E-2	1.85E-3	4.10E-2
SO_2	0	0	1.50E-3	3.32E-2
O_2	0	0	7.49E-4	1.66E-2
Equilibrium at T_r = 825°C				
Species (a)	$\dot{n}_a^o$	y_a^o	$\bar{n}_a$	$\bar{y}_a$
N_2	4.09E-2	0.921	4.09E-2	0.905
SO_3	1.67E-3	3.76E-2	1.31E-4	2.90E-3
H_2O	1.85E-3	4.17E-2	1.85E-3	4.10E-2
SO_2	0	0	1.54E-3	3.41E-2
O_2	0	0	7.69E-4	1.70E-2

From the data in Table 9, equilibrium conversions were calculated using Equation A1 (Appendix A, Section A.3) and compared to conversions obtained during experimental runs. The following table summarises the results obtained.

Table 10 - Comparison of experimental conversions with equilibrium conversions

Base case experimental data		**Base case equilibrium data**	
Temperature (°C)	Conversion (%)	Temperature (°C)	Conversion (%)
700	4.7	700	77.8
725	6.1	725	80.2
750	8.5	750	85.0
775	11.4	775	88.0
800	14.5	800	89.8
825	20.3	825	92.2

Appendix C – Mears Criterion for external diffusion

The Mears criterion to assess whether mass-transfer limitations can be neglected in the experiments and calculations is discussed in Section 2.2.4 and is shown again by the following equation.

$$\frac{-r_a \rho_b R_p \alpha}{k_m} < 0.15 \quad \text{[C1]}$$

Specific units are proposed by Mears for the assessment based on this criterion. These units are tabulated below.

Table 11 - Units associated with the Mears criteria

$Property$	$Units$
r_a	$kmol/kg_{cat}.s$
ρ_b	kg/m^3
R_p	m
α	-
k_m	m/s

Certain assumptions were made in order to evaluate the Mears criterion for this setup.

- The catalyst particles were assumed to be spherical,
- The superficial gas velocity passing the catalyst particles were calculated from the volumetric flow of gas through the bed.

With the reaction rate r_a, the catalyst bulk density ρ_b, the particle radius R_p and the reaction order α known, mostly through measurements, the mass transfer coefficient k_m is the sole unknown. In order to obtain a value for k_m, Incropera & DeWitt (2002:981) proposed a modified Reynolds analogy, also known as the Chilton-Colburn analogy. Following this analogy, the mass transfer coefficient can be obtained from the Stanton number as follow:

$$k_m = v.St_m \quad \text{[C2]}$$

The unknown Stanton number can be calculated from the following equation:

$$St_m = \frac{j_m}{Sc^{2/3}} \quad \text{[C3]}$$

With the Colburn j-factor for mass transfer, j_m, being calculated using the modified Reynolds number, according to the following two equations:

$$j_m = 0.91 Re^{-0.51} \quad \text{[C4]}$$

And

$$Re = \frac{\rho_g.v.d_p}{6.\mu_g.(1-\varepsilon_v)} \quad \text{[C5]}$$

The Schmidt number in Equation C3 is calculated according to Equation C6.

$$Sc = \frac{v}{D_{AB}} \quad [C6]$$

In Equation C7, the binary component diffusion coefficient D_{AB} is calculated from the Fuller-Schettler-Giddings equation (Perry & Green, 1997:5-48):

$$D_{AB} = \frac{0.001T_r^{1.75}.M_{AB}^{0.5}}{P_T\left[(\sum v)_A^{0.333}+(\sum v)_B^{0.333}\right]^2} = \frac{0.001T_r^{1.75}.\left(\frac{1}{M_{N_2}}+\frac{1}{M_{SO_3}}\right)^{0.5}}{P_T\left[(\sum v)_A^{0.333}+(\sum v)_B^{0.333}\right]^2} \quad [C7]$$

Values for the diffusion volumes for nitrogen and sulphur trioxide were obtained from Perry & Green (1997:5-49):

$\sum v_{N_2} = 17.9\ cm^3/mol$

$\sum v_{SO_3} = 46.6\ cm^3/mol$

The obtained (and calculated) values leading to the mass transfer coefficient k_m is shown in Table 12, while Table 13 shows the calculated Mears criterion.

Table 12 - Properties required for determining the mass transfer coefficient

Property	Value	Units
M_{N_2}	14.007	g/mol
M_{SO_3}	80.066	g/mol
M_{AB}	0.084	g/mol
T_r	1098	K
P_t	0.86	atm
ΣV_A	17.90	cm^3/mol
ΣV_B	46.60	cm^3/mol
D_{AB}	1.83	cm^2/s
v	83.34	cm^2/s
Sc	45.51	-
ρ_g	0.275	g/cm^3
d_p	0.004	cm
μ_g	4.91	$g.cm/s$
ε_v	0.70	-
Re	0.0104	-
j_m	9.36	-
ST_m	0.734	-

Table 13 - Evaluation of the Mears criterion

Property	Value	Units
$-r_a$	7.05E-5	$kmol/kg_{cat}.s$
ρ_b	1482	kg/m^3
R_p	2.00E-5	m
α	1.00	-
k_m	0.612	m/s
Mears calculation	3.42E-6	-

This value is significantly lower than the stated criterion in Equation C1, leading to the conclusion that any mass transfer limitations can be neglected in this study.

Appendix D – Acid feed pump calibration

Watson Marlow 120u Peristaltic feed pump

The rate, at which the supplying acid feed pump delivered sulphuric acid to the system, was assessed. The calibration results are subsequently provided.

Table 14 - Calibration data for the Watson Marlow 120u Peristaltic pump

Pump rpm setting	Grams delivered in 5 min	Pump rate (g/min)
0.1	0.454	0.091
0.2	0.849	0.170
0.3	1.400	0.280
0.4	1.831	0.366
0.5	2.306	0.461

This data is presented in the following graph:

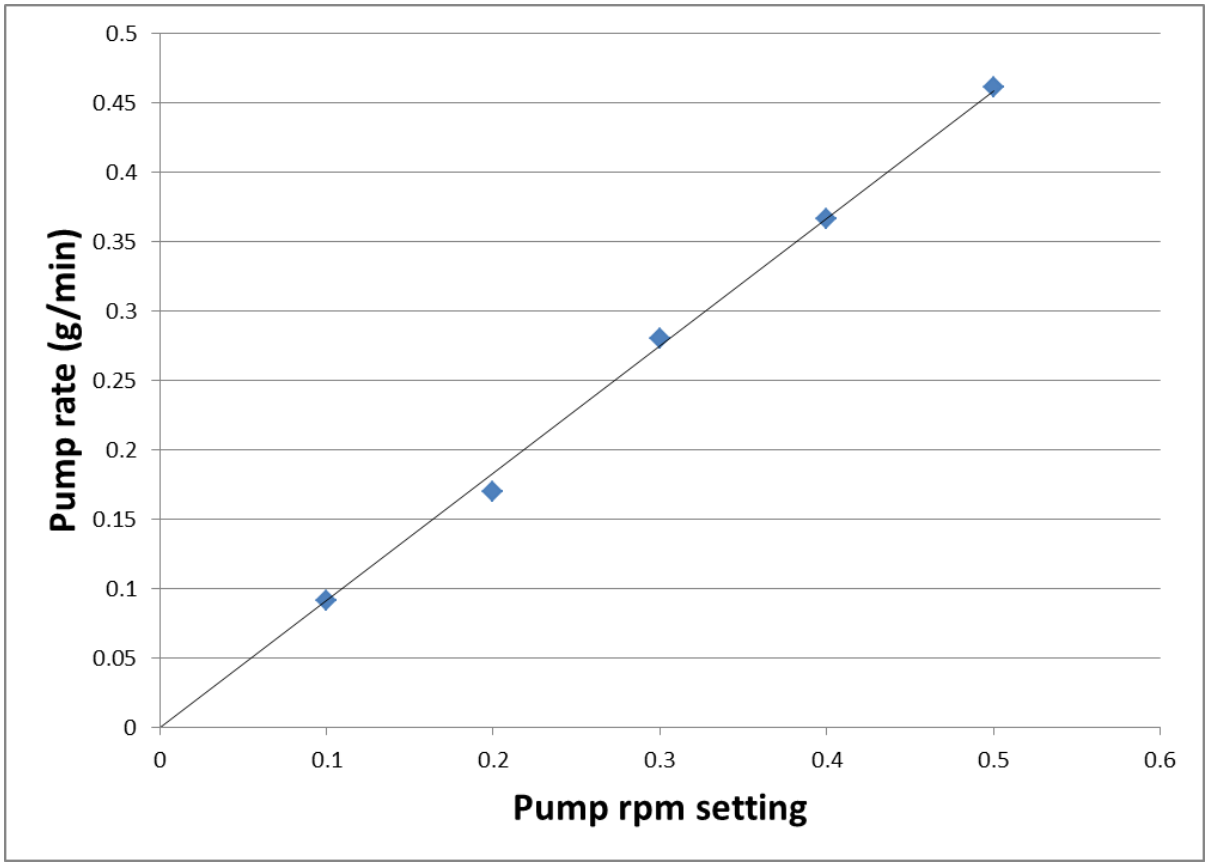

Figure 34 - Watson Marlow 120u pump calibration curve for sulphuric acid

Appendix E – Correction for sulphur dioxide measurements

To compensate for the losses of sulphur dioxide due to dissolution in the liquid traps (point D in Figure 35), the amount of sulphur dioxide that dissolved into the liquid traps was determined for five experiments over all possible feed scenarios i.e. base-case scenario, air scenario, additional water scenario as well as additional sulphur dioxide scenario. The sample from each experiment was subjected to three titrations as outlined in Section 3.1.6. The data in Table 15 shows the results from these titrations, and an estimation of the dissolved sulphur dioxide in the liquid of the liquid traps as well as an estimated dissolution rate is determined for this study.

Table 15 - Titration results used to assess SO_2 dissolution

Iodine titration amounts		**Calculation of SO_2 dissolution rate**	
Experiment number	Iodine used (mℓ)	Concentration SO_2 in trap	$55.505\ mmol/\ell$
1	7.6		
2	8.1	Total SO_2 in trap	$0.555\ mmol$
3	8.5	Molar dissolution rate	$0.046\ mmol/hr$
4	7.2		
5	7.5	Molar dissolution rate	$0.000\ 77\ mmol/min$
Average for samples	7.78		

A correction factor was determined for each experimental run to correct the sulphur dioxide as measured by the analyser. This was done by obtaining the amount of sulphur dioxide in stream E (Refer to Figure 35 in Appendix F) from the analyser data ($\dot{n}_{E(SO_2)}$) as well as a corrected value of sulphur dioxide in stream E, which include the measured value and the amount of sulphur dioxide dissolved in the liquid traps ($\dot{n}^*_{E(SO_2)}$). The correction factor is then determined with the following equation:

$$CF = \frac{\dot{n}^*_{E(SO_2)}}{\dot{n}_{E(SO_2)}} \qquad [E1]$$

By using the correction factor obtained above, the sulphur dioxide measurement from the analyser is then corrected as follows:

$$Y^*_{SO_2} = CF \times Y_{SO_2} \qquad [E2]$$

An average correction factor (CF) of 1.012 was found for all experimental data sets.

Appendix F – Molar flow calculations

The experimental layout is represented in Figure 35. The mole balance of the species will subsequently be discussed for the different experimental scenarios.

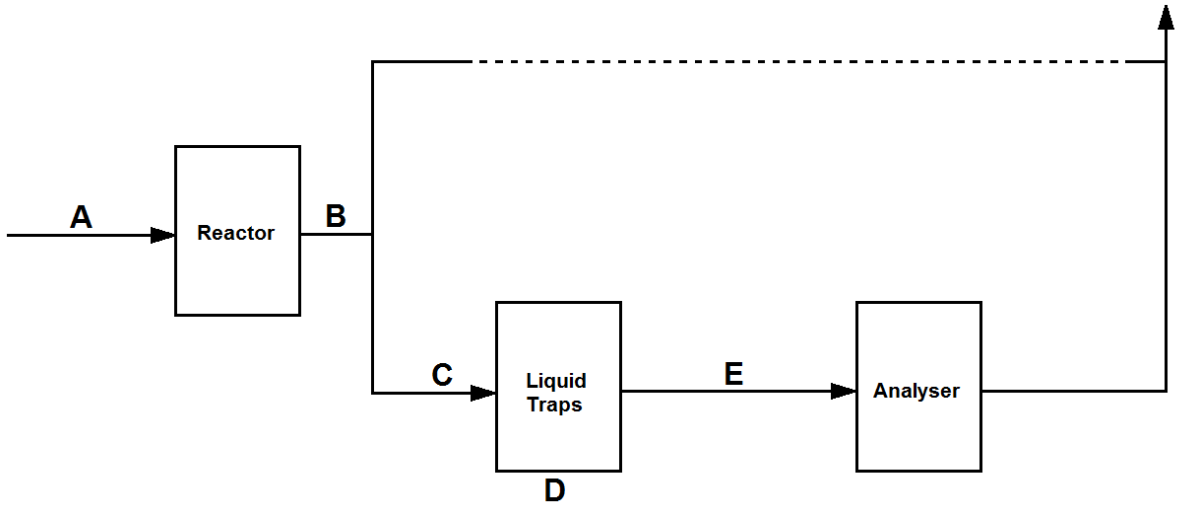

Figure 35 - Block diagram of experimental setup

F.1 Base-case scenario

The base case scenario entails a feed to the reactor consisting of 98%$_{(mass)}$ sulphuric acid and an amount of nitrogen gas as inert carrier. The only variation in the range of base-case experiments was the temperature of the reaction zone.

The molar flow rates at different points in the experimental setup, as is denoted by the letters A through E in Figure 35 is given in the following table.

Table 16 - Molar flow rate formulae over experimental setup for the base-case (nitrogen)

Species	Point in experimental setup (see Figure 35)				
	A	B	C	D	E
N_2	$\dot{n}^o_{N_2}$	$\dot{n}^o_{N_2}$	$S.\dot{n}^o_{N_2}$	0	$S.\dot{n}^o_{N_2}$
SO_3	$\dot{n}^o_{SO_3}$	$\dot{n}^o_{SO_3} - \dot{\xi}$	$S.\dot{n}^o_{SO_3} - S.\dot{\xi}$	$S.\dot{n}^o_{SO_3} - S.\dot{\xi}$	0
H_2O	$\dot{n}^o_{H_2O}$	$\dot{n}^o_{H_2O}$	$S.\dot{n}^o_{H_2O}$	$S.\dot{n}^o_{H_2O}$	0
SO_2	0	$\dot{\xi}$	$S.\dot{\xi}$	$\dot{n}^{(diss)}_{SO_2}$	$S.\dot{\xi} - \dot{n}^{(diss)}_{SO_2}$
O_2	0	$\frac{1}{2}\dot{\xi}$	$\frac{1}{2}.S.\dot{\xi}$	0	$\frac{1}{2}.S.\dot{\xi}$
Total	$\dot{n}^o_{N_2} + \dot{n}^o_{SO_3} + \dot{n}^o_{H_2O}$	$\dot{n}^o_{N_2} + \dot{n}^o_{SO_3} + \dot{n}^o_{H_2O} + \frac{1}{2}\dot{\xi}$	$S\dot{n}^o_{N_2} + S\dot{n}^o_{SO_3} + S\dot{n}^o_{H_2O} + \frac{1}{2}S\dot{\xi}$	$S\dot{n}^o_{SO_3} - S\dot{\xi} + S\dot{n}^o_{H_2O} + \dot{n}^{(diss)}_{SO_2}$	$S\dot{n}^o_{N_2} + \frac{3}{2}S\dot{\xi} - \dot{n}^{(diss)}_{SO_2}$

The flow of the nitrogen carrier gas and the amount of water and sulphur trioxide in the feed stream to the reactor is determined from the mass flow controller and pump calibration data that is presented in Appendix C.

The extent of the reaction ($\dot{\xi}$) is calculated from the sulphur dioxide measurement. The derivation of the equation for this purpose is shown. The measurement of sulphur dioxide is the molar amount of sulphur dioxide in stream E relative to the total moles in stream E.

$$Y_{SO_2} = \frac{S\dot{\xi} - \dot{n}_{SO_2}^{(diss)}}{S\dot{n}_{N_2}^{o} + \frac{3}{2}S\dot{\xi} - \dot{n}_{SO_2}^{(diss)}} \qquad [F1]$$

A correction for the SO_2 measurement based upon dissolution of SO_2 into the liquid traps (point D) is presented in Appendix E. At this point, it can be noted that the corrected measurement ($Y_{SO_2}^{*}$) is expressed as follows:

$$Y_{SO_2}^{*} = \frac{S\dot{\xi}}{S\dot{n}_{N_2}^{o} + \frac{3}{2}S\dot{\xi}} = \frac{\dot{\xi}}{\dot{n}_{N_2}^{o} + \frac{3}{2}\dot{\xi}}$$

$$\therefore \quad \dot{\xi}\left(1 - \frac{3}{2}Y_{SO_2}^{*}\right) = \dot{n}_{N_2}^{o}Y_{SO_2}^{*}$$

$$\therefore \quad \dot{\xi} = \frac{\dot{n}_{N_2}^{o}Y_{SO_2}^{*}}{\left(1 - \frac{3}{2}Y_{SO_2}^{*}\right)} \qquad [F2]$$

In order to determine the split (S) at point B in Figure 35, it was assumed that no water and sulphur trioxide passed the liquid traps. The split (S) was thus determined as follows:

$$S = \frac{\dot{n}_B^{*}}{\dot{n}_E^{*}} \qquad [F3]$$

The value of $\dot{n}_B^{*}$ equals the total moles in stream B less the amount of water and sulphur trioxide present in stream B. The value of $\dot{n}_E^{*}$ equals the total moles in stream E plus the number of moles of sulphur dioxide that was dissolved in the liquid traps, as discussed in Appendix E. The total number of moles in stream E ($\dot{n}_E$) is determined by the amount of gas regulated to the gas analysers.

The measured amount of sulphur dioxide determines the outcome of the molar balance, and a typical mole balance for the base case at 825°C is shown in Table 17.

Table 17 - Base case molar flow rates at 825°C

Species	Point in experimental setup (see Figure 35); Flow (mmol/min)				
	A	B	C	D	E
N_2	44.72	44.72	25.83	0.00	25.83
SO_3	1.67	1.18	0.68	0.68	0.00
H_2O	1.85	1.85	1.07	1.07	0.00
SO_2	0.00	0.49	0.28	0.00	0.28
O_2	0.00	0.24	0.14	0.00	0.14
Total	48.24	48.48	28.01	1.75	26.25

F.2 Additional water in the feed

The mole balance for the case wherein the sulphuric acid was diluted to ensure a 2:1 H_2O:SO_3 ratio as well as a 3:1 ratio, is exactly similar to the base-case mole balance shown in Table 16. Starting each time with 100g of 98%$_{(mass)}$ sulphuric acid, the required amount of water was subsequently calculated to ensure a molar ratio of 2:1 and 3:1 H_2O:SO_3. The following table summarises the calculations regarding these dilutions.

Table 18 - Calculations for dilution of sulphuric acid with water

2:1 Molar ratio (H_2O:SO_3) feed			3:1 Molar ratio (H_2O:SO_3) feed		
$m_{H_2SO_4(98\%)}$	100.245	g	$m_{H_2SO_4(98\%)}$	100.172	g
$m_{H_2SO_4(100\%)}$	98.240	g	$m_{H_2SO_4(100\%)}$	98.169	g
$n_{H_2SO_4(100\%)}$	1.002	$mole$	$n_{H_2SO_4(100\%)}$	1.001	$mole$
$n_{SO_3\ (acid\ decomposition)}$	1.002	$mole$	$n_{SO_3\ (acid\ decomposition)}$	1.001	$mole$
$n_{H_2O(acid\ decomposition)}$	1.002	$mole$	$n_{H_2O(acid\ decomposition)}$	1.001	$mole$
$n_{H_2O(acid\ impurities)}$	0.111	$mole$	$n_{H_2O(acid\ impurities)}$	0.111	$mole$
$n_{H_2O(added\ to\ mix)}$	0.890	$mole$	$n_{H_2O(added\ to\ mix)}$	1.891	$mole$
$m_{H_2O(added\ to\ mix)}$	16.040	g	$m_{H_2O(added\ to\ mix)}$	34.060	g
$n_{H_2O(total)}$	2.003	$mole$	$n_{H_2O(total)}$	3.003	$mole$
$Ratio\ (H_2O:SO_3)$	2.000	-	$Ratio\ (H_2O:SO_3)$	3.000	-

The extent of reaction as well as the split at stream B was calculated in exactly the same manner as for the base case, leaving a typical mole balance of the 2:1 ratio case shown in Table 19 and a typical mole balance for the 3:1 ratio case shown in Table 20, both at 825°C.

Table 19 - 2:1 molar ratio (H_2O:SO_3) molar flow rates at 825°C

Species	Point in experimental setup (see Figure 35); Flow (mmol/min)				
	A	B	C	D	E
N_2	44.72	44.72	26.02	0.00	26.02
SO_3	1.44	1.17	0.68	0.68	0.00
H_2O	2.88	2.88	1.67	1.67	0.00
SO_2	0.00	0.27	0.16	0.00	0.15
O_2	0.00	0.13	0.08	0.00	0.08
Total	49.03	49.17	28.61	2.36	26.25

Table 20 - 3:1 molar ratio (H2O:SO3) molar flow rates at 825°C

Species	Point in experimental setup (see Figure 35); Flow (mmol/min)				
	A	B	C	D	E
N_2	44.72	44.72	26.07	0.00	26.07
SO_3	1.25	1.03	0.60	0.60	0.00
H_2O	3.74	3.74	2.18	2.18	0.00
SO_2	0.00	0.21	0.12	0.00	0.12
O_2	0.00	0.11	0.06	0.00	0.06
Total	49.70	49.80	29.03	2.78	26.25

F.3 Additional oxygen in the feed

In order to assess the influence of oxygen in the reactor feed on the reaction, air was used instead of pure nitrogen as carrier gas. The mole balance for this case differs slightly from the one presented for the base case due to the additional species in the reactor feed, and is shown in Table 21.

Based on the change in stream E, the calculation for the extent of the reaction required a revision from that presented in the base case. The derivation is presented immediately after Table 21 followed by typical molar flow rates for the air-fed case in Table 22.

Table 21 - Molar flow rate formulae over the experimental setup with air as carrier

Species	Point in experimental setup (see Figure 35)				
	A	B	C	D	E
N_2	$\dot{n}^o_{N_2}$	$\dot{n}^o_{N_2}$	$S.\dot{n}^o_{N_2}$	0	$S.\dot{n}^o_{N_2}$
SO_3	$\dot{n}^o_{SO_3}$	$\dot{n}^o_{SO_3} - \dot{\xi}$	$S.\dot{n}^o_{SO_3} - S.\dot{\xi}$	$S.\dot{n}^o_{SO_3} - S.\dot{\xi}$	0
H_2O	$\dot{n}^o_{H_2O}$	$\dot{n}^o_{H_2O}$	$S.\dot{n}^o_{H_2O}$	$S.\dot{n}^o_{H_2O}$	0
SO_2	0	$\dot{\xi}$	$S.\dot{\xi}$	$\dot{n}^{(diss)}_{SO_2}$	$S.\dot{\xi} - \dot{n}^{(diss)}_{SO_2}$
O_2	$\dot{n}^o_{O_2}$	$\dot{n}^o_{O_2} + \frac{1}{2}\dot{\xi}$	$S.\dot{n}^o_{O_2} + \frac{1}{2}.S.\dot{\xi}$	0	$S.\dot{n}^o_{O_2} + \frac{1}{2}.S.\dot{\xi}$
Total	$\dot{n}^o_{N_2} + \dot{n}^o_{SO_3} + \dot{n}^o_{H_2O} + \dot{n}^o_{O_2}$	$\dot{n}^o_{N_2} + \dot{n}^o_{SO_3} + \dot{n}^o_{H_2O} + \dot{n}^o_{O_2} + \frac{1}{2}\dot{\xi}$	$S\dot{n}^o_{N_2} + S\dot{n}^o_{SO_3} + S\dot{n}^o_{H_2O} + S\dot{n}^o_{O_2} + \frac{1}{2}s\dot{\xi}$	$S\dot{n}^o_{SO_3} - S\dot{\xi} + S\dot{n}^o_{H_2O} + \dot{n}^{(diss)}_{SO_2}$	$S\dot{n}^o_{N_2} + S\dot{n}^o_{O_2} + \frac{3}{2}S\dot{\xi} - \dot{n}^{(diss)}_{SO_2}$

Under similar assumptions as for the base case, the extent of the reaction is determined based on the sulphur dioxide analyses according to the following equations:

$$Y^*_{SO_2} = \frac{S\dot{\xi}}{S\dot{n}^o_{N_2} + S\dot{n}^o_{O_2} + \frac{3}{2}S\dot{\xi}} = \frac{\dot{\xi}}{\dot{n}^o_{N_2} + \dot{n}^o_{O_2} + \frac{3}{2}\dot{\xi}}$$

$$\therefore \quad \dot{\xi}\left(1 - \frac{3}{2}Y^*_{SO_2}\right) = \left(\dot{n}^o_{N_2} + \dot{n}^o_{O_2}\right)Y^*_{SO_2}$$

$$\therefore \quad \dot{\xi} = \frac{\left(\dot{n}^o_{N_2} + \dot{n}^o_{O_2}\right)Y^*_{SO_2}}{\left(1 - \frac{3}{2}Y^*_{SO_2}\right)} \qquad [F4]$$

The split fraction (S) was, again, calculated exactly like for the base-case scenario.

Table 22 - Molar flow rates for the air-fed scenario at 825°C

Species	Point in experimental setup (see Figure 35); Flow (mmol/min)				
	A	B	C	D	E
N_2	28.16	28.16	20.29	0.00	20.29
SO_3	1.67	1.14	0.82	0.82	0.00
H_2O	1.85	1.85	1.33	1.33	0.00
SO_2	0.00	0.53	0.38	0.00	0.38
O_2	7.48	7.75	5.58	0.00	5.58
Total	39.16	39.43	28.41	2.15	26.25

F.4 Additional sulphur dioxide in the feed

It was also of interest to assess the influence of additional sulphur dioxide in the reactor feed on the reaction kinetics. For this purpose, a quantity of SO_2 were added to the feed by replacing the pure nitrogen with a 50:50 mixture of pure N_2 and a subsequent mixture of 85.5%$_{(vol)}$ N_2, 10%$_{(vol)}$ SO_2 and 5%$_{(vol)}$ O_2.

The molar flow rate formulae for the case with additional SO_2 in the reactor feed is presented in Table 23 with typical values shown in Table 24.

Table 23 - Molar flow rate formulae over experimental setup with additional SO_2 in feed

Species	Point in experimental setup (see Figure 35)				
	A	B	C	D	E
N_2	$\dot{n}^o_{N_2}$	$\dot{n}^o_{N_2}$	$S.\dot{n}^o_{N_2}$	0	$S.\dot{n}^o_{N_2}$
SO_3	$\dot{n}^o_{SO_3}$	$\dot{n}^o_{SO_3} - \dot{\xi}$	$S.\dot{n}^o_{SO_3} - S.\dot{\xi}$	$S.\dot{n}^o_{SO_3} - S.\dot{\xi}$	0
H_2O	$\dot{n}^o_{H_2O}$	$\dot{n}^o_{H_2O}$	$S.\dot{n}^o_{H_2O}$	$S.\dot{n}^o_{H_2O}$	0
SO_2	$\dot{n}^o_{SO_2}$	$\dot{n}^o_{SO_2} + \dot{\xi}$	$S.\dot{n}^o_{SO_2} + S.\dot{\xi}$	$\dot{n}^{(diss)}_{SO_2}$	$S.\dot{n}^o_{SO_2} + S.\dot{\xi} - \dot{n}^{(diss)}_{SO_2}$
O_2	$\dot{n}^o_{O_2}$	$\dot{n}^o_{O_2} + \frac{1}{2}\dot{\xi}$	$S.\dot{n}^o_{O_2} + \frac{1}{2}.S.\dot{\xi}$	0	$S.\dot{n}^o_{O_2} + \frac{1}{2}.S.\dot{\xi}$
Total	$\dot{n}^o_{N_2} + \dot{n}^o_{SO_3} + \dot{n}^o_{H_2O} + \dot{n}^o_{SO_2} + \dot{n}^o_{O_2}$	$\dot{n}^o_{N_2} + \dot{n}^o_{SO_3} + \dot{n}^o_{H_2O} + \dot{n}^o_{SO_2} + \dot{n}^o_{O_2} + \frac{1}{2}\dot{\xi}$	$S\left(\dot{n}^o_{N_2} + \dot{n}^o_{SO_3} + \dot{n}^o_{H_2O} + \dot{n}^o_{SO_2} + \dot{n}^o_{O_2} + \frac{1}{2}\dot{\xi}\right)$	$S\dot{n}^o_{SO_3} - S\dot{\xi} + S\dot{n}^o_{H_2O} + \dot{n}^{(diss)}_{SO_2}$	$S\dot{n}^o_{N_2} + S\dot{n}^o_{SO_2} + S\dot{n}^o_{O_2} + \frac{3}{2}S\dot{\xi} - \dot{n}^{(diss)}_{SO_2}$

The extent of the reaction is calculated based on similar assumptions as stated for the base case, and was done according to the following derivation:

$$Y^*_{SO_2} = \frac{S\dot{\xi} + S\dot{n}^o_{SO_2}}{S\dot{n}^o_{N_2} + S\dot{n}^o_{SO_2} + S\dot{n}^o_{O_2} + \frac{3}{2}S\dot{\xi}} = \frac{\dot{\xi} + \dot{n}^o_{SO_2}}{\dot{n}^o_{N_2} + \dot{n}^o_{SO_2} + \dot{n}^o_{O_2} + \frac{3}{2}\dot{\xi}}$$

$$\therefore \quad \dot{\xi}\left(1-\frac{3}{2}Y^*_{SO_2}\right)=\left(\dot{n}^o_{N_2}+\dot{n}^o_{SO_2}+\dot{n}^o_{O_2}\right)Y^*_{SO_2}-\dot{n}^o_{SO_2}$$

$$\therefore \quad \dot{\xi}=\frac{\left(\dot{n}^o_{N_2}+\dot{n}^o_{SO_2}+\dot{n}^o_{O_2}\right)Y^*_{SO_2}-\dot{n}^o_{SO_2}}{\left(1-\frac{3}{2}Y^*_{SO_2}\right)} \qquad [F5]$$

The split fraction (S) was calculated similar to the base case scenario.

Table 24 - Molar flow rates for additional SO2 at 825°C

Species	Point in experimental setup (see Figure 35); Flow (mmol/min)				
	A	B	C	D	E
N_2	33.84	33.84	24.16	0.00	24.16
SO_3	1.67	1.54	1.10	1.10	0.00
H_2O	1.85	1.85	1.32	1.32	0.00
SO_2	1.82	1.96	1.40	0.00	1.40
O_2	0.91	0.98	0.70	0.00	0.70
Total	40.09	40.16	28.67	2.42	26.25

Appendix G – Experimental data

The raw data points for the base-case experiments are shown in Figure 36 for all the reaction temperatures of the investigation, i.e. 700°C (red data points), 725°C (dark blue data points), 750°C (green data points), 775°C (purple data points), 800°C (brown data points) and 825°C (blue data points).

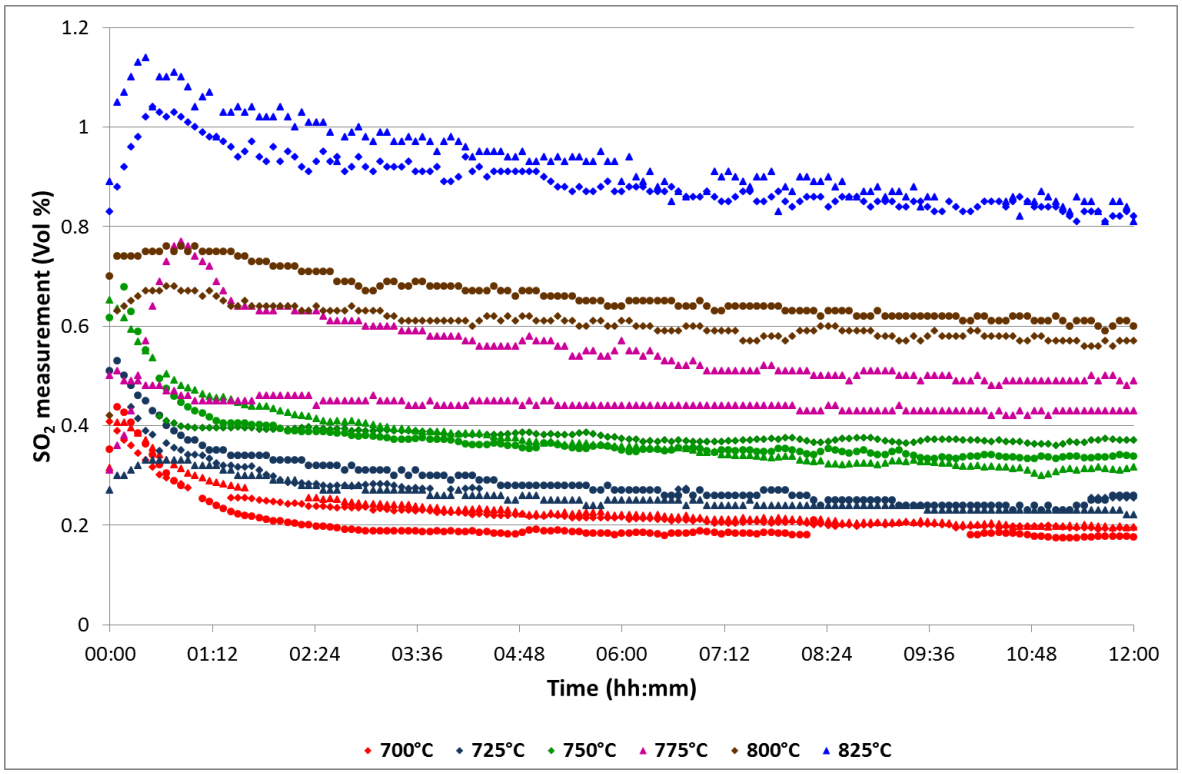

Figure 36 - Raw analyser data for the base-case scenario

Figure 37 and Figure 38 show raw data points used for the qualitative investigation of diluted sulphuric acid as feed to the reactor at three different reaction temperatures, i.e. 700°C (dark blue data points), 750°C (green data points) and 825°C (blue data points). Figure 37 shows data for the 2:1 molar ratio of H_2O:SO_3 in the reactor feed while Figure 38 represents the data for the 3:1 (H_2O:SO_3) feed scenario.

Figure 39 shows raw data points for the scenario wherein additional sulphur dioxide is added to the reactor feed according to Table 4 in Section 3.2.1. Again, the dark blue data points represent the experimental data obtained at a reaction temperature of 700°C, the green data points were obtained for 750°C reaction temperature and the blue data points are representing the measured sulphur dioxide for a reaction temperature of 825°C.

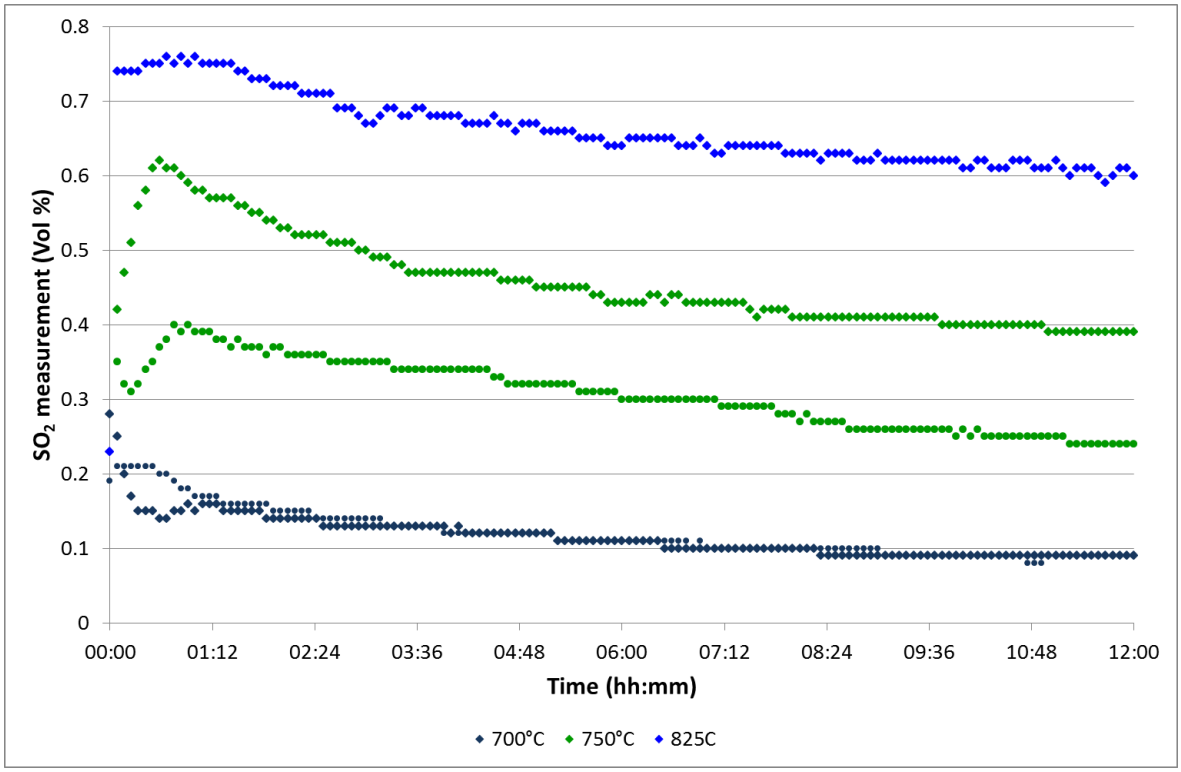

Figure 37 - Raw analyser data for the 2:1 (H_2O:SO_3) feed scenario

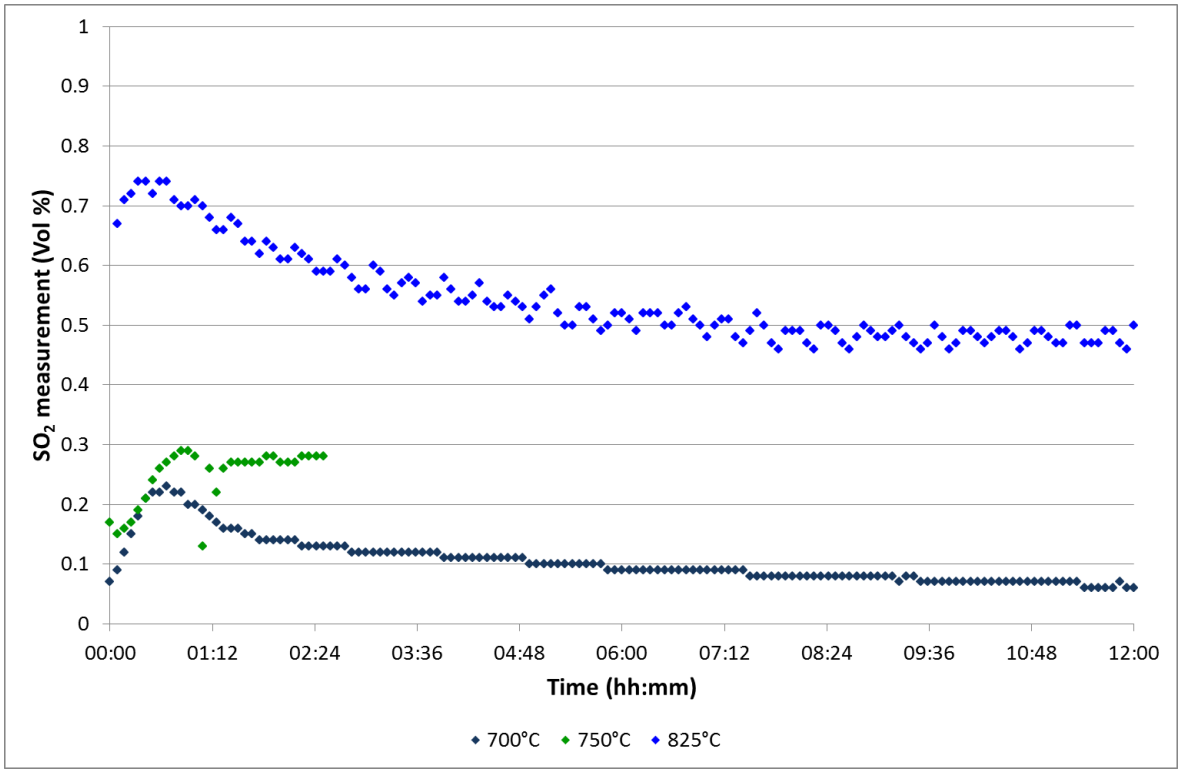

Figure 38 - Raw analyser data for the 3:1 (H_2O:SO_3) feed scenario

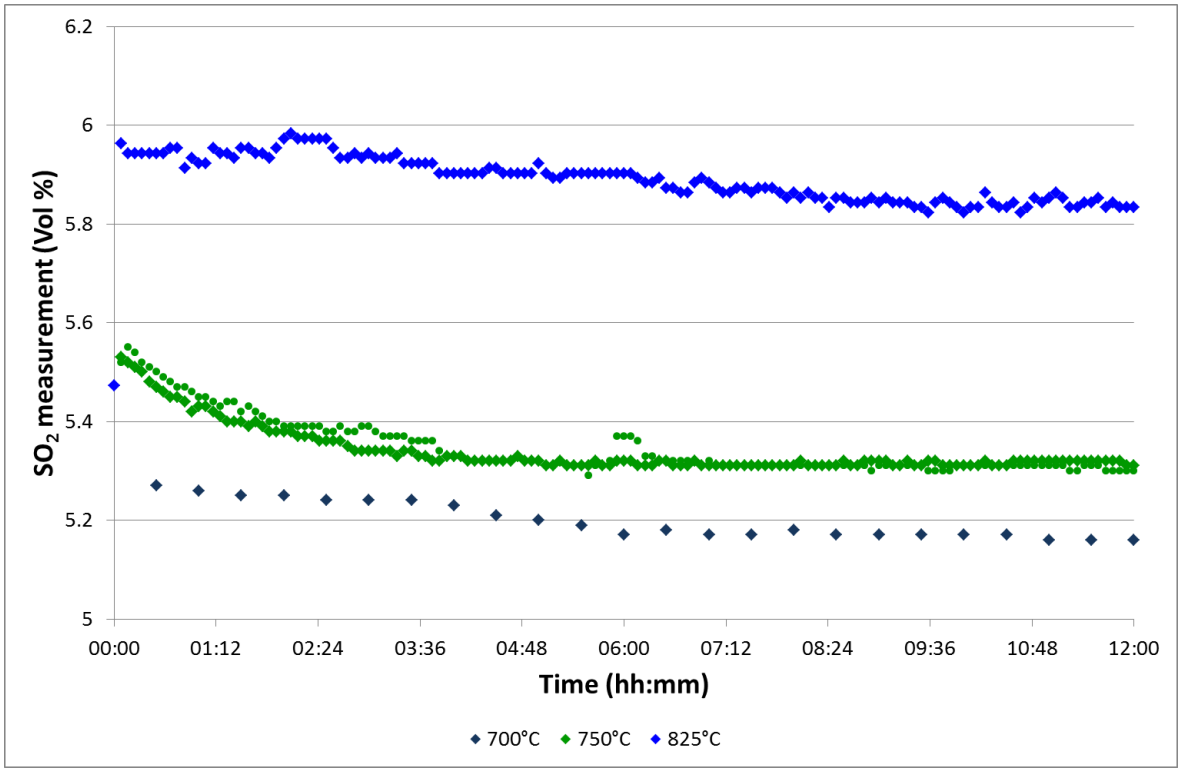

Figure 39 - Raw analyser data for the SO_2-fed scenario

Appendix H – Calculations based on published data

H.1 Calculations conducted on data by Kim *et al.* (2006)

Data for the feed composition to the reactor was obtained from the publication of Kim *et al.* (2006) and was used, in conjunction with the published conversions, to determine the reaction rate constants and subsequently the reaction rates at the different reaction temperatures that correspond with the reaction temperatures used in this study.

Kim *et al.* (2006) specified the following feed conditions to the reactor for all experiments conducted:

- Feed percentage sulphur trioxide of 33.3 $\%_{(mole)}$ with the balance being nitrogen
- Flow rate of sulphur trioxide of 20 cm^3/min
- Flow rate of nitrogen of 40cm^3/min
- Pressure of 1 atmosphere
- Gas hourly space velocity of $72\,000\ cm^3/g_{cat}.hr$

For the different catalysts, which consist of iron (III) oxide on alumina with compositions of 0.25, 0.50, 0.75 & 1.00 molar ratios of iron (III) oxide : alumina, and subsequently a similar arrangement for iron (III) oxide on titania, the following conversions were obtained at the different reaction temperatures:

Table 25 - Conversions obtained for iron-based catalysts (Adapted from Kim *et al.* (2006))

Catalyst type	Reaction temperature	Ratio of Iron (III) oxide to substrate			
		0.25	0.50	0.75	1.00
		Conversion (%)			
Fe/Al	750°C	5 %	18 %	19 %	20 %
	800°C	12 %	26 %	32 %	38 %
	825°C	27 %	42 %	71 %	71 %
Fe/Ti	750°C	22 %	19 %	19 %	18 %
	800°C	36 %	40 %	40 %	42 %
	825°C	58 %	68 %	68 %	70 %

From the data above, the total flow rate to the reactor was calculated as well as the mass of catalyst used. The total flow rate to the reactor was calculated using Equation A10 and the concentration of sulphur trioxide was calculated with Equation A11. Equation A9 was used to obtain the reaction rate constant k, while using Equations A1 & A2 resulted in the flow rate of sulphur dioxide from the reactor ($\dot{n}_{SO_2}\ or\ \dot{\xi}$) and the reaction rate r_{SO_3}. Table 26 summarises the calculated values from the data published by Kim *et al.* (2006) for the 1:1 molar ratio of Fe_2O_3:TiO_2. Similar data is obtained for all other catalyst ratios as discussed in Section 4.2.1.

The calculation of the reaction rates as well as the reaction rate constants were corrected for the iron (III) oxide content in the catalyst based on the specified ratio.

Table 26 - Example of calculated results from data of Kim *et al.* (2006)

Kinetics Data						
T	Conversion	v_o	$C_{so_3(o)}$	k	$\dot{n}_{so_2}$	Reaction rate
(°C)	(%)	m^3/hr	mol/m^3	$m^3/kg_{cat}.hr$	mol/hr	$mol/kg_{cat}.hr$
775	18	0.0127	3.88	75	0.009	265
800	42	0.0130	3.79	212	0.021	618
825	70	0.0133	3.70	479	0.034	1030

Constants		
Total volume Fed v_o	0.002	mol/min
	24.465	Nl/mol
	0.060	Nl/min
	0.004	Nm^3/hr
Init Conc SO_3	13.625	mol/Nm^3
GHSV	72000	$cm^3/g_{cat}.hr$
Mass catalyst	0.050	g_{cat}
Mass Fe_2O_3	0.033	g_{cat}

Species	Feed		
	Vol(%)	Flow (Nml/min)	Flow (mmol/min)
N_2	33	40.0	1.63
SO_3	67	20.0	0.82
H_2O	0	0.0	0.00
SO_2	0	0.0	0.00
O_2	0	0.0	0.00
Total	100	60.0	2.45

The reaction rate constants as well as the reaction rates obtained through calculations on the results published by Kim *et al.* (2006) are compared to the reaction rate constants and reaction rates obtained for pure iron (III) oxide in this study and are discussed in Section 4.2.1. The calculated values are reported in the following two tables.

Table 27 - Comparison of reaction rate constants of Kim et al. (2006) with values in this study

	Fe-Al (Molar Ratio)				Fe-Ti (Molar Ratio)				This study
	0.25	0.50	0.75	1.00	0.25	0.50	0.75	1.00	Pure Fe_2O_3
T (K)	**Reaction Rate Constant (k) - $(m^3/kg_{cat}.hr)$**								
1048	46	114	99	93	80	126	89	75	347
1073	118	178	185	203	372	231	221	618	460
1098	297	329	608	538	568	460	504	479	680

Table 28 - Comparison of reaction rates of Kim et al. (2006) with values in this study

	Fe-Al (Molar Ratio)				Fe-Ti (Molar Ratio)				This study
	0.25	0.50	0.75	1.00	0.25	0.50	0.75	1.00	Pure Fe_2O_3
T (K)	**Reaction Rate ($-r_a$) - $(m^3/kg_{cat}.hr)$**								
1048	174	402	345	321	294	432	311	265	143
1073	418	581	581	611	1119	707	654	618	182
1098	941	938	1289	1141	1502	1138	1112	1030	254

H.2 Calculations conducted on data by Kondamudi & Uphadhyayula (2012)

The reactor feed conditions applied by Kondamudi & Uphadhyayula (2012) are summarised as follow:

- Catalyst mass of 0.002 kg
- Concentration of sulphur trioxide in the reactor feed of 7%$_{(mole)}$
- Sulphuric acid feed rate of 0.0024 ℓ/hr
- Pressure of 1 atmosphere
- WHSV of 0.146 – 0.731 kmol/kg$_{cat}$.hr

Kondamudi & Uphadhyayula (2012) conducted experiments with iron (III) oxide supported on alumina (Al_2O_3) and published conversions at reaction temperatures of which some correspond with reaction temperatures of this study, i.e. 775°C, 800°C and 825°C. Conversions obtained by Kondamudi & Uphadhyayula (2012) are 28% at 775°C, 50% at 800°C and 75% at 825°C.

Similar to the calculations as described for Kim *et al.* (2006) in Section H1, Equations A1, A2 & A9 through A11 were applied to obtain reaction rate constants and reaction rates at the mentioned reaction temperatures. Due to a lack of information on the iron (III) oxide load in the supported catalyst, it was not possible to correct these calculated results for the iron content alone. The results of the calculations are presented in Table 29.

Table 29 - Example of calculated results from data of Kondamudi & Uphadhyayula (2012)

Kinetics Data						
T	Conversion	v_o	$C_{SO_3(o)}$	k	n_{SO_2}	Reaction rate
(°C)	(%)	m^3/hr	mol/m^3	$m^3/kg_{cat}.hr$	mol/hr	$mol/kg_{cat}.hr$
775	28	0.0551	0.81	91	0.013	63
800	50	0.0565	0.79	196	0.022	112
825	75	0.0578	0.78	400	0.034	168

H_2SO_4 in Feed			
l/hr	ml/min	g/min	mmol/min
0.0024	0.040	0.073	0.75
Purity	96	%	0.78
SG_{H2SO4}	1.834	kg/l	
M_{H2SO4}	98.079	g/mol	

Constants		
	0.0107	mol/min
Total volume	24.5	Nl/mol
Fed	0.261	Nl/min
v_o	0.016	Nm^3/hr
Init Conc SO_3	2.86	mol/Nm^3
WHSV	0.46	$kmol/kg_{cat}.hr$
Mass catalyst	0.200	g_{cat}

Species	Feed		
	Vol(%)	Flow (Nml/min)	Flow (mmol/min)
N_2	85.7	224	9.16
SO_3	7.0	18	0.75
H_2O	7.3	19	0.78
SO_2	0	0.000	0.00
O_2	0	0.000	0.00
Total	100	261	10.69

Table 30 shows the values calculated for the case presented by Kondamudi & Uphadhyayula (2012) as well as the values obtained in this study. A complete discussion on the comparison is presented in Section 4.2.2.

Table 30 - Comparison of calculations of Kondamudi & Uphadhyayula (2012) with values obtained in this study

	Reaction Rate ($-r_a$) - $(m^3/kg_{cat}.hr)$	
T (K	Supported Fe_2O_3	Pure Fe_2O_3
1048	63	143
1073	112	182
1098	168	254
	Reaction Rate Constant (k) - $(m^3/kg_{cat}.hr)$	
T (K	Supported Fe_2O_3	Pure Fe_2O_3
1048	91	347
1073	196	460
1098	400	680

H.3 Calculations conducted on data by Giaconia *et al.* (2011)

Giaconia *et al.* (2011) specified different reactor feed conditions for different experiments that were conducted. Three investigations were conducted using iron (III) oxide pellets with three more using Fe_2O_3-coated SiSiC honeycomb fragments. The conditions for the six investigations are summarised in Table 8 in Section 4.2.4.

Important to note is the way in which Giaconia *et al.* (2011) calculated the WHSV. Rather than following the formula used in this study, as depicted by Equation A3 (Appendix A), the following formula was used:

$$WHSV = \frac{\dot{w}^{o}_{H_2SO_4}}{m_{cat}} \qquad [H1]$$

The mass of catalyst each time used by Giaconia *et al.* (2011) could be obtained by using Equation H1.

Following similar routes for the calculations as discussed in Sections H1 & H2 for other authors, the values obtained for the reactor flow rate, inlet concentration of sulphur trioxide, the reaction rate constant, flow of sulphur dioxide from the reactor as well as the reaction rate was calculated for each reaction temperature. The calculated reaction rates and reaction rate constants were corrected for the average amount of iron (III) oxide in the catalyst specified by Giaconia *et al.* (2011) at around 16.7%$_{wt}$. An example of the calculations is displayed for the Fe_2O_3-coated SiSiC honeycomb fragments (experiment C – refer to Table 8 in Section 4.2.3) in Table 31.

Table 31 - Example of calculated results from data of Giaconia *et al.* (2011)

Kinetics Data							Constants		
T	Conversion	v_o	$C_{so_3(o)}$	k	$\dot{n}_{so_2}$	Reaction rate			
(°C)	(%)	m^3/hr	mol/m^3	$m^3/kg_{cat}.hr$	mol/hr	$mol/kg_{cat}.hr$	Total volume Fed	0.013	mol/min
								24.5	Nl/mol
								0.330	Nl/min
775	10	0.0696	5.0	10.8	0.035	51	v_o	0.020	Nm^3/hr
800	19	0.0713	4.9	22.1	0.066	97			
825	34	0.0729	4.8	44.7	0.118	174	Init Conc SO_3	17.6	mol/Nm^3
							WHSV	8.400	hr^{-1}
							Mass catalyst	4.063	g_{cat}
							Mass Fe_2O_3	0.679	g_{cat}

H_2SO_4 in Feed			
mmol/min	mol/hr	g/hr	ml/min
5.8	0.3	34.1	0.31
Purity	96	%	0.32
SG_{H2SO4}	1.834	kg/l	
M_{H2SO4}	98.079	g/mol	

Species	Feed		
	Vol(%)	Flow (Nml/min)	Flow (mmol/min)
N_2	5	17	0.67
SO_3	43	142	5.80
H_2O	52	172	7.01
SO_2	0	0	0.00
O_2	0	0	0.00
Total	100	330	13.49

The reaction rate constants and the reaction rates of the six experiments of Giaconia *et al.* (2011) were compared to the values obtained in this study using pure, micronized, unsupported iron (III) oxide. Details of this discussion can be found in Section 4.2.3. The reaction rate constants calculated for the data obtained by Giaconia *et al.* (2011) as well as those obtained in this study are shown in Table 32 while the reaction rates are tabulated in Table 33.

Table 32 - Comparison of reaction rate constants of Giaconia et al. (2011) with values obtained in this study

	Fe (III) oxide pellets			SiSiC Fragments			This study
	(A)	(B)	(C)	(A)	(B)	(C)	Pure Fe_2O_3
T (K)	**Reaction Rate Constant (k) - $(m^3/kg_{cat}.hr)$**						
1048	17	17	13	6	17	11	347
1073	30	25	20	6	33	22	460
1098	45	38	29	12	57	45	680

Table 33 - Comparison of reaction rates of Giaconia et al. (2011) with values obtained in this study

	Fe (III) oxide pellets			SiSiC Fragments			This study
	(A)	(B)	(C)	(A)	(B)	(C)	Pure Fe_2O_3
T (K)	**Reaction Rate $(-r_a)$ - $(mol/kg_{cat}.hr)$**						
1048	85	78	53	30	82	51	143
1073	136	108	74	30	153	97	182
1098	195	152	98	60	245	174	254